REPORT T-150 JANUARY 1985

CSL COORDINATED SCIENCE LABORATORY

NUMERICAL SOLUTION OF THE NONLINEAR SHIP WAVE PROBLEM

R. R. CHAMBERLAIN
S. M. YEN

UNIVERSITY OF ILLINOIS AT URBANA-CHAMPAIGN

SECURITY CLASSIFICATION OF THIS PAGE

REPORT DOCUMENTATION PAGE

1a. REPORT SECURITY CLASSIFICATION Unclassified	1b. RESTRICTIVE MARKINGS None
2a. SECURITY CLASSIFICATION AUTHORITY N/A	3. DISTRIBUTION/AVAILABILITY OF REPORT Approved for public release, distribution unlimited.
2b. DECLASSIFICATION/DOWNGRADING SCHEDULE N/A	
4. PERFORMING ORGANIZATION REPORT NUMBER(S) T-150	5. MONITORING ORGANIZATION REPORT NUMBER(S) N/A
6a. NAME OF PERFORMING ORGANIZATION Coordinated Science Lab., Univ. of Illinois 6b. OFFICE SYMBOL (If applicable) N/A	7a. NAME OF MONITORING ORGANIZATION Office of Naval Research
6c. ADDRESS (City, State and ZIP Code) 1101 W. Springfield Avenue Urbana, Illinois 61801	7b. ADDRESS (City, State and ZIP Code) 800 N. Quincy Street Arlington, VA 22217
8a. NAME OF FUNDING/SPONSORING ORGANIZATION Office of Naval Research 8b. OFFICE SYMBOL (If applicable)	9. PROCUREMENT INSTRUMENT IDENTIFICATION NUMBER Contract #N00014-80-C-0740 (NR334-004)
8c. ADDRESS (City, State and ZIP Code) 800 N. Quincy Street Arlington, VA 22217	10. SOURCE OF FUNDING NOS. PROGRAM ELEMENT NO.: N/A; PROJECT NO.: N/A; TASK NO.: N/A; WORK UNIT NO.: N/A
11. TITLE (Include Security Classification) Numerical Solution of the Nonlinear Ship Wave Problem.	
12. PERSONAL AUTHOR(S) R. R. Chamberlain and S. M. Yen	
13a. TYPE OF REPORT Technical 13b. TIME COVERED FROM _____ TO _____	14. DATE OF REPORT (Yr., Mo., Day) January, 1985 15. PAGE COUNT 131
16. SUPPLEMENTARY NOTATION N/A	
17. COSATI CODES FIELD / GROUP / SUB. GR.	18. SUBJECT TERMS (Continue on reverse if necessary and identify by block number) Nonlinear ship wave, wave resistance, Wigley hull, numerical solution, finite difference method.

19. ABSTRACT (Continue on reverse if necessary and identify by block number)

This work is a systematic development of a general numerical method for the solution of the nonlinear ship wave problem. Analytical approaches to this problem must always be linearized and are often unable to handle arbitrary and complicated hull geometry in the presence of a free surface. Other numerical approaches often provide inconsistent results for the physical quantities of interest, particularly the wave resistance. The present work unifies the numerical approach to the ship wave problem and considers all of the major aspects of the numerical method. Many of the features of the method are novel in the sense that they do not agree with the presently accepted views of the numerical ship hydrodynamics community.

The solution method is a time dependent finite difference technique which couples the time advancement of the free surface boundary conditions to a fast direct solution of the Laplace equation for the interior flow. The direct solver is optimized in the sense that

- continued on other side -

20. DISTRIBUTION/AVAILABILITY OF ABSTRACT UNCLASSIFIED/UNLIMITED ☒ SAME AS RPT. ☐ DTIC USERS ☐	21. ABSTRACT SECURITY CLASSIFICATION Unclassified
22a. NAME OF RESPONSIBLE INDIVIDUAL	22b. TELEPHONE NUMBER (Include Area Code) 22c. OFFICE SYMBOL None

DD FORM 1473, 83 APR EDITION OF 1 JAN 73 IS OBSOLETE.

Unclassified

SECURITY CLASSIFICATION OF THIS PAGE

numerical solution in the entire domain need not be calculated or stored. A new type of mesh system is also developed so as to accurately accommodate the exact hull geometry, and the fast Laplace solver is modified by the capacitance matrix technique in order to implement the hull boundary condition. Furthermore, it is found that by increasing the size of the computational region so that the downstream boundary is far from the ship, an effective open boundary condition which is far simpler than what has been proposed in the past may be implemented.

Results are obtained for the thin ship and Neumann-Kelvin problems and are compared to existing solutions and to experiments. It is generally found that the linearized, inviscid models presently in use are unable to adequately predict in a quantitative way the extremely small values of wave resistance over a wide range of Froude numbers. It is therefore shown in detail how the numerical groundwork developed in this research may be extended to solve the full non-linear ship wave problem.

NUMERICAL SOLUTION OF THE NONLINEAR SHIP WAVE PROBLEM

BY

ROBERT REXFORD CHAMBERLAIN, JR.

B.S., Denison University, 1978
M.S., University of Illinois, 1980

THESIS

Submitted in partial fulfillment of the requirements
for the degree of Doctor of Philosophy in
Aeronautical and Astronautical Engineering
in the Graduate College of the
University of Illinois at Urbana-Champaign, 1984

Urbana, Illinois

Numerical Solution of the Nonlinear Ship Wave Problem

Robert Rexford Chamberlain, Jr., Ph.D.
Department of Aeronautical and Astronautical Engineering
University of Illinois at Urbana-Champaign, 1984

This thesis is a systematic development of a general numerical method for the solution of the nonlinear ship wave problem. Analytical approaches to this problem must always be linearized and are often unable to handle arbitrary and complicated hull geometry in the presence of a free surface. Other numerical approaches often provide inconsistent results for the physical quantities of interest, particularly the wave resistance. The present work unifies the numerical approach to the ship wave problem and considers all of the major aspects of the numerical method. Many of the features of the method are novel in the sense that they do not agree with the presently accepted views of the numerical ship hydrodynamics community.

The solution method is a time dependent finite difference technique which couples the time advancement of the free surface boundary conditions to a fast direct solution of the Laplace equation for the interior flow. The direct solver is optimized in the sense that the numerical solution in the entire domain need not be calculated or stored. A new type of mesh system is also developed so as to accurately accommodate the exact hull geometry, and the fast Laplace solver is modified by the capacitance matrix technique in order to implement the hull boundary condition. Furthermore, it is found that by increasing the size of the computational region so that the downstream boundary is far from the ship, an effective open boundary condition which is far simpler than what has been proposed in the past may be implemented.

Results are obtained for the thin ship and Neumann-Kelvin problems and are compared to existing solutions and to experiments. It is generally found that the linearized, inviscid models presently in use are unable to adequately predict in a quantitative way the extremely small values of wave resistance over a wide range of Froude numbers. It is therefore shown in detail how the numerical groundwork developed in this thesis may be extended to solve the full nonlinear ship wave problem.

DEDICATION

TO MY WIFE, AMI, AND MY DAUGHTER, KATIE.

ACKNOWLEDGEMENTS

I wish to thank my advisor, Professor S.M. Yen, for his encouragement and support during this research project. I am also grateful to him for sharing with me his keen insight into the use of numerical experiments.

My wife, Ami, is a patient and understanding person, and I was glad to have her support, encouragement and love.

TABLE OF CONTENTS

CHAPTER 1. INTRODUCTION

Surface wave problems are in general characterized by the motion of a free boundary in response to a disturbance. A free surface which lacks surface tension is defined as a boundary which always contains the same fluid particles and along which the pressure is zero. The resulting motion of a free boundary must therefore proceed in such a way that this definition is continuously satisfied. This leads to three primary computational difficulties, namely those due to geometry, boundary conditions and flow conditions. Since the free surface geometry is unknown and must be determined as a part of the solution, we see that the difficulties due to geometry and boundary conditions are coupled in an essential way.

Many problems involving free surfaces are common in engineering applications. For instance, body motion problems involving heave and sway of oil rigs in the open sea are of interest for the design of structural integrity and stability. Material scientists are often concerned with the properties of melting solids in which the liquid-solid interface forms a free boundary. Other examples typically involve the formation of waves, and naval hydrodynamicists seek to determine the wave resistance experienced by a free surface piercing body. This will be our present topic of physical interest.

Naval ship hydrodynamics has had a long history of analytical and experimental research. The primary goal is to accurately predict the wave pattern of full scale ships in an effort to minimize or at least reduce the associated wave resistance during the design phase of new hull forms. This ultimate goal, however, has never been realized. The apparent reason for this is that analytical and quasi-analytical approaches must necessarily resort to linearized theory which often gives inconsistent results for conventional ship forms. Even purely numerical treatments have not been developed to the point where they can provide adequate predictions. Therefore, in an effort to better understand the problems associated with the determination of ship wave resistance, a brief review of several important methods will be given.

Purely analytical methods have long dominated ship hydrodynamics. The foundations of the potential theory underlying flows about thin bodies are well understood, and consequently an extension to flows with a free surface has been made. The classical thin ship theory given by Michell [1] in 1898 provides an explicit expression for the wave resistance in terms of hull geometry and speed. He linearized the full nonlinear problem to first order about the free stream velocity and applied the free surface condition at the location of the undisturbed free surface. In addition, the thin ship assumption allowed him to apply the body boundary condition on the centerplane of the hull rather than on the actual solid surface. Under these assumptions, an appropriate Green's function can be found which satisfies the Laplace equation, the free surface condition and a condition at infinity, namely that there exist only downstream waves. Such a Green's function is called a Havelock source. A collection of these sources can be distributed below the free surface and over the centerplane of the hull in such a way as to satisfy the thin ship condition. Once the velocity potential is known from the distribution of Havelock sources, other quantities of interest, such as wave profiles and wave resistance, can be calculated. The determination of wave resistance, for instance, involves the evaluation of a quintuple integral known as Michell's integral.

That Michell's theory so dominated the subject of ship hydrodynamics is seen from the fact that it was the only well founded theory in consistent use even as recently as thirty years ago. However, the age of high speed computer technology brought not only easier evaluation of Michell's integral but also provided the opportunity for improvements in the theory itself. The assumption of potential flow is apparently overshadowed in importance by the thin ship and linearized free surface approximations in the sense that the latter simplifications are most often singled out for improvement. By far the easier condition to improve is the thin ship assumption. A simple extension of the Michell theory is due to Guilloton [2]. Emerson [3] and Gadd [4] have applied Guilloton's method with reasonable success. The procedure is based on the intuitive observation that the flow over the linearized hull can be related to the flow over a real hull by a suitable transformation of coordinates. Thus, once the Michell solution is obtained,

one can find the real hull to which the linearized solution applies. The inverse procedure, that is, finding the linearized hull which corresponds to a given real hull, is an iterative process. While this method must ultimately rely upon a linearized calculation, the wave profiles along the real hull are in better accord with experiment than the linearized theory alone. Gadd argues that this is primarily due to a better accommodation of the free surface conditions. The Michell approximation allows the streamlines to actually pass through the physical hull since the hull boundary condition is applied on the centerplane of the ship. The Guilloton transformation, on the other hand, provides coordinate displacements in all three directions so that better account is taken of the actual free surface and solid body locations. Therefore, the linearized hull surface streamline along the centerplane is transformed into the wave profile or the curved free surface streamline along the real hull. The results of Gadd and Emerson are similar and both show some improvement over the first order theory.

The preceding discussion would seem to indicate that the deficiencies of the Michell theory can be largely overcome by applying the desired boundary conditions at the proper locations. In fact, the exact body condition can be satisfied by distributing Kelvin sources over the actual hull surface rather than over the centerplane. Since in this formulation, known as the Neumann-Kelvin problem, the free surface conditions remain linearized while the hull condition is exact, it is often argued that the approach is mathematically inconsistent. Further controversy also exists over the use of a line source distribution along the waterline of a ship. Since a surface piercing hull does not actually form a closed surface, Brard [5] argues that such an additional source distribution should be considered so that the shape, and therefore the flow around, the physical hull is more accurately represented. He reported that the inclusion of the line integral term along with the source distribution on the hull gave better results for the wave resistance, especially at low Froude numbers.

It is often convenient and more accurate to linearize the wavemaking problem about the double model potential rather than the free stream potential. This extension is the so called

double body approximation (often referred to as the zero Froude number approximation) and represents the flow that would exist if the free surface was replaced by a rigid plate. In practice, one determines the double body potential by reflecting the hull in the undisturbed free surface, thereby forming an image hull. The required source strengths may then be determined either analytically or numerically. As a first approximation, this potential provides a more accurate representation of the flow since the streamlines flow around the hull rather than through it, as in thin ship theory. The result is similar to the desired effect of Guilloton's method.

Gadd [6] uses the double model potential, represented by Kelvin sources distributed on the actual hull, to obtain wave profiles and wave resistance curves for a series of models at several Froude numbers. The procedure used in determining the source strengths, which allow satisfaction of the slip condition on the body, is outlined as follows. The ship is divided into n panels on which Kelvin wavemaking sources are uniformly distributed. Such a distribution may usually be regarded as a single point source concentrated at the center of a panel. The total velocity at each of the centers is evaluated in terms of the unknown source strengths on all the panels. Special consideration is given to the influence of a particular panel upon itself as well as upon its image panel. The requirement that the normal velocity at the center of each of the n panels be zero then yields n equations for the n unknown source strengths. Gadd is then able to calculate far field waves, hull wave profiles and surface pressure and velocity distributions. He brings the wave resistance results more into line with experiment by the addition of an empirical stern wave damping factor which effectively reduces the amplitude of the stern waves. This ad hoc procedure is justified by presuming that viscous effects must be important near the stern, especially if the body shape is bluff. The results for the several models investigated show qualitative agreement with existing Michell and second order theories (Gadd [7]), although there seems to be no marked improvement in either hull wave profile or wave resistance predictions. Guilloton's method still appears to provide better results in these areas.

Another approach which uses the double body potential is low speed theory, first introduced by Baba and Takekuma [8]. Baba and Hara [9] present calculations for a semi-submerged sphere as well as several ship forms, while Baba [10] provides results for more conventional ship hulls. Low speed theory is a representation of ship wave resistance in the asymptotic limit of zero Froude number. The velocity potential is assumed to be the sum of two parts. The first potential is that due to the double body, while the second is called the surface layer potential and represents the wave motion. The total potential must satisfy a nonlinear form of the free surface conditions, but only the double model potential is required to satisfy the solid body condition. The disturbance on the free surface is represented by products of derivatives of the known double body potential, and this is taken to be the only nonlinear effect on the free surface. At infinity, the wavy potential vanishes and there exists only uniform flow. Then, in the low speed limit, a solution for the free surface layer potential is found to be an integral involving only derivatives of the double model potential. The wave resistance can be derived from this expression, and this constitutes one of the main results of low speed theory. Early calculations [8,9] showed promise, especially for mathematical models in which the bow and stern are sharp (e.g., the Wigley hull). For conventional bluff forms, such as the HSVA tanker or the Series 60 hull, the theory was found to yield unacceptable results for the wave resistance (Baba [10]). It was later concluded by Tulin [11] that most low speed theories do not perform well.

An apparently successful method has been introduced by Dawson [12] in which the double model solution is improved by treating a portion of the free surface near the body separately from the outer part of the free surface away from the body. On the symmetry line between a two dimensional body and its image, the free surface condition is linearized in terms of the free stream velocity. This boundary condition is then satisfied by a line source distribution along the undisturbed free surface. The symmetry condition is a good approximation upstream where there is no disturbance. Downstream, however, Dawson argues that it represents the average condition of zero disturbance. Since the problem as stated up to this

point does not have a radiation condition at infinity, the solution will not be unique, and upstream waves will satisfy the boundary conditions just as well as downstream waves. Therefore, in order to prevent upstream waves, Dawson uses a four point, one sided upstream difference operator when applying the free surface condition for the velocity potential. This effectively allows waves to propagate only downstream. Furthermore, Dawson also found that it was necessary to include a damping region near the downstream boundary in order to prevent unwanted oscillations. Such a damping region is the usual approach for steady state formulations in which the proper numerical radiation condition at the downstream boundary is unknown. Although Israeli and Orszag [13] have shown that care must be taken in constructing a proper damping region, Dawson claims that a two point upstream difference operator works well and has limited upstream influence. This approach has also been extended to three dimensions, and the results of Dawson [12] and particularly of Dawson [14] show reasonable agreement with experiment for five ship hulls over a typical range of Froude numbers. It is apparently the general consensus [11] that the method due to Dawson shows the most overall promise. A similar method due to Gadd [15,16] is less consistent and is still not as close to experimental hull wave profiles as Guilloton's method, especially in the bow region.

All of the methods previously discussed for wave resistance computations fall into the broad category known as the Green's function approach. These procedures are characterized by steady state formulations of the problem in which the solution is obtained by an appropriate distribution of singularities on the boundaries. They have the distinct advantage that the Laplace equation for the potential function is automatically satisfied by the Green's function, and thus the computational burden does not involve calculating the details of the entire flow field. However, this type of approach runs into difficulty when trying to deal with nonlinear boundary conditions by superimposing linear combinations of component Laplace solutions. Thus, when applying the full nonlinear free surface conditions, it is necessary to abandon the Green's function approach and proceed by a more direct method of solution.

In contrast to the singularity methods, the class of direct simulation techniques is characterized by a finite element or finite difference solution of the Laplace equation. Most of the computational effort, especially in three dimensional problems, is consequently associated with this endeavor. The opportunity to handle the exact free surface conditions, however, is now more readily available. Most of the methods in this class attempt to satisfy the free surface conditions (both the linearized and the nonlinear forms) as accurately as possible while using any convenient technique for the remainder of the flow field.

Direct methods can be further divided into the steady state and the time dependent approaches. The steady state approach seeks only to determine the final wave pattern over the entire free surface. Oomen [17,18] used this approach based in part on a method developed by Korving and Hermans [19]. The Laplace equation is solved by a finite element method with a Neumann condition at the assumed location of the free surface. Small changes in the conditions at the free surface are calculated using the linearized boundary conditions, after which the problem is systematically solved until these changes become negligible. As in the Green's function approach, the proper outflow condition for this steady state formulation is also unknown. This is perhaps one of the most serious difficulties associated with any direct numerical approach to the steady state ship wave problem. One could specify the downstream boundary values, but there is never any assurance that the values one chooses would be correct. Oomen's solution to this problem was to introduce a pressure damping region near the downstream boundary of the truncated domain. Then, with no waves present, he specified uniform outflow. Bai [20], using a simple test problem, claims that this procedure is appropriate, although it would seem that additional numerical experimentation is necessary in order to completely understand the upstream influence of artificial damping regions in the flow field.

Although Oomen attempted to consider the nonlinear effects on the free surface, his results do not agree well with experiment. The hull wave profiles for the Series 60 ship show a phase shift aft relative to the experimental profiles. The wave resistance predictions, com-

puted for three Froude numbers from far field wave profiles, also appear to be rather poor. It may be that taking only three vertical planes to represent the depth variation of the velocity potential is not justified for full ships. The method, however, is still significant since it represents a purely numerical attack on the ship wave resistance problem.

Of the two types of direct techniques, the time dependent approach is perhaps a more natural and appealing concept when dealing with free surface wave phenomena. The transient solution is calculated, and the flow is assumed to approach the steady state after a long time. The free surface conditions are treated as a separate initial value problem, after which the Laplace equation is solved numerically with Dirichlet conditions at the moving boundary. The sole reason for using the time dependent approach over the steady state formulation is that the downstream boundary condition can be specified more precisely. That is, there is less guess work involved since artificial damping regions do not have to be designed. The idea is rather to allow the transient waves to propagate out of the truncated domain as if there was no boundary at all. For this reason, the downstream boundary is often referred to as an open boundary.

Although the difficulty of merely specifying the downstream boundary condition has been overcome in the time dependent approach, new computational difficulties regarding the actual implementation of an open boundary condition have been introduced. The open boundary treatment which is most often preferred is the use of a one dimensional advection model based on the Sommerfeld radiation condition. This model has been shown by Wu and Wu [21] to work well for long wave (i.e., shallow water) pressure distribution problems in which the exact wave speed is known. Except for situations of limited physical interest, their open boundary treatment is not applicable to ship wave resistance computations since the proper wave speed for deep water problems is unknown. Thus the major difficulty to be dealt with in implementing an effective open boundary condition is the accurate calculation of the phase speed of the waves approaching the truncation boundary. This calculation must be accurate in order for the waves to propagate cleanly (i.e., without reflection) out of the region. This idea

was originally proposed by Orlanski [22], who suggested that the wave speed could be numerically calculated near the open boundary and then used in the Sommerfeld radiation condition. Chan [23] revised Orlanski's original scheme so that it was nondissipative and applied the modified method to a ship wave problem. His purpose was to decrease the size of the computational region so that an excessive number of grid points was not required and hence so that relative efficiency in the Laplace solution could be maintained. He claimed that the boundary treatment was successful, but it is believed that further study is needed in this regard, especially since, as pointed out by Yeung [24], ship waves approaching the open boundary are two dimensional and should actually be considered using a two dimensional advection model.

Additional work of significance concerning the issue of the open boundary condition has been performed by Yen and Hall [25]. They first recognized the importance of studying the side effects of implementing a numerical radiation condition. Their advection experiments concentrated on the procedures and the errors involved in calculating the phase speed near the open boundary. By using a two dimensional pressure distribution problem as a test case, they compared wave height results for both a fixed and an expanding domain. The open boundary implementation was found to cause two grid interval oscillations near the boundary. If these spurious wave components were not eliminated, they believed that the solution in the region of interest could be severely contaminated. In order to eliminate these oscillations, the authors proposed the filtering scheme of Shapiro [26], but found it to be effective at early times only. For long time solutions they suggested the use of a dissipative time marching scheme, even though no physical viscosity was assumed to be present. They do caution, however, that further study is needed in order to ascertain the overall influence of damping on the solution. This work is nonetheless unique in the sense that it does not oversimplify or misjudge the problems encountered in developing and implementing an accurate open boundary condition.

Another difficult issue which is encountered in the direct approaches to the ship wave problem is the representation of irregular and arbitrary geometry (e.g., the hull and free sur-

faces) on a finite difference mesh. The approach taken by Chan [23] was to use a body fitted coordinate system throughout the physical domain. He was able to accurately accommodate arbitrary hull geometry, but he had to increase the computational complexity by transforming the Laplace equation into a general elliptic equation in the new coordinate system. The solution method used was successive over relaxation (SOR), which is known to have a very slow convergence rate, especially when an optimum relaxation parameter is not known. The solution of the transformed elliptic equation was thus an extreme computational burden at each time step. In order to improve the efficiency of the Laplace solution, Ohring [27] described a fast direct solution method based on the Fast Fourier Transform (FFT). Ohring and Telste [28] applied this solution technique, with second order spatial differencing, to the problem of a translating hull form. Their method of handling the exact hull condition, described in [29], is rather unconventional. They expand the Neumann condition at the hull, as well as two of its derivatives in two surface directions, in a Taylor series about the hull location. After manipulating the resulting expressions and incorporating the Laplace equation, they obtain a boundary condition which they apply at the mesh plane immediately adjacent to the exact hull. They thus completely avoid the problem of actually representing the hull form in their mesh system. This is an interesting approach, but it does not maintain second order spatial accuracy since many of the approximations in the Taylor expansion are only first order.

Given the present state of the art in ship wave resistance computations, it is desired to develop a new, general finite difference method for accurately and efficiently predicting ship wave resistance. This thesis represents a unified and systematic development of such a method for the full nonlinear ship wave problem. We shall consider only the Wigley hull, although the method shall be applicable to surface piercing bodies of arbitrary shape. In Chapter 2, we present both the nonlinear and linearized formulations of the ship wave problem. Chapter 3 is devoted to a discussion of the proposed numerical methods as well as a review of some other Laplace solution techniques so that the differences can be more easily illustrated. Chapter 4 establishes the validity of the present time dependent approach by solving the linearized, thin

ship problem for the Wigley hull. Numerical experiments are also performed to investigate the sensitivity of the solutions to changes in the computational parameters. Chapter 5 introduces the concept of the locally body fitted coordinate system which both maintains spatial resolution near the hull as well as superior efficiency in the Laplace solution. This chapter then describes the modification of the fast direct Laplace solver, which is required to handle the irregular hull geometry, and presents results for the Neumann-Kelvin problem. Chapter 6 uses the guidelines set forth in Chapters 4 and 5 to extend the method to the full nonlinear case. Wave profile results for this case are obtained and are compared to those of the linearized Neumann-Kelvin problem. The general conclusions of this work as well as indications for further research in the area of numerical ship hydrodynamics are finally outlined in Chapter 7.

CHAPTER 2. FORMULATION OF THE SHIP WAVE PROBLEM

We now present the mathematical formulation for the free surface flow about a hull. Consider the Cartesian coordinate system which is moving with a ship at an instantaneous speed U_s in the $-x$ direction (Fig. 2.1). The x-axis is aligned with the forward motion, the y-axis is perpendicular to this motion, and the z-axis is directed opposite to the force of gravity. Since the flow is symmetric about the centerplane, we need to consider only half of the ship. For an inviscid fluid without surface tension, there exists a velocity potential Φ which satisfies the Laplace equation

$$\nabla^2\Phi = \Phi_{xx} + \Phi_{yy} + \Phi_{zz} = 0. \tag{2.1}$$

Subscripts are used to denote partial differentiation, e.g., $\Phi_{xx} = \frac{\partial^2\Phi}{\partial x^2}$. We also note that the fluid velocity components are defined in terms of the potential as $(u,v,w) = (\Phi_x, \Phi_y, \Phi_z)$.

The domain of interest is enclosed by the upstream and downstream boundaries, the symmetry, lateral and bottom planes, and by the hull and free surfaces. Appropriate boundary conditions must also be specified for Eq. (2.1). On the free surface, there are two physical requirements. The first is that no fluid is allowed to cross the boundary. If we define the function $\zeta = z - \eta(x,y,t)$, where η is the free surface height above the reference plane $z = 0$, then clearly $\zeta = 0$ on $z = \eta$. The kinematic boundary condition is thus

$$\frac{D\zeta}{Dt} = \zeta_t + \Phi_x\zeta_x + \Phi_y\zeta_y + \Phi_z\zeta_z = 0. \tag{2.2}$$

Expanding the particle derivative and writing Eq. (2.2) in terms of $\eta(x,y,t)$, we have

$$\eta_t + \Phi_x\eta_x + \Phi_y\eta_y = \Phi_z \tag{2.3}$$

on $z = \eta(x,y,t)$.

The second physical requirement on the free surface is that the pressure must remain atmospheric. The velocity and pressure are related by Bernoulli's equation, which can be

written in a moving frame of reference as

$$\Phi_t + \frac{1}{2}(\Phi_x^2 + \Phi_y^2 + \Phi_z^2) + gz + P/\rho = P_a/\rho + \frac{1}{2}U_s^2 + x\frac{dU_s}{dt} . \tag{2.4}$$

The symbol ρ is used for the fluid density, g for gravitational acceleration, P for the pressure and U_s for the instantaneous speed of the ship in the $-x$ direction. For convenience, let us define $\mathrm{P} = P - P_a$ so that $\mathrm{P} = 0$ on $z = \eta$. The dynamic boundary condition then becomes

$$\Phi_t + \frac{1}{2}(\Phi_x^2 + \Phi_y^2 + \Phi_z^2) + \eta/Fr^2 = \frac{1}{2}U_s^2 + x\frac{dU_s}{dt} . \tag{2.5}$$

In equations (2.1), (2.3) and (2.5), lengths have been nondimensionalized by the ship length, L, velocity by the free stream velocity, U_∞, and time by L/U_∞. We note that the range for U_s is now $0 \leqslant U_s \leqslant 1$ since the maximum speed of the ship is U_∞. Furthermore, the nondimensional parameter Fr is the Froude number and is defined as $Fr = \dfrac{U_\infty}{(gL)^{1/2}}$.

At the upstream boundary, free stream conditions exist so that we require $\Phi_x = U_s$. The same is true for the lateral and bottom boundaries, both presumed to be far from the ship, so that we have $\Phi_y = 0$ and $\Phi_z = 0$ there, respectively. On the symmetry plane the proper condition is $\Phi_y = 0$, while on the hull, the normal velocity vanishes, i.e., $\Phi_n = 0$. Far downstream of the ship we require that no energy is generated, i.e., waves are only allowed to propagate downstream. This requirement can be expressed mathematically as $\Phi_x \rightarrow U_s$ as $x \rightarrow \infty$. Computationally, however, it will be necessary to truncate the domain and assume that $\Phi_x = U_s$ at the downstream boundary. As we shall see, numerical experiments are required to determine the appropriate domain length such that this downstream boundary approximation is valid.

It is often convenient to consider a perturbation potential ϕ defined by

$$\Phi = U_s x + \phi , \tag{2.6}$$

where ϕ represents a small deviation from the instantaneous hull speed. Substituting Eq. (2.6) into Eqs. (2.1), (2.3) and (2.5), we obtain the following governing equation and free surface

boundary conditions:

$$\phi_{xx} + \phi_{yy} + \phi_{zz} = 0\,, \tag{2.7}$$

subject to

$$\eta_t + (U_s + \phi_x)\eta_x + \phi_y \eta_y = \phi_z \tag{2.8}$$

and

$$\phi_t + U_s \phi_x + \frac{1}{2}(\phi_x^2 + \phi_y^2 + \phi_z^2) + \eta/Fr^2 = 0 \tag{2.9}$$

on $z = \eta(x, y; t)$. The conditions on the remaining boundaries are then expressed as

$$\begin{aligned} \phi_x &= 0, \quad \text{upstream} \\ \phi_x &= 0, \quad \text{downstream} \\ \phi_y &= 0, \quad \text{symmetry} \\ \phi_y &= 0, \quad \text{lateral} \\ \phi_z &= 0, \quad \text{bottom.} \end{aligned} \tag{2.10}$$

In order to express the hull boundary condition, we define the shape of the hull by the function $y = f(x, z)$. The components of the unit normal vector (positive when pointing into the fluid), expressed in terms of direction cosines, are $\hat{n} = (\cos\alpha, \cos\beta, \cos\gamma)$. The unit normal can also be expressed as $\hat{n} = (-f_x/\gamma_1, 1/\gamma_1, -f_z/\gamma_1)$, where the normalizing factor γ_1 is defined as $\gamma_1 = [1 + f_x^2 + f_z^2]^{1/2}$. In terms of the perturbation potential, the hull boundary condition becomes

$$-f_x \phi_x + \phi_y - f_z \phi_z = U_s f_x \tag{2.11}$$

on $y = f(x, z)$.

Equations (2.7)–(2.11) are the governing equation and the boundary conditions for the full nonlinear ship wave problem. The initial conditions are $\phi = \eta = 0$ at $t = 0$, after which the ship accelerates, either impulsively or gradually, with nondimensional speed U_s. It is interest-

ing to note that the governing equation is linear while the free surface boundary conditions are highly nonlinear. This is a consequence of the fact that the boundary shape is determined as a part of the solution and that one of the boundary conditions specifies the pressure rather than the velocity. There are no analytical solutions to this set of equations, nor are there any existence or uniqueness proofs. It is therefore difficult to assess the accuracy of any numerical solution to this problem.

The complexity of the full nonlinear ship wave problem is due primarily to a time dependent boundary whose shape is unknown *a priori*. The way to circumvent this difficult is to linearize the problem by neglecting certain higher order quantities, such as $\phi_x \eta_x$ or ϕ_x^2, which may be assumed to be small in some cases. The linearized kinematic and dynamic conditions then become, respectively,

$$\eta_t + U_s \eta_x = \phi_z \tag{2.12}$$

and

$$\phi_t + U_s \phi_x + \eta / Fr^2 = 0 \tag{2.13}$$

on $z = 0$. We may also apply the hull boundary condition on the centerplane of the ship to obtain the thin ship condition, which is expressed as

$$\phi_y = U_s f_x \tag{2.14}$$

on $y = 0$. The Laplace equation is thus to be solved subject to the boundary conditions in Eqs. (2.10), (2.12), (2.13) and (2.14). The initial conditions are the same as for the nonlinear case.

The linearized ship wave problem is much simpler than the full nonlinear problem for several important reasons. The boundary conditions have been simplified both in form and in the way in which they are applied. The linearized free surface conditions are applied on the plane $z = 0$ rather than on the free surface $z = \eta(x, y, t)$. Furthermore, the hull boundary condition is applied on the ship's centerplane ($y = 0$) rather than on the exact hull ($y = f(x, z)$). Major simplification in the geometrical complexity of the full nonlinear ship wave problem has

thus been achieved by linearizing the free surface conditions and by employing the thin ship condition. These additional approximations are physically justified under fairly restrictive conditions, however. It must be assumed that the actual vessel being considered does not disturb the free surface so violently that the wave height and slope become too large. In addition, the beam of the ship must be small in comparison to all other length scales in order for the thin ship approximation to be rigorously justified. These two restrictions are compatible, however, in the sense that a thin ship will not disturb the free surface to a great extent, and therefore the linearized problem can be used in a consistent fashion.

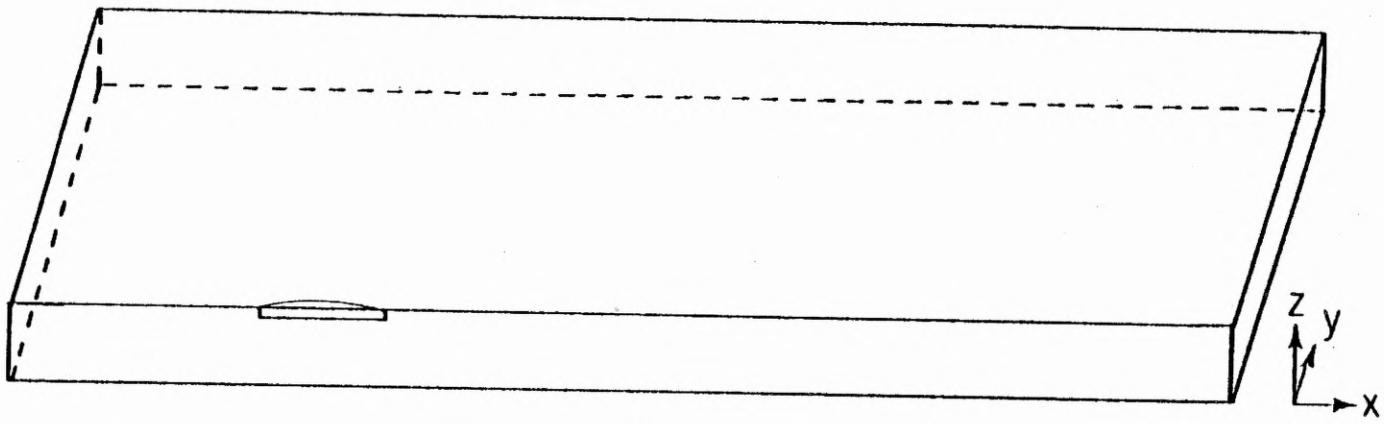

Figure 2.1 Placement of the ship within the Cartesian coordinate system, denoted by (x, y, z). The coordinate system follows the forward ($-x$ direction) motion of the ship.

CHAPTER 3. THE NUMERICAL METHOD

There are two distinct types of equations which are encountered in the ship wave problem. The Laplace equation is elliptic, while the free surface conditions, when coupled to this governing equation, are hyperbolic. As different as these two types of equations are mathematically, so too is there a great difference in the numerical methods which must be used to solve them. Since the overall effect of the free surface conditions and the Laplace equation is to describe the propagation of gravity waves on the surface of water, it is necessary to construct a numerical scheme which properly reflects this physical attribute. This chapter shall therefore be concerned with the principle features of the present numerical approach to the ship wave problem and shall also deal explicitly with the details of the numerical method.

The present method uses a time dependent, finite difference approach to obtain steady state solutions for the thin ship, Neumann-Kelvin and full nonlinear ship wave problems. The underlying assumption is that a steady state solution exists and that it can be found after a finite number of time steps. The time dependent approach is used primarily so that a physically appropriate downstream boundary condition can be defined. Furthermore, we use an explicit time marching scheme on the free surface in order to decouple the free surface boundary conditions from the solution of the Laplace equation. It is therefore necessary to solve the Laplace equation only once during each time step, subject to a Dirichlet condition on the free surface and to Neumann conditions at all the other boundaries.

The present approach to the numerical solution of the Laplace equation uses a general fast Poisson solver which is based on the Fast Fourier Transform (FFT). It is found that by exploiting certain characteristics of the Fourier Transform, an elliptic solver which is optimized in terms of storage and execution time can be derived. This means that it is neither necessary to compute or store the elliptic solution in the entire domain. Since the solution of the Laplace equation represents the bulk of the computational burden, an explicit scheme for the free sur-

face conditions and an optimized fast direct method for the Laplace equation are considered essential to the efficiency and accuracy of the present approach.

The choice of a fast direct method for the Laplace solver is motivated by the fact that this elliptic equation will be solved many times during the calculation, and we therefore require maximum computational efficiency. A fast Poisson solver is the most efficient and accurate means of solving the Laplace equation, but its use is restricted to rectangular regions. The application of this technique therefore requires that we use a Cartesian grid. This in turn changes the way in which the Neumann boundary condition on the exact hull has previously been handled. The usual approach has been to transform the Laplace equation into a general body fitted coordinate system so that the mesh planes coincide exactly with the hull surface. However, a fast Poisson solver cannot be used in arbitrary curvilinear regions of body fitted coordinates which extend throughout the entire domain. It is therefore necessary to localize the body fitted mesh only near the hull so that the bulk of the region can be represented by a rectangular grid. In this way, we can maintain spatial resolution on the ship as well as efficiency in the Laplace solver since the fast direct method can be modified to handle the Neumann condition on the curvilinear surface of a ship which is embedded in a locally body fitted region. The modification method used in this work will be considered in detail in Chapter 5 when we investigate the Neumann-Kelvin problem.

Another particularly interesting numerical feature contained in the present implementation is the treatment of the open boundary condition in the truncated domain. Previous approaches have used a one dimensional advection model based on the Sommerfeld radiation condition as a means to supply a Dirichlet condition for ϕ at the open boundary. It is found to be more convenient and efficient, however, to specify a Neumann boundary condition at the downstream boundary, and, as we shall see in this chapter, the most efficient choice is $\phi_x = 0$ (i.e., the free stream condition). A numerical experiment which verifies that this condition is acceptable is devised and performed on the linearized, thin ship problem in Chapter 4. It is

thus possible to avoid altogether the complicated open boundary treatment which has so often been believed to be necessary for the ship wave problem.

In this chapter, we shall consider only the numerical methods which are used to solve the free surface and Laplace equations. We first discuss the implementation of the free surface conditions and then turn to a general numerical discussion of the Laplace equation. Since the solution of elliptic finite difference equations is usually accomplished by iterative techniques, a brief review of some of the classical methods will be given so that a better comparison with the present optimized direct method can be made. We shall delay consideration of the details of the mesh systems and implementation of the Neumann and open boundary conditions until specific computational examples are presented in Chapters 4-6.

Numerical Implementation of the Free Surface Conditions

The present scheme for the free surface conditions was developed and used by Chan [23] for a ship-like floating body. This scheme can be characterized as an explicit, upwind centered scheme which is neutrally stable for pure advections at constant speed. To investigate this method, we write the free surface equations in the following form

$$Q_t + u^* Q_x + v^* Q_y = \Delta^* , \tag{3.1}$$

in which the scalar Q represents either η or ϕ, and u^*, v^* and Δ^* may be functions of Q. Notice that by the appropriate choice of u^*, v^* and Δ^*, both the nonlinear and linearized versions of the free surface conditions (Eqs. (2.8), (2.9) and (2.12), (2.13), respectively) can be written in the form (3.1). When specific computational examples are discussed in Chapters 4-6, the exact definitions of u^*, v^* and Δ^* will be given.

We now center Eq. (3.1) about an upstream point on the free surface. This point is shown in the (x,t) plane in Fig. 3.1. Using the standard notation of $Q^n_{i,j}$ to represent $Q(i\Delta x, j\Delta y, n\Delta t)$, we make the following finite difference replacements to center the calculation about the point $[(i-\frac{1}{2})\Delta x, j\Delta y, n\Delta t]$:

$$Q_t = \frac{1}{2\Delta t}\left|(Q^{n}_{i,j}{}^{+1} + Q^{n}_{i-1,j}) - (Q^{n}_{i,j} + Q^{n}_{i-1,j}{}^{-1})\right|$$

$$Q_x = \frac{1}{\Delta x}(Q^{n}_{i,j} - Q^{n}_{i-1,j}) \tag{3.2}$$

$$Q_y = \frac{1}{4\Delta y}(Q^{n}_{i,j+1} - Q^{n}_{i,j-1} + Q^{n}_{i-1,j+1} - Q^{n}_{i-1,j-1})$$

These finite difference approximations are substituted into Eq. (3.1), and the result is an explicit expression for $Q^{n}_{i,j}{}^{+1}$. We thus advance the values of η and ϕ in time using the following general expression

$$Q^{n}_{i,j}{}^{+1} = Q^{n}_{i-1,j}{}^{-1} + \alpha(Q^{n}_{i,j} - Q^{n}_{i-1,j}) - 2\Delta t\,[v^{*}(Q_y)^{n}_{i-1/2,j} - \Delta^{*}]\,, \tag{3.3}$$

where $\alpha = 1 - \dfrac{2u^{*}\Delta t}{\Delta x}$. The quantities u^{*}, v^{*} and Δ^{*} are all evaluated at $[(i-\tfrac{1}{2})\Delta x, j\,\Delta y, n\,\Delta t]$, which means that the required values are averaged at $[(i-1)\Delta x, j\,\Delta y, n\,\Delta t]$ and $[i\,\Delta x, j\,\Delta y, n\,\Delta t]$. For the case in which u^{*} and v^{*} are constant and $\Delta^{*} = 0$, the linear von Neumann stability analysis, given in Appendix A, provides the following stability condition

$$|c_y + 2c_x| \leqslant 1 + \sqrt{2} \tag{3.4}$$

where $c_x = \dfrac{u^{*}\Delta t}{\Delta x}$ and $c_y = \dfrac{v^{*}\Delta t}{\Delta y}$. When $v^{*} = 0$, as in the linearized case, this restriction is shown in Appendix A to reduce to the usual Courant condition

$$\left|\frac{u^{*}\Delta t}{\Delta x}\right| \leqslant 1\,. \tag{3.5}$$

This condition guarantees that no information will travel faster than one mesh interval in one time step. For the nonlinear case, Eq. (3.4) should be observed locally at all points on the free surface. This is the safest practice for a situation in which linear stability analysis is applied to a nonlinear problem. It should be pointed out that numerical experimentation may still be necessary in order to determine the computational parameters which produce a stable calculation. For the linearized case, however, Eq. (3.5) is well known and is sufficient to guarantee stability.

We now make several observations concerning how the scheme in Eq. (3.3) is started and how it is applied at the boundary intersections. Since this is a three time level scheme, it cannot be used to start the calculation from $t = 0$ since the solution at $t = -\Delta t$ is not known. We must therefore consider the use of some other starting scheme. However, any explicit starting scheme which one wishes to use will always lead to the same result, i.e., $Q_{i,j}^{n+1} = 0$ at $t = \Delta t$ for all points on the free surface. This is because, by virtue of the initial conditions, all of the forcing terms contained in Δ^* are equal to zero at $t = 0$. It is therefore possible to use Eq. (3.3) for all values of t with the understanding that the scheme begins at $t = 2\Delta t$ and that the solution is zero at $t = 0$ and $t = \Delta t$.

Chan's scheme does require some modification at the intersection of the free surface with some of the other boundaries. At the symmetry, hull and far field boundaries, one sided differencing is used for Q_y so as to avoid introducing unknown values outside of the domain. At the upstream boundary, one sided (downstream) differencing for Q_x is avoided since we want to retain the upwind bias of the scheme. We thus choose to impose the additional computational boundary conditions $\phi_x = 0$ and $\eta_x = 0$ at the intersection of upstream boundary with the free surface. This is again necessary in order not to introduce unknowns outside of the domain. It is physically justified on the grounds that the perturbations do not propagate upstream, and thus free stream conditions will hold at the upstream boundary. In order to implement these conditions, it would be possible to use Eq. (3.3) with $Q_{i-1,j}^n = Q_{i,j}^n$ and with $Q_{i-1,j}^{n-1} = Q_{i,j}^{n-1}$ at the upstream points. However, it is preferred to use the formula $Q_{i,j}^{n+1} = Q_{i,j}^n - \Delta t[v^*(Q_y)_{i,j}^n - \Delta^*]$ so as to avoid centered time differencing. This formula is obtained by using a forward time, centered space approximation to Eq. (3.1) with $Q_x = 0$. The centered space formula is used only in the y-direction so that Q_y is evaluated as previously discussed. Finally, we remark that at the downstream boundary, no additional unknowns outside of the domain are introduced (i.e., only upstream points are used) so that the explicit scheme is used in its original form.

Numerical Solution of the Laplace Equation

The Laplace equation occurs in many physical applications, and consequently its numerical solution is quite often needed. In this section, we shall discuss the present optimized direct method for the efficient numerical solution of this elliptic equation. The present solution technique is much more efficient and accurate than any iterative method, and it is therefore considered to be essential to the success of the time dependent approach in which the Laplace equation must solved accurately at each time step. In order to demonstrate the superiority of the optimized fast Poisson solver, we shall begin with a discussion of some classical iterative methods and of the preconditioned conjugate gradient technique.

The result of applying finite difference approximations to the Laplace equation is a linear system of the form

$$Ax = b\,. \tag{3.6}$$

The matrix A is large (N x N) and sparse, i.e., there are many more zeros than non-zeros in each of its rows. Methods to solve the system (3.6) fall into two primary categories, direct and iterative. The direct methods theoretically obtain the exact solution to Eq. (3.6) in a finite number of arithmetical operations. Iterative methods, on the other hand, successively approximate the solution vector x and must be terminated when a sufficiently accurate approximation is obtained. We shall briefly discuss some of the classical iterative methods as well as the higher order conjugate gradient technique before turning to a presentation of the proposed direct method.

Complete advantage of the sparsity of A is taken by iterative methods. This means that only the non-zero elements of the matrix need to be stored. We first split A into the form

$$A = I - L - U\,, \tag{3.7}$$

where I is the identity matrix and L and U are strictly lower and upper triangular matrices, respectively. Equation (3.6) then becomes

$$(I - L - U)x = b\,, \tag{3.8}$$

from which we can define the iterative process

$$Ix_{i+1} = (L + U)x_i + b \quad (i = 0,1,2,\ldots)\,, \tag{3.9}$$

where the x_i $(i = 0,1,2,\ldots)$ represent successive approximations to the actual solution vector x. This particular iterative process is called the point Jacobi method. If we use the most recent approximations as soon as they become available, then we have the Gauss-Seidel iterative method, defined as

$$(I - L)x_{i+1} = Ux_i + b \quad (i = 0,1,2,\ldots)\,. \tag{3.10}$$

These two methods comprise particular cases of the more general iteration

$$x_{i+1} = Bx_i + c \quad (i = 0,1,2,\ldots)\,, \tag{3.11}$$

in which $B = L + U$ and $(I - L)^{-1}U$ for the point Jacobi and the Gauss-Seidel methods, respectively.

To investigate the convergence of these methods, we define the error in the i^{th} iterate as

$$e_i = x_i - x \quad (i = 0,1,2,\ldots)\,, \tag{3.12}$$

where x is the exact solution. Inserting Eq. (3.12) into Eq. (3.11) and realizing that x satisfies

$$x = Bx + c\,, \tag{3.13}$$

we obtain

$$e_{i+1} = Be_i \quad (i = 0,1,2,\ldots)\,. \tag{3.14}$$

Hence we conclude that

$$e_i = B^i e_0 \tag{3.15}$$

and that $e_i \to 0$ as $i \to \infty$, if $B^i \to 0$. The matrix B is then said to be convergent if and only if $\rho(B) < 1$, where $\rho(B)$ is the spectral radius (largest eigenvalue) of B.

We now discuss the particular method known as successive overrelaxation (SOR). We use the splitting of Eq. (3.8) and define an intermediate iterate $\bar{x}_{i+1}$ as

$$I\bar{x}_{i+1} = Lx_{i+1} + Ux_i + b\,. \tag{3.16}$$

The accepted value x_{i+1} is then

$$x_{i+1} = x_i + \omega(\bar{x}_{i+1} - x_i) \tag{3.17}$$

where $0 < \omega < 2$ for stability. Equation (3.17) can be interpreted as increasing (overrelaxing) the displacement vector $(\bar{x}_{i+1} - x_i)$ by a factor ω when $\omega > 1$. We note that Eq. (3.17) reduces to the Gauss-Seidel method when $\omega = 1$.

We now eliminate $\bar{x}_{i+1}$ from Eqs. (3.16) and (3.17) to obtain

$$(I - \omega L)x_{i+1} = [\omega U + (1 - \omega)I]x_i + \omega b \tag{3.18}$$

from which it follows that

$$x_{i+1} = (I - \omega L)^{-1}[\omega U + (1 - \omega)I]x_i + \omega(I - \omega L)^{-1}b\,. \tag{3.19}$$

The so called iteration matrix for the SOR method is then seen from Eq. (3.19) to be defined as $B_\omega = (I - \omega L)^{-1}[\omega U + (1 - \omega)I]$. Thus, from the general theory of iterative methods of the form (3.11), the SOR method will converge if and only if $\rho(B_\omega) < 1$.

The success of the SOR method really depends on the knowledge of an optimum relaxation parameter, ω_o, as well as on the initial guess, x_0. Young [30] shows that the convergence rate of SOR is extremely sensitive to the choice of ω, especially when $\omega \approx \omega_o$. As can be seen from Eq. (3.15), SOR will converge in the fewest number of iterations if $\rho(B_\omega)$ is as small as possible. Thus the determination of ω_o depends on minimizing the largest eigenvalue of B_ω with respect to ω. In practice, the calculation of ω_o is non-trivial and often takes as much time as the solution to $Ax = b$ with ω_o known exactly. Thus, for cases in which the elements of A may be time dependent, as in the nonlinear free surface wave problem, it is not likely that SOR will succeed due to the difficulty and cost of estimating ω_o at each time step.

An alternative to the SOR method is the conjugate gradient (CG) technique. This was originally developed as a direct method by Hestenes and Stiefel [31], but was found not to work well as such in practice. It was later reported by Reid [32], however, to be an excellent iterative method. Recently, Concus, Golub and O'Leary [33] discussed how CG could be used to accelerate already convergent iterative processes. This method has several advantages over SOR in the sense that it requires no restrictions on the coefficient matrix other than symmetry and positive definiteness, although the extension to the nonsymmetric case has been carried out by Concus and Golub [34]. Furthermore, no estimation of acceleration parameters is required, as in SOR, since they are determined as a part of the solution.

The basic idea of the unmodified CG algorithm for solving the system (3.6) is to minimize the quadratic form of the error given by

$$E(x_k) = \frac{1}{2}(x - x_k)^T A(x - x_k) . \tag{3.20}$$

The minimum of $E(x_k)$ is of course zero at $x = x_k$. We now define a search direction p_k such that the new iterate, x_{k+1}, minimizes E in the direction p_k. Thus, using the definition

$$x_{k+1} = x_k + \beta_k p_k , \tag{3.21}$$

we find β_k such that $E(x_k + \beta_k p_k)$ is minimized. Then, defining r_k to be the residual at the k^{th} step, i.e., $r_k = b - Ax_k$, we choose the next search direction , p_{k+1}, to be the component of r_{k+1} which is conjugate to all the previous search directions, i.e., $p_0, p_1, p_2, ..., p_k$. Thus we have

$$p_{k+1} = r_{k+1} + \alpha_k p_k , \tag{3.22}$$

where α_k is chosen such that

$$p_{k+1}^T A p_j = 0 \quad (j = 0,1,2,...k) . \tag{3.23}$$

Putting these concepts together to form the complete algorithm, we define the following four steps as the conjugate gradient method :

(i) given x_0, $r_0 = b - Ax_0$ and $p_0 = r_0$,
for $k = 0,1,2,\ldots$, compute

(ii) $x_{k+1} = x_k + \beta_k p_k$, $\beta_k = \dfrac{r_k^T r_k}{p_k^T A p_k}$

(iii) $r_{k+1} = r_k - \beta_k A p_k$

(iv) $p_{k+1} = r_{k+1} + \alpha_k p_k$, $\alpha_k = \dfrac{r_{k+1}^T r_{k+1}}{r_k^T r_k}$.

The exact solution is obtained in at most N steps, where N is the order of A. For this reason, the algorithm was originally classified as a direct method. However, in the presence of roundoff error, the orthogonality of the sequence p_k is lost and so too is the finite-termination property. Fortunately, however, a satisfactory approximation x_k is usually obtained in a number of steps which is small compared to N. It is for this reason that Reid suggested the use of CG as an iterative technique.

Although the CG algorithm may be used as an iterative method in its own right, it is more often used to accelerate slowly convergent iterative processes. This extension is known as the preconditioned conjugate gradient algorithm, and the process to be accelerated is called the preconditioner. The essence of this approach is to replace Eq. (3.6) by

$$M^{-1}Ax = M^{-1}b \tag{3.24}$$

with the idea that $M^{-1}A$ should be close to the identity matrix. For example, if we precondition CG with SOR, then we have

$$M = \frac{1}{\omega}(I - \omega L) \tag{3.25}$$

in view of Eq. (3.19).

We now apply the standard CG algorithm to the system (3.24) and obtain the preconditioned conjugate gradient algorithm, which may now be defined in terms of the following four modified steps :

(i) given x_0, $r_0 = b - Ax_0$ and $p_0 = M^{-1}r_0$,
for $k = 0,1,2,\ldots$, compute

(ii) $x_{k+1} = x_k + \beta_k p_k$, $\beta_k = \dfrac{r_k^T M^{-1} r_k}{p_k^T A p_k}$

(iii) $r_{k+1} = r_k - \beta_k A p_k$

(iv) $p_{k+1} = M^{-1}r_{k+1} + \alpha_k p_k$, $\alpha_k = \dfrac{r_{k+1}^T M^{-1} r_{k+1}}{r_k^T M^{-1} r_k}$.

In this algorithm, one must solve during each iteration a linear system of the form

$$Mz_k = r_k \ . \tag{3.26}$$

This suggests that systems involving M should be easily solved. Meijerink and van der Vorst [35] suggest preconditioning by incomplete Cholesky decomposition. Kershaw [36] extends these ideas and also explores incomplete LU decomposition as a preconditioner, while Khosla and Rubin [37] prefer strongly implicit factorization. It is often possible to precondition by fast Poisson solvers, as described in [33].

Efficient implementation of the CG algorithm is discussed by Reid [32] and by Concus, et.al. [33]. However, the method still requires the storage of the vectors x_k, r_k, p_k and Ap_k in addition to the non-zero elements of A. Thus the requirement is greater than that for SOR, but it is offset by the fact that the acceleration parameters (i.e., α_k and β_k) do not need to be estimated. Furthermore, the convergence rate of CG has been found in practice to be much greater than that of SOR [37,38]. Since one of the objectives in the ship wave problem is to efficiently obtain an accurate potential solution at each time step, it would appear that CG is a likely candidate. It turns out, however, that this algorithm has some serious drawbacks which limit its effectiveness for the three dimensional ship wave problem. Specifically, the amount of storage required, even for modestly sized domains with adequate spatial resolution, is in fact too great to be practical without using out of core storage. This would be a severe disadvantage because of the amount of time required to perform I/O operations. Another limitation is that no advantage can be taken of the fact that the same matrix is being inverted for a variety of

different right hand sides (a new right hand side at each time step). Thus a tremendous amount of computational effort is wasted by repeatedly performing the same operations. As a result of these considerations, direct methods for the solution of Eq. (3.6) were investigated and were found to be superior in every respect when applied to this problem. We shall now take up a discussion of the direct method which is to be used in the present approach to the ship wave problem.

Remarkable advances in fast Poisson technology are described by Buzbee, Golub and Nielson [39]. Most of the so called fast direct methods are based on the Fast Fourier Transform (FFT), however other techniques are described in [39] as well as in a review on the subject by Dorr [40]. These methods require a highly regular structure in the coefficient matrix, which makes them ideally suited to Cartesian mesh systems and rectangular regions. The present method uses Fourier analysis to successively reduce the system (3.6) to a sequence of simpler problems. This approach was first discussed by Hockney [41,42]. The basic idea is to Fourier analyze the solution and the right hand side vectors in two of the three mesh directions as a means of uncoupling the unknowns in these directions. The result is a sequence of tridiagonal systems which must be solved for the Fourier amplitudes of the solution. These amplitudes are then used to reconstruct the exact solution by Fourier synthesis. Full details of this procedure are given in Appendix B. The tremendous efficiency of the method is due in part to the availability of an FFT routine which performs the analysis and synthesis. The Fast Fourier Transform is an efficient way to compute sums involving trigonometric functions since it utilizes the symmetry of these functions to significantly reduce the number of required operations.

We now describe how additional, significant computational savings, both in terms of storage and execution time, can be attained when applying the algorithm given in Appendix B specifically to the ship wave problem. In step 1 (Appendix B), it is not necessary to transform any vector sequence which is entirely zero since all of the Fourier amplitudes are also zero. In this problem, the right hand side is entirely zero except on the hull or centerplane (nonhomo-

geneous Neumann condition) and near the free surface (a nonhomogeneous Dirichlet boundary). Thus, the right hand side is transformed only if non-zeros appear on the particular mesh line under consideration. This strategy takes complete advantage of the fact that the right hand side contains mostly zeros, and thus the operation count in this step is reduced significantly. We now see that the choice of $\phi_x = 0$ at the downstream boundary is the most efficient for the simple reason that it introduces no additional non-zeros on the right hand side.

In step 2, we recognize several important observations. First, the solution for the velocity potential is needed only on the hull or the centerplane (to calculate the wave resistance by pressure integration) and just below the free surface (to advance the free surface conditions in time by computing ϕ_z in Eqs. (2.8) and (2.9)). The solution in the rest of the domain is really of no physical interest. Second, the reconstruction of the solution (Eqs. (B.9) and (B.10)) in the regions of physical interest does not require knowledge of the Fourier components in the entire domain. These two observations motivate one not to compute the Fourier components or the velocity potential in the entire domain but rather to efficiently compute only that part of the solution which is absolutely needed.

Such a strategy can be realized in step 2 in the following manner. Starting from the bottom of the domain, the forward elimination part of the tridiagonal solution for the Fourier components (Eq. B.6) is performed all the way up to the free surface. The backward substitution, however, proceeds only as far down as the keel of the ship. Thus, only the Fourier coefficients between the keel and the free surface are computed since these are the only ones which are needed to reconstruct the velocity potential solution in this region. We note that since the Fourier coefficients below the keel are never needed, it is not necessary to allocate any additional storage for them.

In step 3, during the reconstruction of the potential solution from the Fourier components, it is necessary to compute the Fourier amplitudes $\bar{\phi}^l_{j,k}$ for all values of l, j and k between the keel and the free surface. However, when using Eq. (B.10) to compute the solution $\phi_{i,j,k}$, we

only obtain this solution on and near the hull (centerplane) and just below the free surface. Thus, in most of the region between the keel and the free surface, the velocity potential is never Fourier synthesized. We note, however, that storage must be allocated in this entire region since all of the amplitudes $\bar{\Phi}^{l}_{j,k}$ are needed in Eq. (B.10).

From the previous discussion of the steps involved in obtaining the potential solution by the Fourier series method, we have seen why it is not necessary to compute or store the solution in the region below the keel of the ship. This strategy possesses two significant computational advantages. First, the number of operations is reduced since not every Fourier sum nor every tridiagonal system must be computed or solved. Second, the amount of core storage required is much smaller and remains nearly constant, even for domains of essentially arbitrary depth. The present direct method is thus optimized in terms of efficiency and storage since every computational advantage is exploited.

We now consider again the use of iterative methods for this problem in light of the fast Poisson solver. By comparison, all computational advantage is lost since all iterative methods must update the entire solution vector at each step in the iteration. Thus the storage and computation time requirements increase substantially as the size of the domain increases. Furthermore, iterative methods cannot produce as accurate a solution in as little time as the present optimized direct method. For example, a typical convergence level for the two norm of the residual in the CG method is 10^{-6}. By contrast, the direct method, using less computation time, gives a residual which is much less than 10^{-10}. Therefore, in addition to minimizing the accumulation of error at each time step, fast direct methods offer significant computational advantages over iterative methods and are thus preferred for use in the ship wave problem.

The entire computational algorithm which has been developed for both the linearized and the nonlinear ship wave problems can be summarized in the following steps :

(1) Initialize the flow field by setting $\phi = \eta = 0$ throughout the domain.

(2) Advance ϕ and η in time at the free surface using Eq. (3.3) applied to

either the nonlinear or linearized free surface boundary conditions.

(3) Solve the Laplace equation with ϕ at the free surface given from step (2). The Neumann boundary conditions for the other five boundaries and the hull are given by Eqs. (2.10) and (2.11), respectively.

(4) Repeat steps (2) and (3) until the steady state is reached.

Specific criteria for the termination of this solution process will be given in the next chapter. This algorithm will then be applied directly to the case of a translating hull under the linearized, thin ship assumption. In this particular problem, the domain is entirely rectangular, and the optimized direct method can therefore be used without modification. We shall see, however, that some modification of the fast Poisson solver will be necessary when implementing the exact hull boundary condition in a locally body fitted mesh system. The necessary extension of the direct method to the exact hull case will be given in Chapter 5 and Appendix C when the Neumann-Kelvin problem is considered. This modified direct method will then be directly applicable to the nonlinear ship wave problem, which will finally be dealt with in Chapter 6.

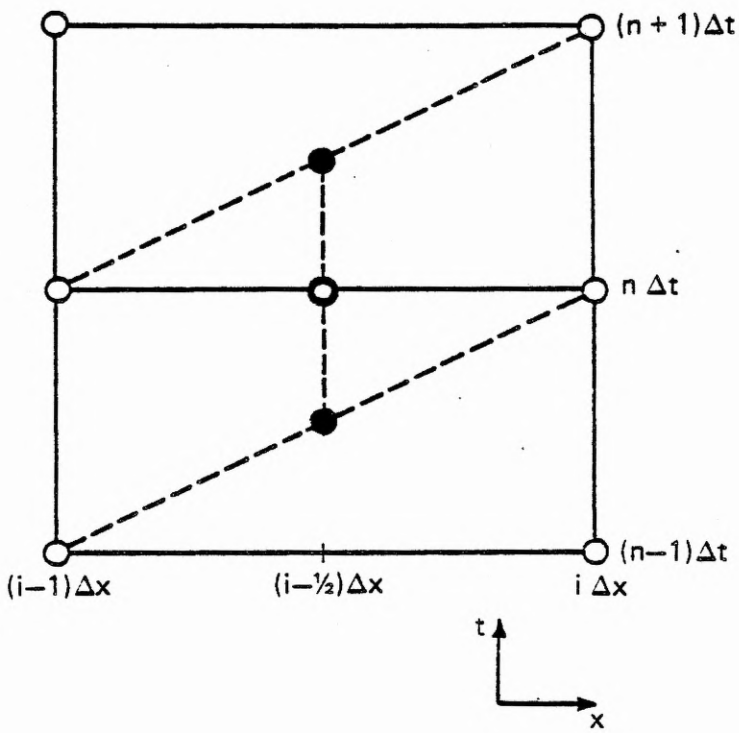

Figure 3.1 View in the (x,t) plane of the upstream point $[(i-\frac{1}{2}\Delta x)]$ about which the time marching scheme is centered.

CHAPTER 4. THE LINEARIZED, THIN SHIP PROBLEM

The first step in the systematic development of a general numerical method to solve the full nonlinear ship wave problem is the consideration of a simple test problem. It is necessary to investigate the underlying numerical features of any method by studying typical computational characteristics such as accuracy, execution time, storage requirements and the effects of changes in the parameters on the solutions. In this chapter, we investigate in numerical detail the linearized, thin ship problem for the free surface flow about a simple hull geometry. This problem is significant because it offers the opportunity to study the features of the proposed numerical approach in a situation which is free of the geometrical and computational complexity present in the full nonlinear problem. Furthermore, the linearized, steady state problem possesses an analytical solution for simple hull geometries. Although it is usually nontrivial to evaluate this solution, the thin ship theory of Michell [1] has nonetheless been applied to a simple hull form which is a special case of a series of algebraically defined models proposed by Wigley [43]. Before actually applying the present time dependent approach to this problem, however, we shall discuss the Wigley hull form, the mesh system to be used, the implementation of the boundary conditions and the calculation of the ship wave resistance.

The Wigley ship is a simple mathematical hull form defined as

$$f(x,z) = \frac{b}{2}(1 - 4x^2)(1 - (z/h)^2) \tag{4.1}$$

for $-1/2 \leqslant x \leqslant 1/2$ and $-h \leqslant z \leqslant 0$. The parameters b and h are the beam and draft of the ship and are set equal to 0.10 and 0.0625, respectively. These values are chosen to agree with those of an experimental towing tank model of the Wigley hull which has already been and tested. A perspective view of this hull is shown in Fig. 4.1. It is seen to be a symmetric hull characterized by a sharp bow and stern as well as a very shallow draft. This is an attractive hull to consider because of its convenient definition.

The linearized, thin ship problem has already been formulated in Chapter 2 and is defined by Eqs. (2.7), (2.10) and (2.12)-(2.14). We recall that the linearized free surface conditions (Eqs. (2.12) and (2.13)) are applied on the plane $z = 0$, while the thin ship condition (Eq. (2.14)) is applied on the centerplane of the hull ($y = 0$). The domain is thus entirely rectangular, and the optimized direct method of Chapter 3 and Appendix B is therefore directly applicable. The free surface equations, which supply the Dirichlet boundary condition for ϕ in the Laplace equation, are advanced in time using Eq. (3.3). The following definitions are used for the quantities u^*, v^* and Δ^* appearing in this time marching scheme :

Dynamic condition for ϕ :

$$u^* = U_s$$

$$v^* = 0$$

$$\Delta^* = -\eta/Fr^2$$

Kinematic condition for η :

$$u^* = U_s$$

$$v^* = 0$$

$$\Delta^* = \phi_z$$

The initial conditions are $\phi = \eta = 0$ at $t = 0$, after which the ship is linearly accelerated for 20 time steps ($\Delta t = 0.02$) to its final (free stream) velocity. This simply means that U_s is a linear function of t for $0 \leqslant t \leqslant 20\Delta t$ and is a constant (= 1) for $t > 20\Delta t$.

The Mesh System

A Cartesian mesh system is used to describe the rectangular computational domain. Since the physical dimensions of the domain will need to be changed frequently, it is convenient to define mesh system parameters which control the size of the domain, the grid spacing and the number of mesh points in each coordinate direction. One of the goals of this research is to

determine the sensitivity of the numerical solutions to changes in these computational parameters. Numerical experiments will be performed in order to investigate the solutions obtained under a variety of operating conditions, and we therefore find it convenient to define the grid system in terms of the mesh system parameters as follows :

$$x_i = -(0.49 + 30\Delta x) + (i-1)\Delta x \quad (1 \leqslant i \leqslant L),$$

$$y_j = (j-1)\Delta y \quad (1 \leqslant j \leqslant M) \tag{4.2}$$

$$z_k = \begin{cases} -\mathrm{d} + 0.2(k - k_1) & (k_1 \leqslant k \leqslant 24) \quad \text{(far below the ship)} \\ z(k) & (24 \leqslant k \leqslant 34) \quad \text{(transition region)} \\ z(34) + (k - 34)\Delta z & (34 \leqslant k \leqslant 40) \quad \text{(on the hull).} \end{cases}$$

In this mesh system, the grid spacing is uniform in the x- and y-directions. In the z-direction, however, there are three distinct mesh regions. The spacing on the ship and far below the ship is constant but unequal. A transition region consisting of nonuniform grid intervals is used to smoothly match the mesh in the two constant spacing regions. Considerations for the proper development of the vertical grid distribution will be given at the end of this section.

The grid is seen to consist of L x M x (41 - k_1) mesh points in the x-, y- and z-directions, respectively. The size of the domain is controlled by the parameters L, M and d. The upstream boundary is set at $x = -(0.49 + 30\Delta x)$, and we recall that the ship is located between $x = -1/2$ and $x = 1/2$. The parameter k_1 is used in conjunction with d to determine the depth of the domain.

Throughout this work, the values Δx = 0.98/19, Δy = 2.0/(M-1) and Δz = h/6.5 are used, unless otherwise noted. The values of Δx and Δz are chosen so that the Wigley hull (defined for $31 \leqslant i \leqslant 50$ and $34 \leqslant k \leqslant 40$) is covered by 20 x 7 grid points and so that mesh lines straddle the bow, stern and keel. This is a necessary aspect of the mesh system since the directions normal to the Wigley hull at these locations are not precisely defined.

The design of the grid distribution in the vertical (z-) direction requires careful consideration. We must reconcile the relatively small grid intervals on the centerplane (h/6.5)

with the larger intervals (0.2) far below the ship. It is thus necessary to use a nonuniform mesh in this direction. The spacing remains constant on the centerplane and far below the ship, but in between these constant grid interval regions we define a transition region which smoothly matches the mesh spacing. These transition values, denoted by $z(k)$ for $24 \leqslant k \leqslant 34$ in Eqs. (4.2), are given in Table 4.1, and they shall be used in all of the mesh systems for the thin ship problem. The parameters which therefore remain free to be chosen are L, M, k_1 and d. The specific values for these parameters will be given later in this chapter when the numerical experiments are discussed.

Vertical Mesh Spacings	
k	z
24	−0.4000
25	−0.2800
26	−0.2000
27	−0.1600
28	−0.1300
29	−0.1100
30	−0.0962
31	−0.0865
32	−0.0769
33	−0.0673
34	−0.0577

Table 4.1 The values of z vs. k in the vertical mesh transition region, defined by $24 \leqslant k \leqslant 34$.

Implementation of the Boundary Conditions

We now discuss specifically how the boundary conditions for the Laplace equation are implemented using the grid defined in Eqs. (4.2). In order to apply the thin ship condition ($\phi_y = U_s f_x$) on $y = 0$ ($j=1$), we first write the finite difference form of the Laplace equation on the centerplane. This equation is of the form (cf. Eq. (B.1))

$$C_1\left[\phi_{i-1,1,k} - 2\phi_{i,1,k} + \phi_{i+1,1,k}\right] + C_2\left[\phi_{i,0,k} - 2\phi_{i,1,k} + \phi_{i,2,k}\right] +$$

$$a_k \phi_{i,1,k-1} - b_k \phi_{i,1,k} + c_k \phi_{i,1,k+1} = 0 . \tag{4.3}$$

We note that $\phi_{i,0,k}$ lies outside of the computational domain since the allowed values of the index j are $1 \leqslant j \leqslant M$ (cf. Fig. 5.3a). We must therefore use the thin ship condition to eliminate $\phi_{i,0,k}$ from Eq. (4.3). Approximating ϕ_y by a central difference, we write the thin ship condition as

$$\phi_{i,0,k} = \phi_{i,2,k} - 2\Delta y U_s f_x . \tag{4.4}$$

The finite difference representation of the Laplace equation on the centerplane thus becomes

$$C_1\left[\phi_{i-1,1,k} - 2\phi_{i,1,k} + \phi_{i+1,1,k}\right] + 2C_2\left[\phi_{1,2,k} - \phi_{i,1,k}\right] +$$

$$a_k \phi_{i,1,k-1} - b_k \phi_{i,1,k} + c_k \phi_{i,1,k+1} = \frac{2}{\Delta y} U_s f_x , \tag{4.5}$$

since $C_2 = \frac{1}{\Delta y^2}$. The effect of the Neumann boundary condition on the centerplane is thus seen to add a source term on the right hand side of the Laplace equation. This nonzero term accounts for the wave disturbance to the free surface in the absence of a real (physical) hull. We note that an analogous procedure is followed for all other boundaries on which ϕ_n is specified. It turns out, however, that no additional source terms appear on the right hand side since $\phi_n = 0$ on the remaining Neumann boundaries. We also note that Eq. (4.5) is equivalent to one in which $\phi_y = 0$ with a nonzero right hand side, so that the direct method of Appendix B for the more general Poisson equation is appropriate.

In the case of the Dirichlet condition on $z = 0$ (k=40), we immediately put the known solution on the right hand side to obtain

$$C_1\left[\phi_{i-1,j,39} - 2\phi_{i,j,39} + \phi_{i+1,j,39}\right] + C_2\left[\phi_{i,j-1,39} - 2\phi_{i,j,39} + \phi_{i,j+1,39}\right] +$$

$$a_k \phi_{i,j,38} - b_k \phi_{i,j,39} = -c_k \phi_{i,j,40} . \tag{4.6}$$

Finite difference equations of this form are applied at all points just below the free surface.

We note that at the intersection of the free surface and the centerplane, the Neumann boundary condition leads to additional modification of the right hand side, as previously discussed.

Calculation of the Wave Resistance

In addition to calculating hull wave profiles and ship wave patterns, one of the primary objectives of this research is to estimate the wave resistance. A ship traveling in an inviscid fluid with a free surface experiences a resistance to its motion due to the fact that the surface velocity, and hence the pressure, are not symmetric fore and aft of the midship section. Thus, the integral of the x-component of the surface pressure on the hull is nonzero. We therefore define the resistance as

$$R = -2\iint_S P n_x \, dS \ , \tag{4.7}$$

where n_x is the x-component of the unit normal vector (equal to $-f_x/\gamma_1$), S is the wetted hull surface area at rest, and P is equal to $P - P_a$. We can transform the integral in Eq. (4.7) to an equivalent integral over the centerplane area A by choosing $dS = \frac{dx\,dz}{n_y}$. We thus obtain

$$R = 2\iint_A P f_x \, dx \, dz \ , \tag{4.8}$$

where f_x is the x-slope of the Wigley hull, and n_y is equal to $1/\gamma_1$.

The pressure is calculated from Bernoulli's equation (Eq. (2.13) applied on the centerplane), and for the present linearized case we have

$$P = -\left[\phi_t + U_s \phi_x + z/Fr^2\right] . \tag{4.9}$$

Then, defining the wave resistance coefficient, C_w, as

$$C_w = \frac{R}{\frac{1}{2}\rho U_\infty^2 S} \ , \tag{4.10}$$

we obtain finally

$$C_w = -\frac{4}{S}\int_{-h}^{0}\int_{-1/2}^{1/2}(\phi_t + U_s\phi_x)f_x\,dx\,dz\ , \tag{4.11}$$

where $(\phi_t + U_s\phi_x)$ is evaluated on the Wigley hull centerplane. In Eq. (4.11) we have used the fact that the integral of z/Fr^2 over this symmetric hull is zero since f_x is an odd function of x. Furthermore, the value of S (nondimensionalized by the square of the ship length) is obtained from

$$S = 2\int_{-h}^{0}\int_{-1/2}^{1/2}(1 + f_x^2 + f_z^2)^{1/2}\,dx\,dz\ , \tag{4.12}$$

and this value for the Wigley hull is found to be $S = 0.1487906$.

Numerical Experiments

Three key numerical experiments have been performed in order to determine the effects of changes in the computational parameters on the hull wave profiles and the wave resistance. The computational parameters under consideration are: **1)** the domain depth (i.e., the choice of k_1 in Eqs. (4.2)), **2)** the domain length (i.e., the choice of L in Eqs. (4.2)) and **3)** the order of the difference approximation for ϕ_z in Eq. (2.12) (i.e., first or second order one-sided differencing on $z = 0$). These experiments are considered to be most important in determining the characteristic features of the present time dependent approach to the steady state solution of the linearized, thin ship problem.

Experiments **1)** and **2)** are necessary for two reasons. First, since the Laplace equation must be solved many times during the calculation, we want to minimize the computational effort by allowing the domain to be as small as possible. The proper choice for the domain size must be based upon numerical evidence which establishes that the placement of artificial boundaries does not contaminate the solution near the ship. We thus seek to determine a finite domain size which both maintains efficiency during the Laplace solution and which also best

approximates an infinite region.

The second reason involves simplicity and efficiency in the implementation of the downstream (open) boundary condition. Various complicated alternatives for the implementation of an open boundary condition have been proposed (e.g., Orlanski [22], Chan [23] and Yen and Hall [25]). These methods attempt to calculate the phase velocity of the waves near the downstream boundary and then allow the disturbances to advect out of the region at the proper speed. In principle, this procedure should minimize the wave reflection from the open boundary and hence reduce the effects near the ship. It would also then be theoretically possible to place the downstream boundary very close to the ship since the finite cutoff is assumed to be transparent to wave propagation. In practice, however, it is very difficult to accurately estimate the required wave speed. Furthermore, only one dimensional advection models have been considered, and it is well known that ship waves meet the downstream boundary at a nonzero angle, thus requiring a two dimensional propagation model. Therefore, for ease of implementation, it is proposed that a simple downstream boundary condition be used (i.e., $\phi_x = 0$). This condition eliminates the necessity of calculating the wave speed, and it is also physically justified, as long as no disturbance is present. When a disturbance has reached the downstream boundary, however, we must be concerned about wave reflection and its possible contamination of the solution on the ship. It is therefore necessary to experimentally determine the appropriate length of the computational domain such that an accurate steady state solution on the ship is obtained. We must thus balance our requirement of efficiency against the demand for accuracy by performing numerical experiments to establish the optimum operating conditions for the numerical towing tank.

Finally, experiment **3)** is important since the term ϕ_z in Eq. (2.12) couples the free surface boundary conditions to the interior flow and hence strongly influences the development of the solution. Chan [23] used first order one-sided differencing for ϕ_z at the free surface and thus did not maintain overall second order accuracy in space. In this work, the order of the

difference approximations is considered to be worthy of careful investigation since it will clearly affect the accuracy of the results.

We now turn to a discussion of the experimental procedures and the results. It should be kept in mind that throughout this exposition, the computational procedure outlined at the end of Chapter 3 is always used. One of the most important features of this method is the use of the optimized Laplace solver. By contrast, the conjugate gradient iterative technique, preconditioned by incomplete Cholesky decomposition, was first applied to the thin ship problem, but it was found that an affordable convergence level could not be maintained at each time step. Furthermore, the additional accumulation of error due to a relatively inaccurate potential solution can seriously affect the results, especially for C_w, which is particularly sensitive to this error. Therefore, a direct method must be used in order to efficiently obtain at each time step the most accurate elliptic solution possible.

The numerical experiments are carried out on three different mesh systems (Mesh I, Mesh II and Mesh III), each of which are defined by specifying the parameters in Eqs. (4.2). These parameters, given below in Table 4.2, complete the definitions of the mesh systems which are used in this chapter. The three mesh systems contain 129 x 33 x 20, 97 x 33 x 20 and 97 x 33 x 40 grid points and represent domain sizes of 6.6 x 2.0 x 1.0, 4.95 x 2.0 x 1.0 and 4.95 x 2.0 x 5.0, respectively. Mesh systems I and II are shown in Figs. 4.2-4.3, in which the placement of the ship is also indicated. We note that Mesh III is identical to Mesh II when the depth is increased to d = 5.0.

The Mesh Systems		
Mesh I	Mesh II	Mesh III
L = 129	L = 97	L = 97
M = 33	M = 33	M = 33
k_1 = 21	k_1 = 21	k_1 = 1
d = 1.0	d = 1.0	d = 5.0

Table 4.2 The computational parameters in Eqs. (4.2) which define the three mesh systems used in the numerical experiments.

In all of the numerical experiments, we consider three Froude numbers (Fr = 0.266, 0.350 and 0.452) which are chosen to be representative of typical values used for the Wigley hull. In the first experiment, we compare, using mesh systems II and III for the two domain depths, the hull wave profiles and the wave resistance at t = 9.0. The value t = 9.0 represents 450 time steps with Δt = 0.02, and we shall see presently that t = 9.0 represents a sufficiently long time such that the steady state solution is obtained on the centerplane. Figures 4.4-4.6 show the hull wave profiles for the three Froude numbers under consideration, each with the depth of the domain equal to 1.0 and to 5.0. We note that in these plots the longitudinal coordinate is x/l (l is half of the ship length), while the wave elevation η is nondimensionalized by $U_\infty^2/2g$. For all three Froude numbers, there are negligible quantitative differences between the respective solutions for each of the domain depths. It is also found that the wave resistance does not vary to any significant degree in this depth comparison. Figure 4.7 shows C_w vs. Fr for these cases and also compares the results to the Michell resistance and to an experiment by Ju [44]. The residual resistance seen in this figure is defined as the total hull resistance (measured) minus a viscous component. The viscous component in this experimental result is assumed to be equivalent to that of a flat plate with a total wetted surface area equal to that of the Wigley hull. The general trend for the linearized, thin ship theory is to overestimate the wave resistance. However, there is good agreement between the Michell theory and the present time dependent approach.

In Figs. 4.8-4.9, we show the time history of C_w for Fr = 0.452 with the depth equal to 1.0 and 5.0, respectively. There is essentially no difference between these two cases, even in the actual transition to the steady state. Furthermore, from the C_w vs. t curve for this Froude number, we note that C_w has settled down by t = 9.0, and the solution on the centerplane is therefore considered to be steady. It has been observed, however, that for the lower Froude numbers, the wave resistance oscillates about its steady state value. Figures 4.10-4.11 for Fr = 0.266 show that the frequency of the oscillation increases with decreasing Froude number but remains independent of the depth. Therefore, in order to obtain the steady state value for C_w,

it is necessary to take an average by integrating the $C_w(t)$ curve in the interval $4.0 \leqslant t \leqslant 9.0$ and by dividing the result by the duration of the interval (5.0 in this case). This procedure has been followed for all cases in which C_w is reported.

The depth experiment has shown that the solution on the Wigley centerplane is insensitive to large variations in the depth and that a domain depth equal to 1.0 is sufficient to approximate a very deep region. It should also be pointed out that because of the nature of the optimized Laplace solver, the two depth cases required essentially the same amount of storage, and the d = 5.0 case required only 10% more execution time. This should be compared to iterative methods for the Laplace equation in which the storage requirements would be doubled and the execution time would increase far more than 10% for the d = 5.0 case.

The second numerical experiment is more critical than the first since the treatment of the downstream boundary condition is usually thought to be a more difficult issue in numerical ship hydrodynamics. Physically, the propagating disturbances must always move downstream and must therefore leave the finite computational domain without reflection. Numerically, however, we cannot easily enforce this condition. We therefore impose the much simpler free stream condition ($\phi_x = 0$) and experimentally determine the proper domain length such that this open boundary condition does not affect the solution on the centerplane. We thus consider two domain lengths, 6.6 and 4.95, which are represented by mesh systems I and II, respectively (Figs. 4.2-4.3). In Fig. 4.2, the downstream boundary is located 4.06 ship lengths from the stern, while in Fig. 4.3 this distance is decreased to 2.41 ship lengths. The wave profiles for these domain lengths are compared for the three Froude numbers at $t = 9.0$ in Figs. 4.12-4.14. It is again noted that there are no substantial quantitative differences between the solutions. Furthermore, the wave resistances for both cases are found to be identical and are the same as shown in Fig. 4.7 for the depth experiment. It is thus concluded that, within the limits considered, the placement of the downstream boundary relative to the stern and the use of the condition $\phi_x = 0$ at the open boundary have a negligible influence on the solution on and near the

centerplane.

The previous result is rather surprising since the present treatment of the downstream boundary is completely contrary to what is usually considered to be a more standard approach to wave propagation problems in truncated domains. The physical appeal of using a one dimensional advection model to allow the disturbances to leave the domain at the proper speed is attractive. However, this concept overlooks the fact that the disturbances near the boundary may be small enough that $\phi_x = 0$ is a valid approximation, which seems to be the case here. It is thus of interest to examine more closely the events taking place at the open boundary by plotting the surface wave pattern generated by the moving ship. A time sequence of ship wave patterns for $Fr = 0.266$ is shown in Figs. 4.15-4.17 for the domain lengths 6.6 (Long Domain) and 4.95 (Short Domain). At early times, the wave disturbances are only approaching the downstream boundary in both domains. After the disturbances have reached the outflow boundary, we see immediately that no wave reflection is evident. Furthermore, there is no evidence of distortion in the wave patterns near either downstream boundary, even long after the disturbances have reached the limits of the domain. It is especially interesting to note that the wave patterns for both domains are essentially identical if one imagines that the long domain is truncated to the short domain. It is thus apparent from this numerical experiment that the disturbances are indeed small enough such that the condition $\phi_x = 0$ is justified. Moreover, this boundary condition is simple and efficient to implement, so its use is greatly preferred over more complicated open boundary schemes. We therefore conclude that the domain of length 4.95 is a sufficient approximation to a much longer domain and shall henceforth be used as such.

In the final numerical experiment, we investigate a computational parameter which is associated with the finite difference approximations rather than with the mesh system. Specifically, it is desired to compare the results when both first and second order approximations are used for the vertical free surface velocity (ϕ_z) in Eq. (2.12). The wave profiles for these two cases are compared for the three Froude numbers in Figs. 4.18-4.20. It is seen from these

figures that the qualitative features of the wave profiles do not depend significantly on the order of the ϕ_z differencing. There is, however, a slight upstream phase shift for all three Froude numbers in the second order case, and this is considered to be the correct trend. This can be seen by comparing each of the wave profiles with the Michell (steady state) profile for Fr = 0.266 (Figs. 4.21-4.22). There is slightly better phase and amplitude agreement in the bow region for the second order ϕ_z differencing. This trend can also be seen in Figs. 4.23-4.24, in which the Fr = 0.350 profile is compared to an experiment by Shearer and Cross [45]. The bow wave is not only better predicted for the second order case, but the downstream profile on the Wigley hull is also in better qualitative agreement with experiment. We also show the thin ship wave profiles vs. experiment for Fr = 0.266 and Fr = 0.452 in Figs. 4.25-4.26, respectively. The second order ϕ_z profiles for all three Froude numbers compare quite favorably with this experiment, especially when one considers that viscous effects are ignored in this calculation.

We finally compare the wave resistance predictions for both types of ϕ_z differencing. As shown in Fig. 4.27, the second order ϕ_z greatly improves the wave resistance relative to the linear source distribution theory, especially at Fr = 0.452. At Fr = 0.266, the trend is to approach the Michell resistance. At Fr = 0.350, however, there is little change, which is perhaps a consequence of the fact that Michell and the experiment agree fairly well at this Froude number. Based on all of the above observations, we conclude that the one-sided second order ϕ_z differencing is more accurate and should therefore be used in order to maintain overall second order spatial accuracy.

Summary

The purpose of this chapter has been to implement and test an efficient, time dependent method for obtaining the steady state solution for the free surface flow about the Wigley hull. Numerical tests were conducted under simplified conditions so that the underlying features of

the method could be examined apart from the geometrical and computational complexity present in the full nonlinear problem. It is concluded that the present approach reproduces the qualitative features of the wave profiles, patterns and resistance for the Wigley hull shape. Furthermore, the numerical experiments demonstrated that the 4.95 x 2.0 x 1.0 domain, containing 97 x 33 x 20 grid points, was sufficient to approximate a much longer and deeper domain since the solutions were relatively insensitive to large changes in the domain size. It was also demonstrated that second order ϕ_z differencing at the free surface gives better results than first order differencing. In addition, the implementation of the open boundary condition presented here is contrary to the presently understood approach to this issue. The results, however, nonetheless proved that the present implementation is successful in effectively allowing the waves to leave the computational region without reflection or distortion of the wave pattern. More importantly, however, this simple open boundary condition was found to have no influence on the hull wave profiles or the wave resistance.

It is interesting to note that the present optimized fast Poisson solver has performed very well in the solution of the thin ship problem. The exact numerical solution of the Laplace equation is obtained at each time step with relatively little computational effort or cost. This effort has been compared to that for the conjugate gradient technique, preconditioned by incomplete Cholesky decomposition, and has been found to be substantially less. For example, using the same spatial resolution on the centerplane, the preconditioned CG algorithm required twice as much storage and seven times as much execution time as the fast Poisson solver to obtain essentially the same steady state solution to this problem. This is a dramatic difference which cannot be ignored, and it is therefore considered crucial that fast direct methods in general be used for time dependent elliptic problems.

In the next chapter, we shall use the solution guidelines prepared in this chapter to investigate the Neumann-Kelvin problem. In this case, the exact hull boundary condition is implemented, but the linearized free surface conditions are retained. We shall see that the use of an

optimized Laplace solver based on the FFT will determine the mesh system to be used and the way in which the exact hull boundary condition is implemented. Some modification of the Laplace solver will be required, but the overall efficiency and accuracy are maintained since it is still possible to use fast direct methods for the elliptic finite difference system. Although the Neumann-Kelvin problem may be considered mathematically inconsistent, the extension of the present method to handle the exact hull boundary condition will be needed in Chapter 6 when the full nonlinear ship wave problem is considered.

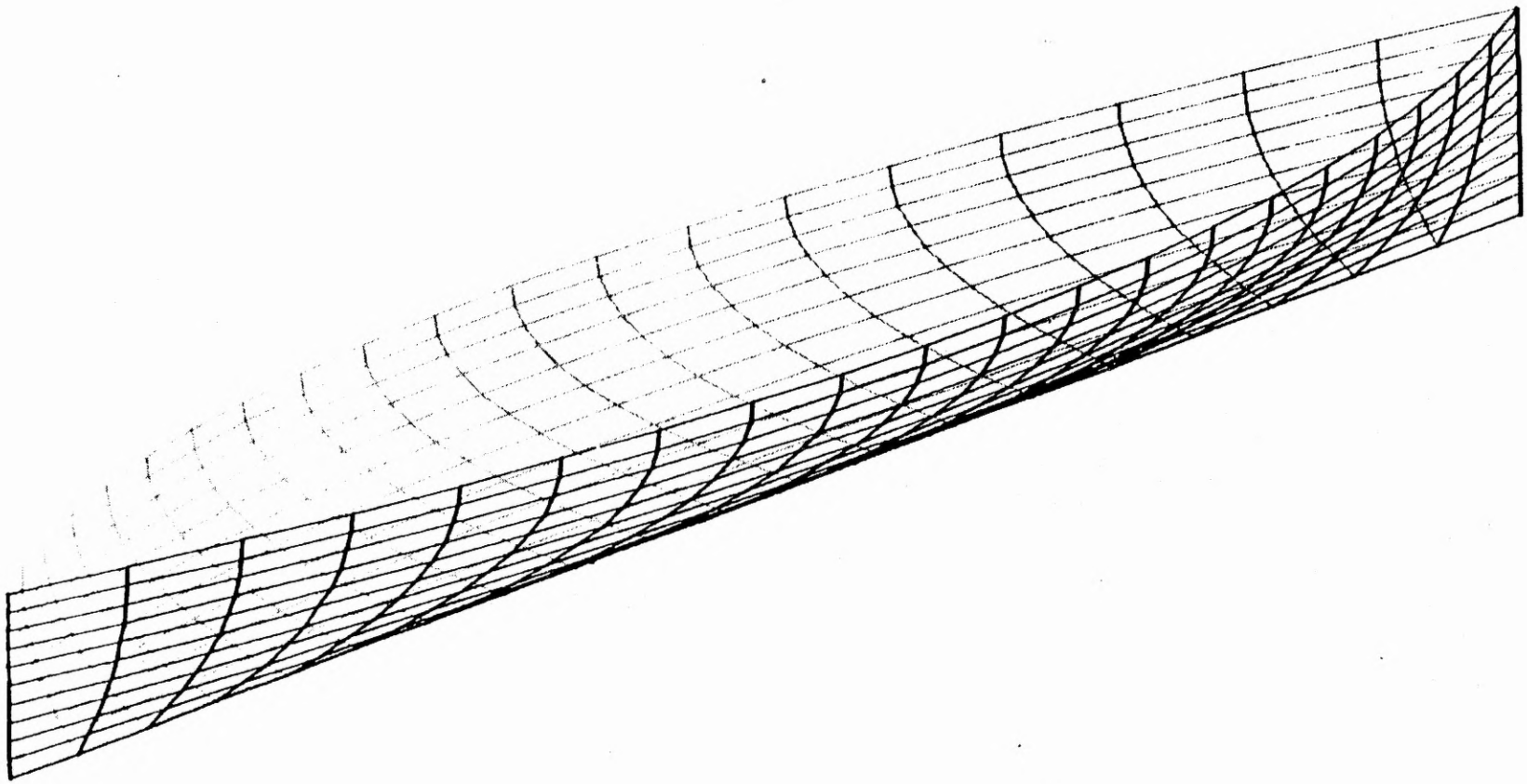

Figure 4.1 Perspective view of the Wigley parabolic hull. The vertical scale is enlarged by a factor of two for clarity. Note the sharp bow, stern and keel.

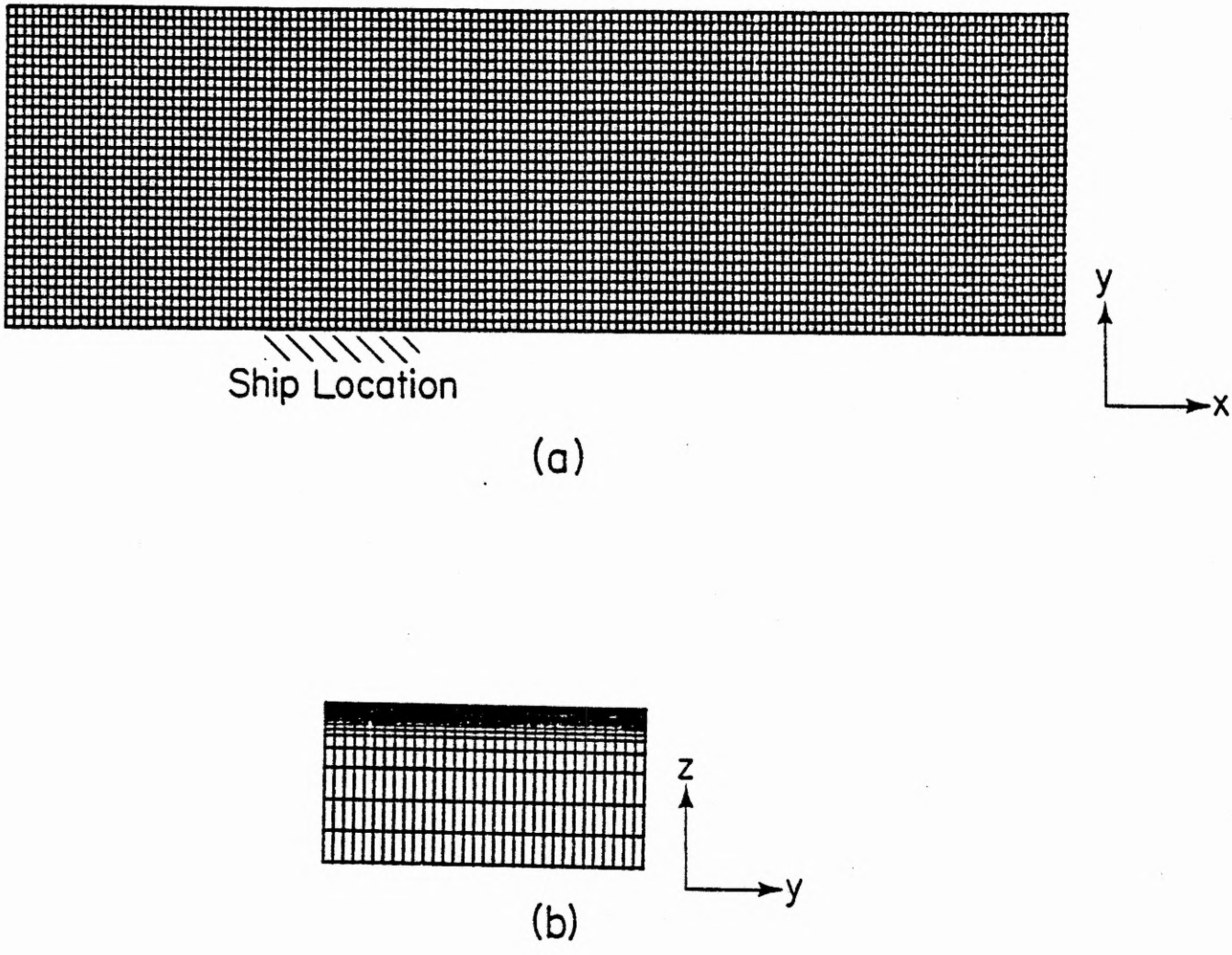

Figure 4.2 Cartesian mesh system for the 6.6 x 2.0 x 1.0 domain. **(a)** Top view of the (x,y) plane showing the constant grid intervals. **(b)** Side view of the (y,z) plane. Note the concentration of mesh lines near the free surface so that the shallow draft of the Wigley hull can be accommodated.

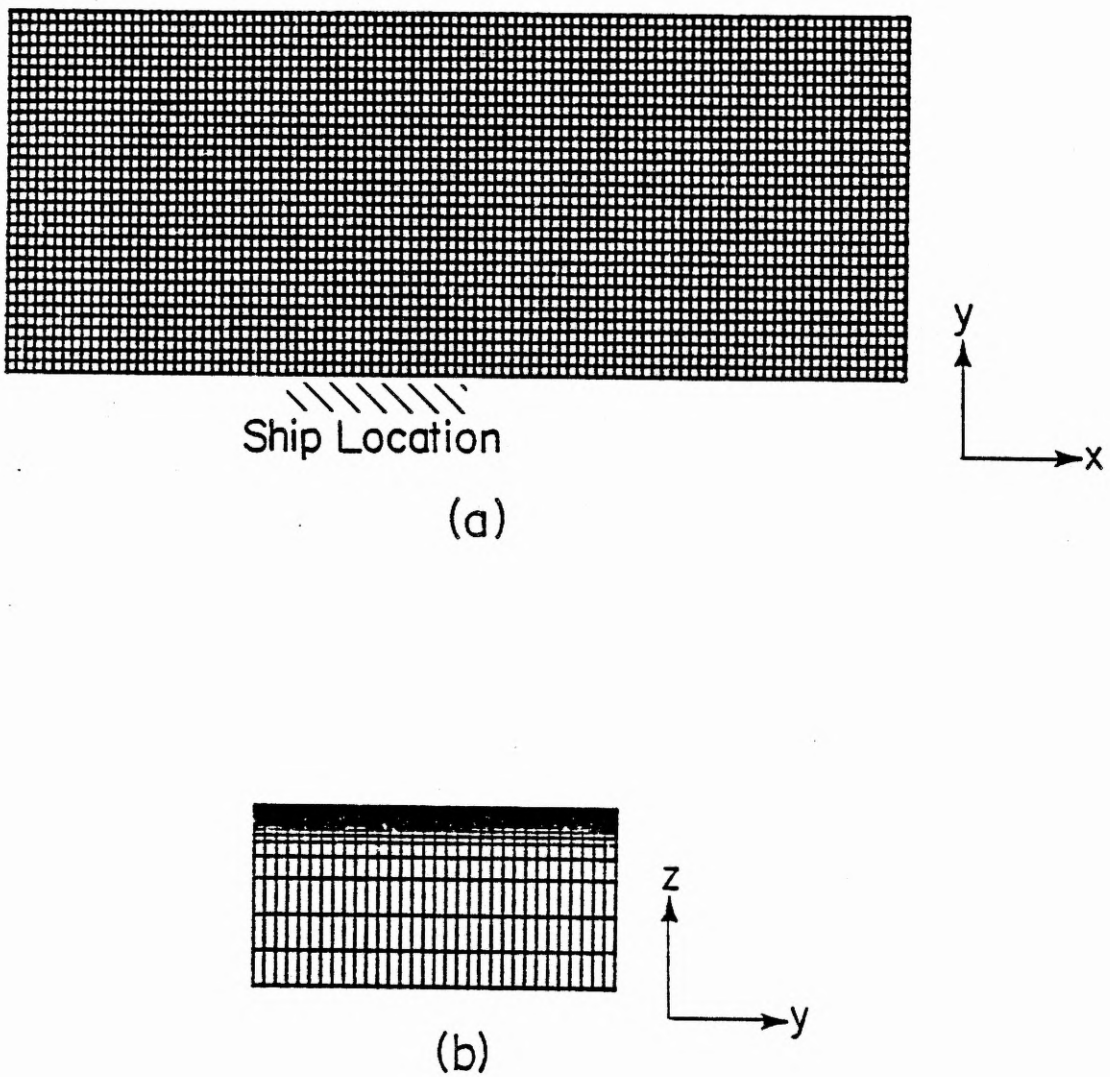

Figure 4.3 Cartesian mesh system for the 4.95 x 2.0 x 1.0 domain. **(a)** Top view of the (x,y) plane showing the constant grid intervals. **(b)** Side view of the (y,z) plane. Note the concentration of mesh lines near the free surface so that the shallow draft of the Wigley hull can be accommodated.

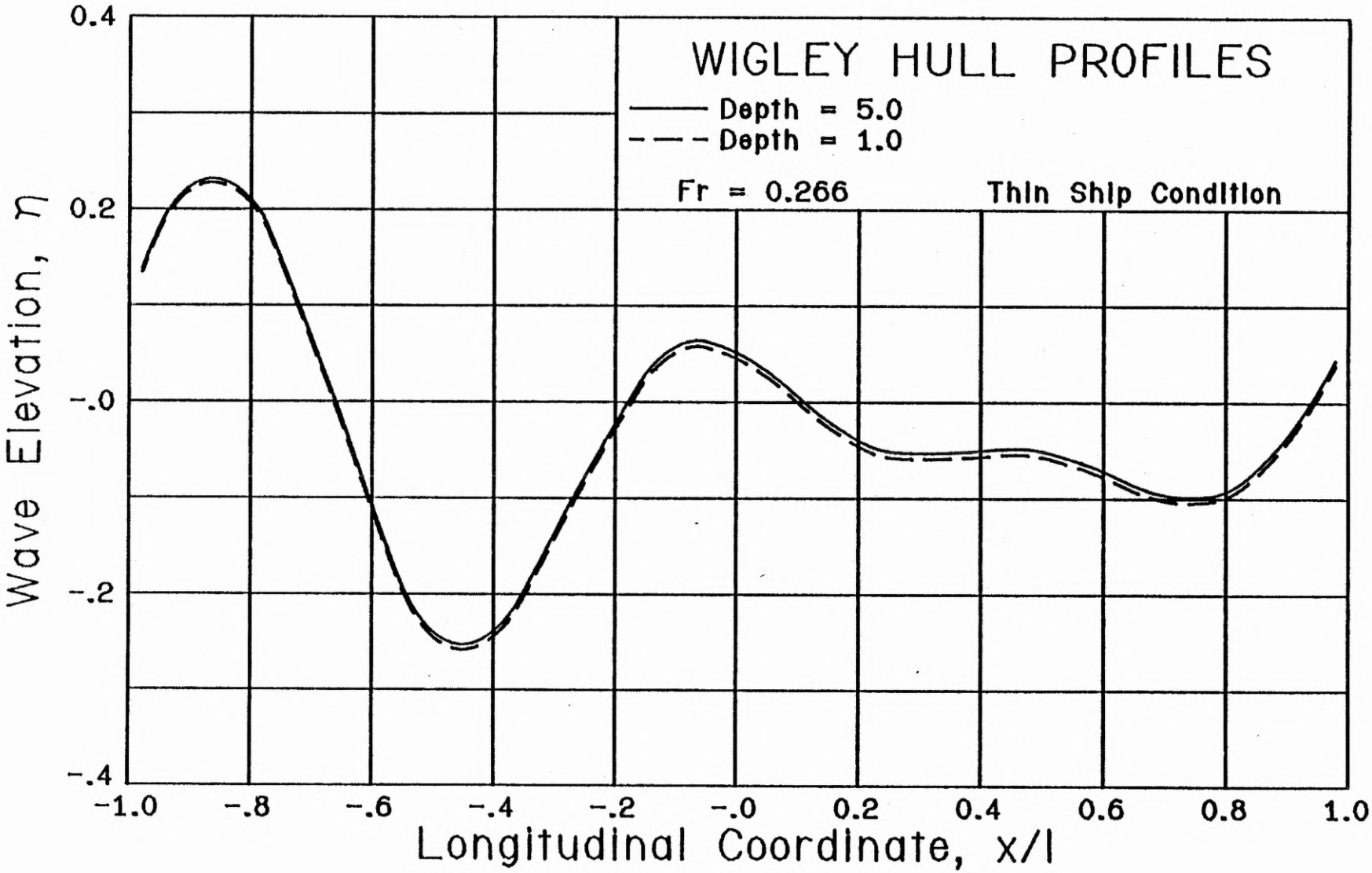

Figure 4.4 Comparison of the Wigley hull wave profiles using the thin ship condition for the depth equal to 1.0 and 5.0 and for $Fr = 0.266$.

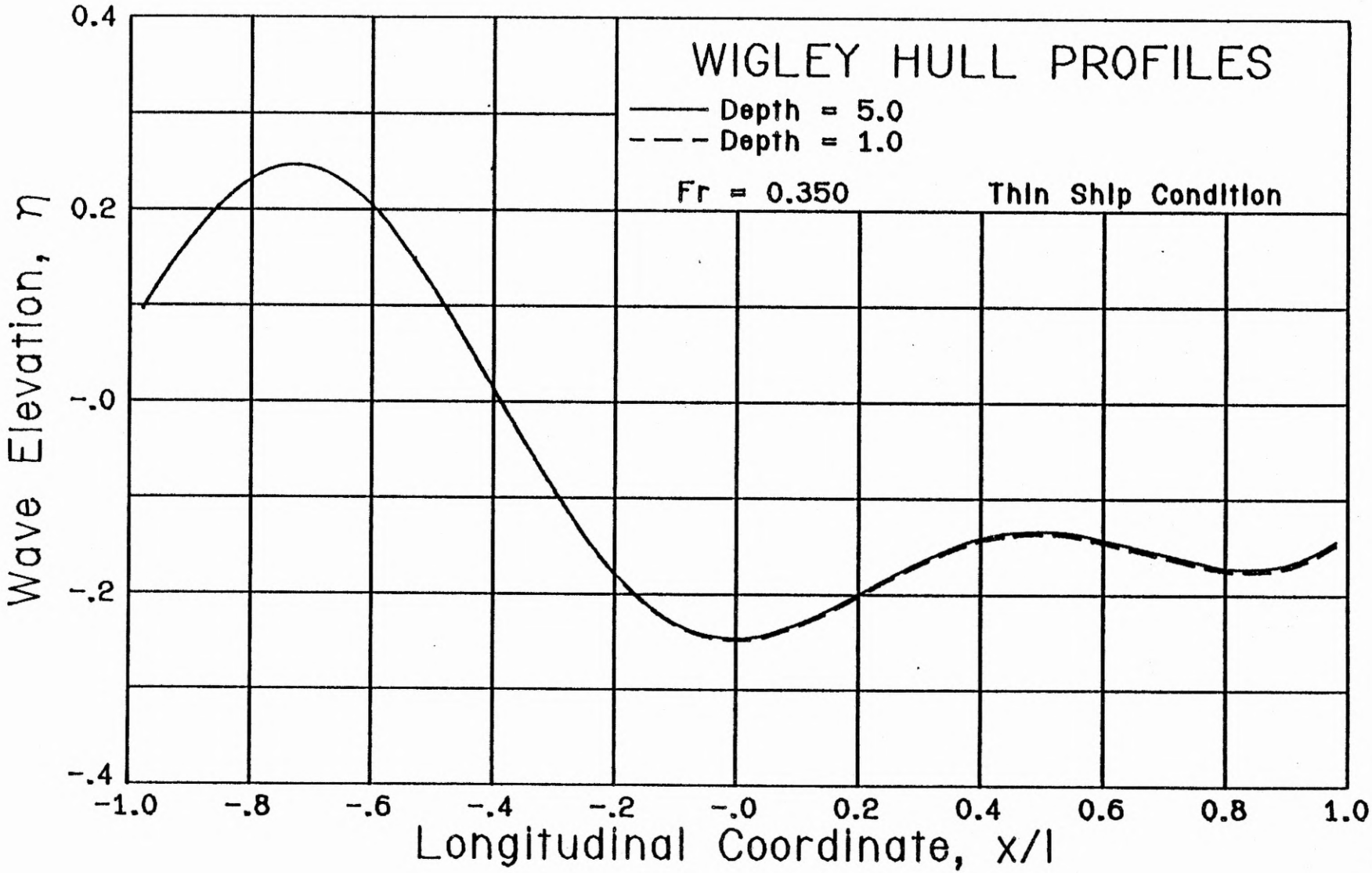

Figure 4.5 Comparison of the Wigley hull wave profiles using the thin ship condition for the depth equal to 1.0 and 5.0 and for $Fr = 0.350$.

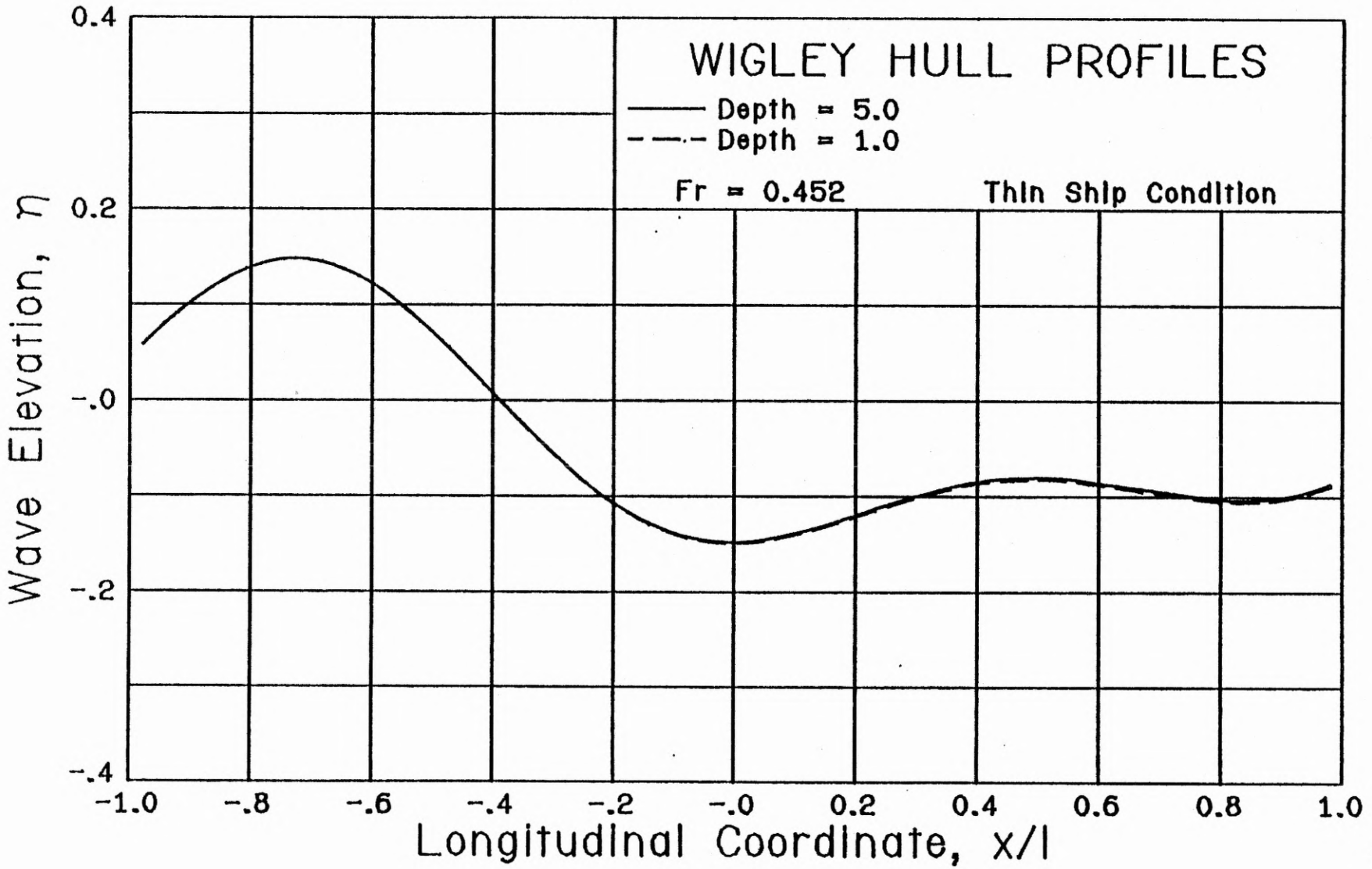

Figure 4.6 Comparison of the Wigley hull wave profiles using the thin ship condition for the depth equal to 1.0 and 5.0 and for Fr = 0.452.

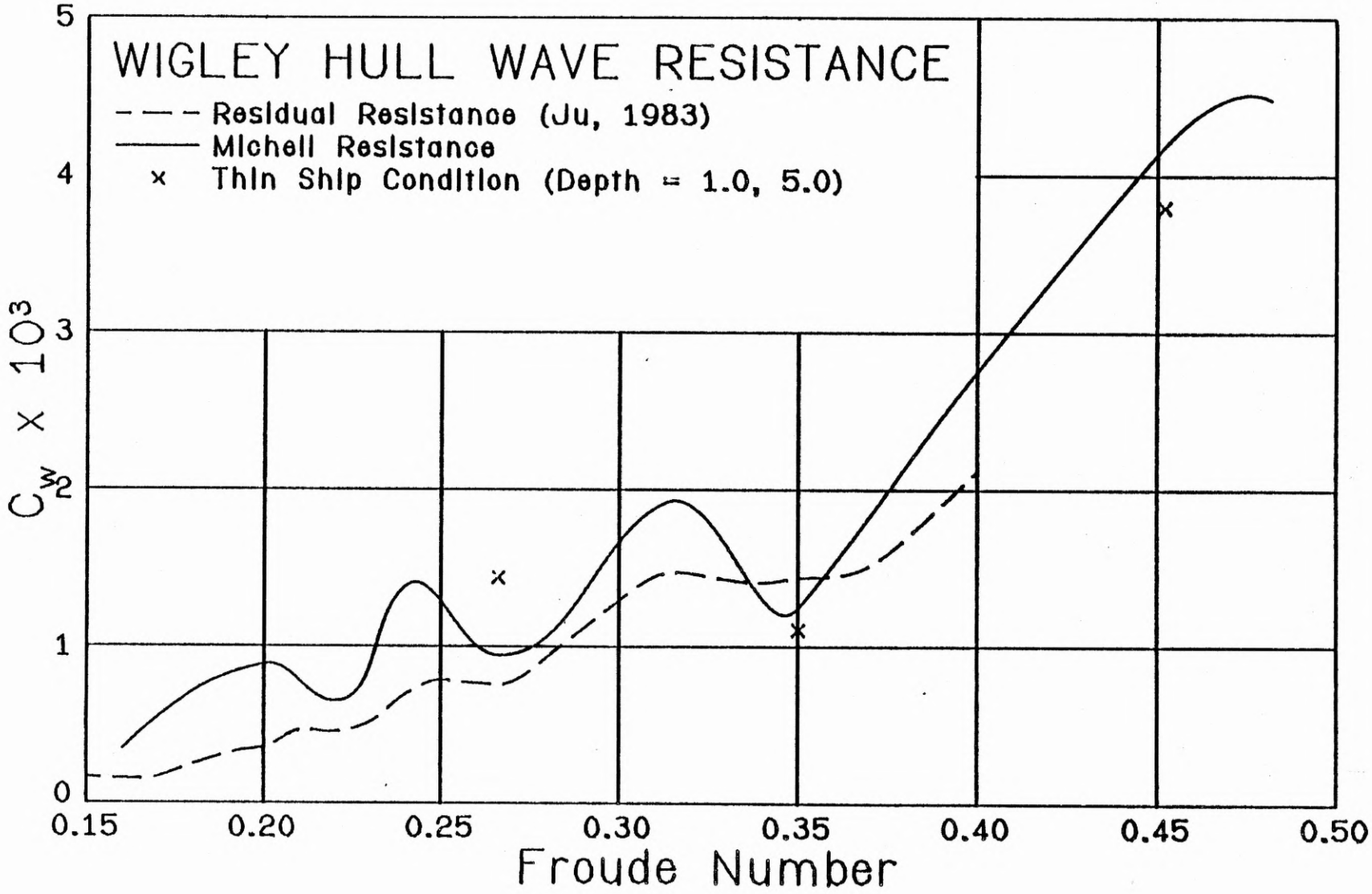

Figure 4.7 Wigley hull wave resistance vs. Froude number using the thin ship condition for the depth equal to 1.0 and 5.0 compared to the Michell resistance and an experiment.

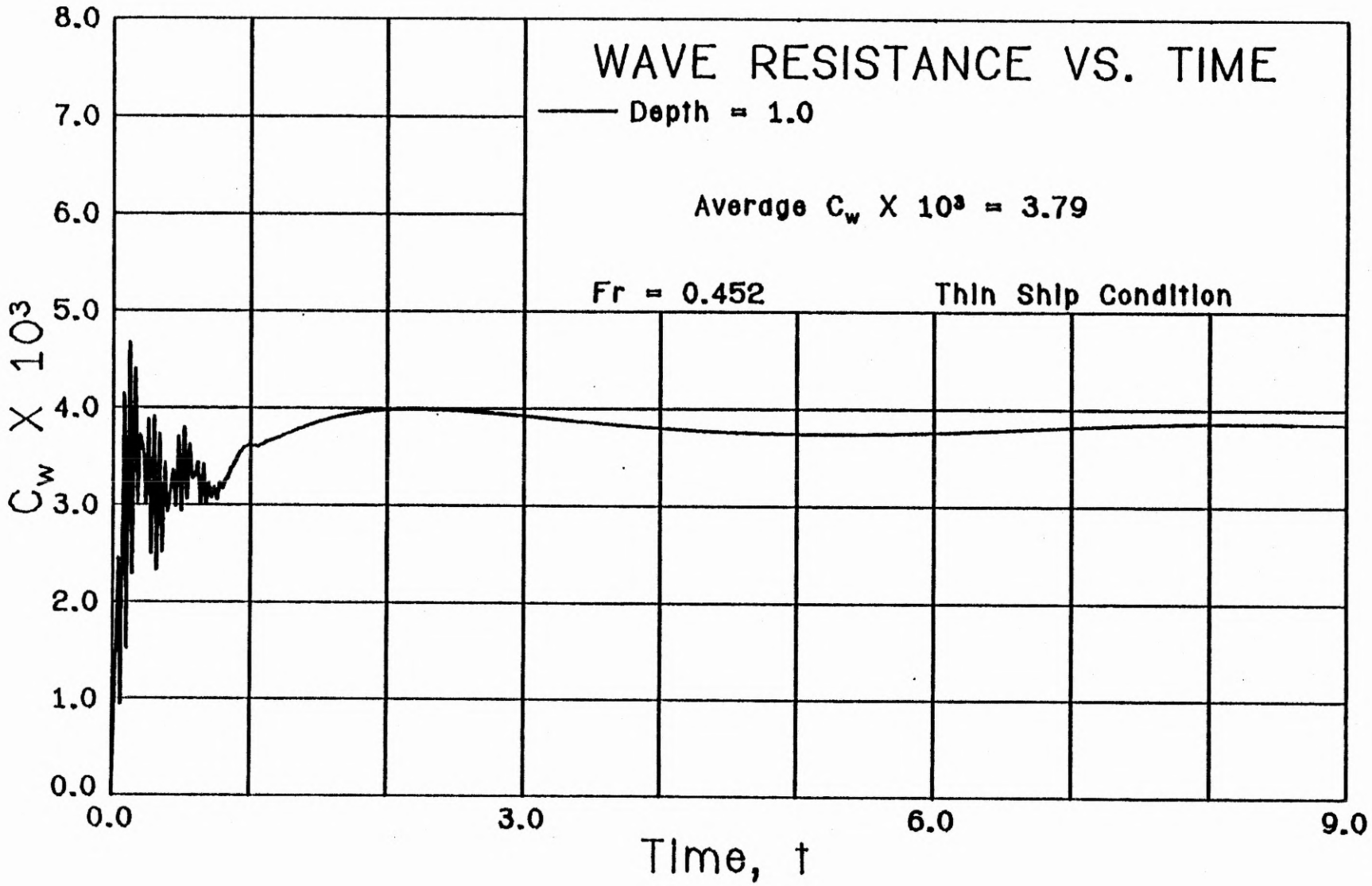

Figure 4.8 Wigley hull wave resistance vs. time using the thin ship condition for the depth equal to 1.0 with $Fr = 0.452$.

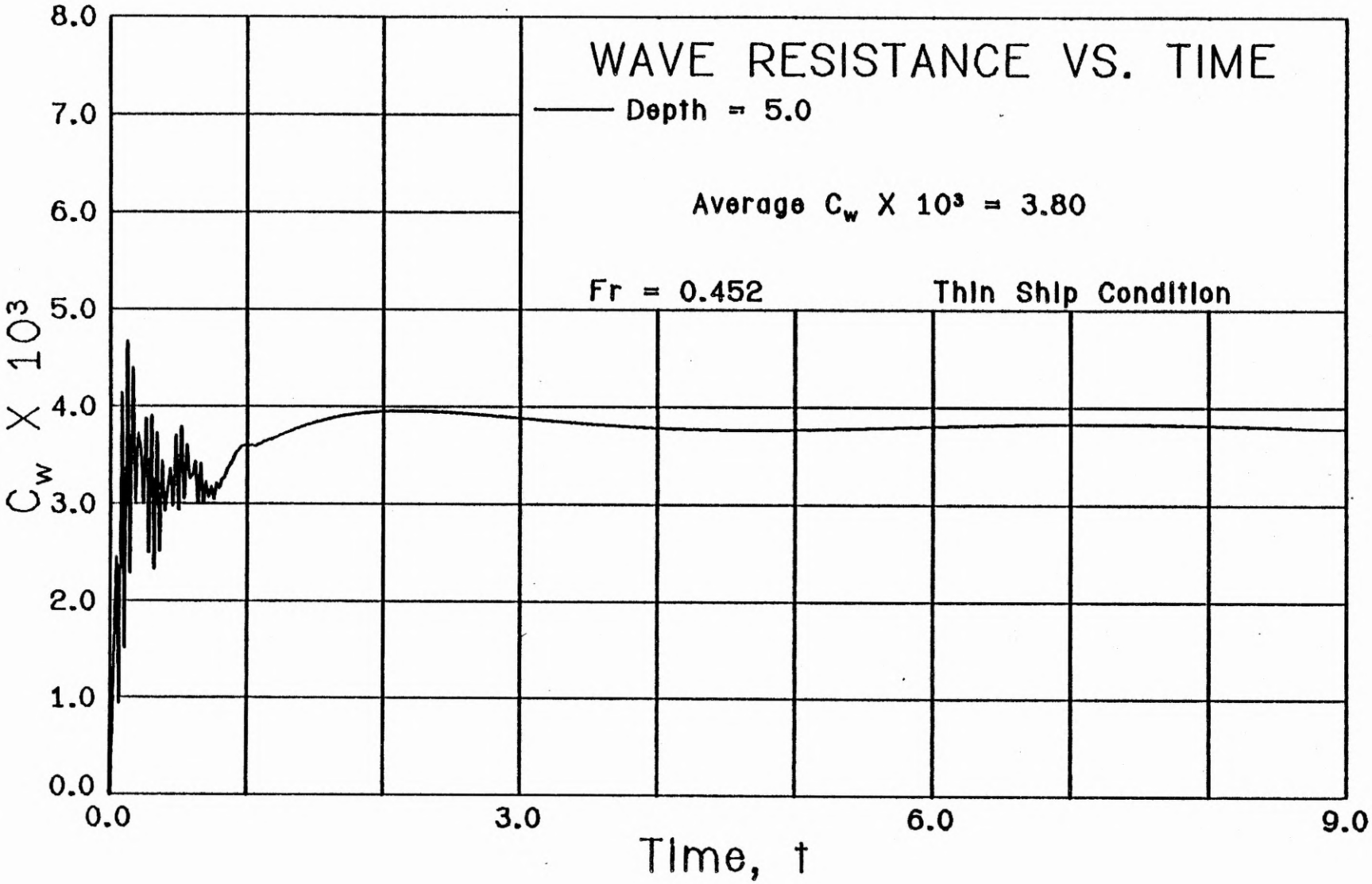

Figure 4.9 Wigley hull wave resistance vs. time using the thin ship condition for the depth equal to 5.0 with Fr = 0.452.

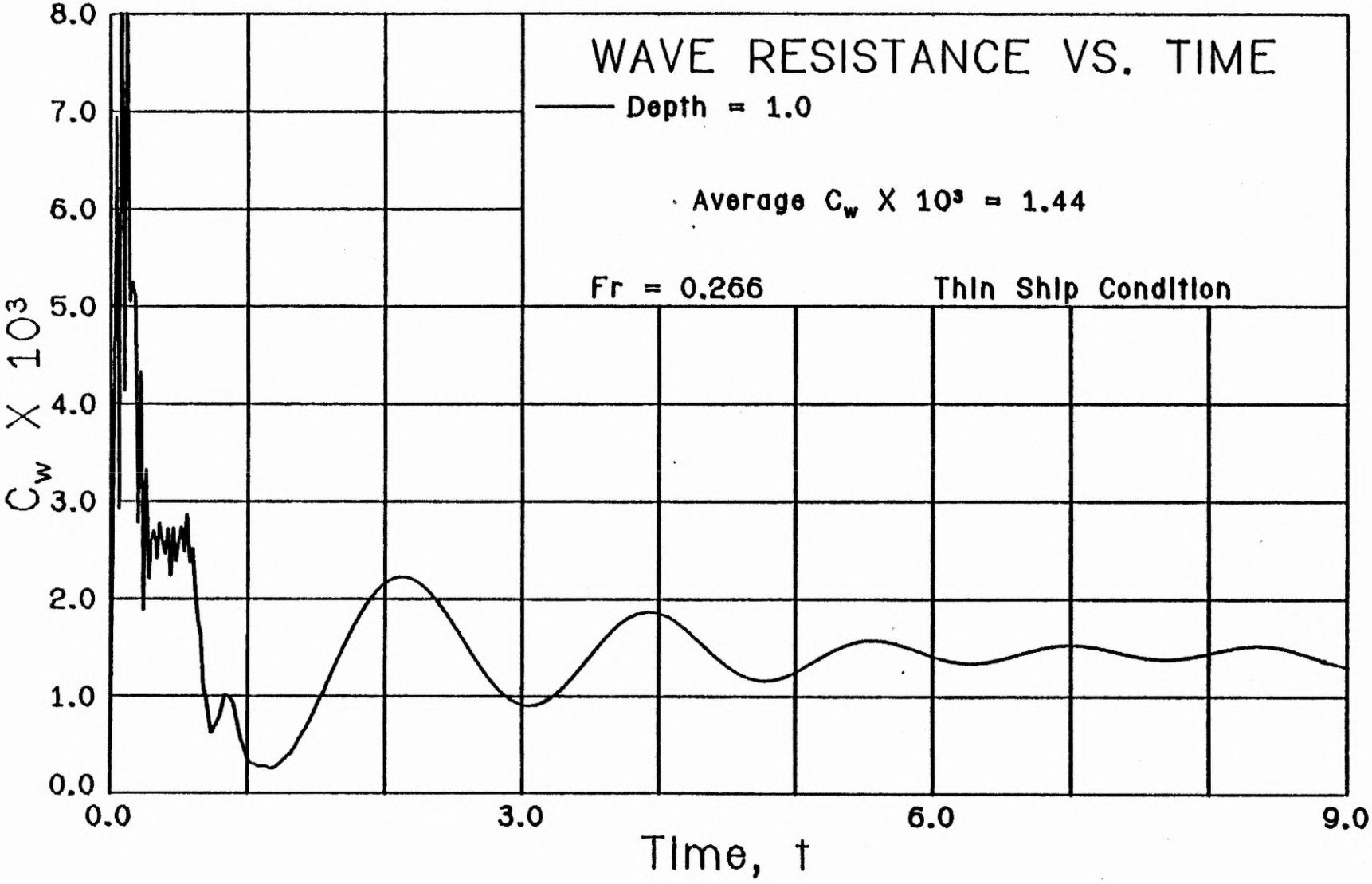

Figure 4.10 Wigley hull wave resistance vs. time using the thin ship condition for the depth equal to 1.0 with Fr = 0.266.

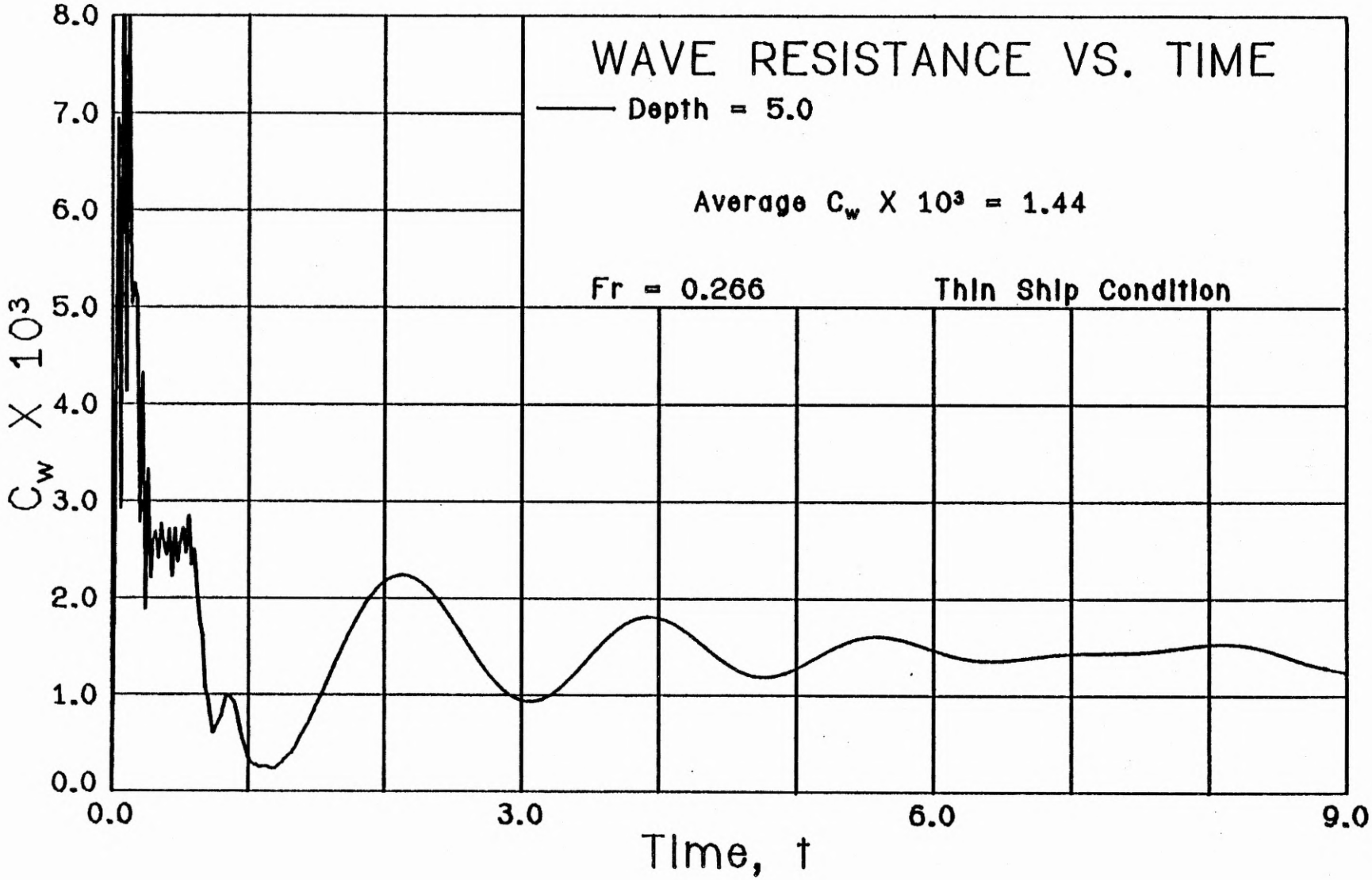

Figure 4.11 Wigley hull wave resistance vs. time using the thin ship condition for the depth equal to 5.0 with Fr = 0.266.

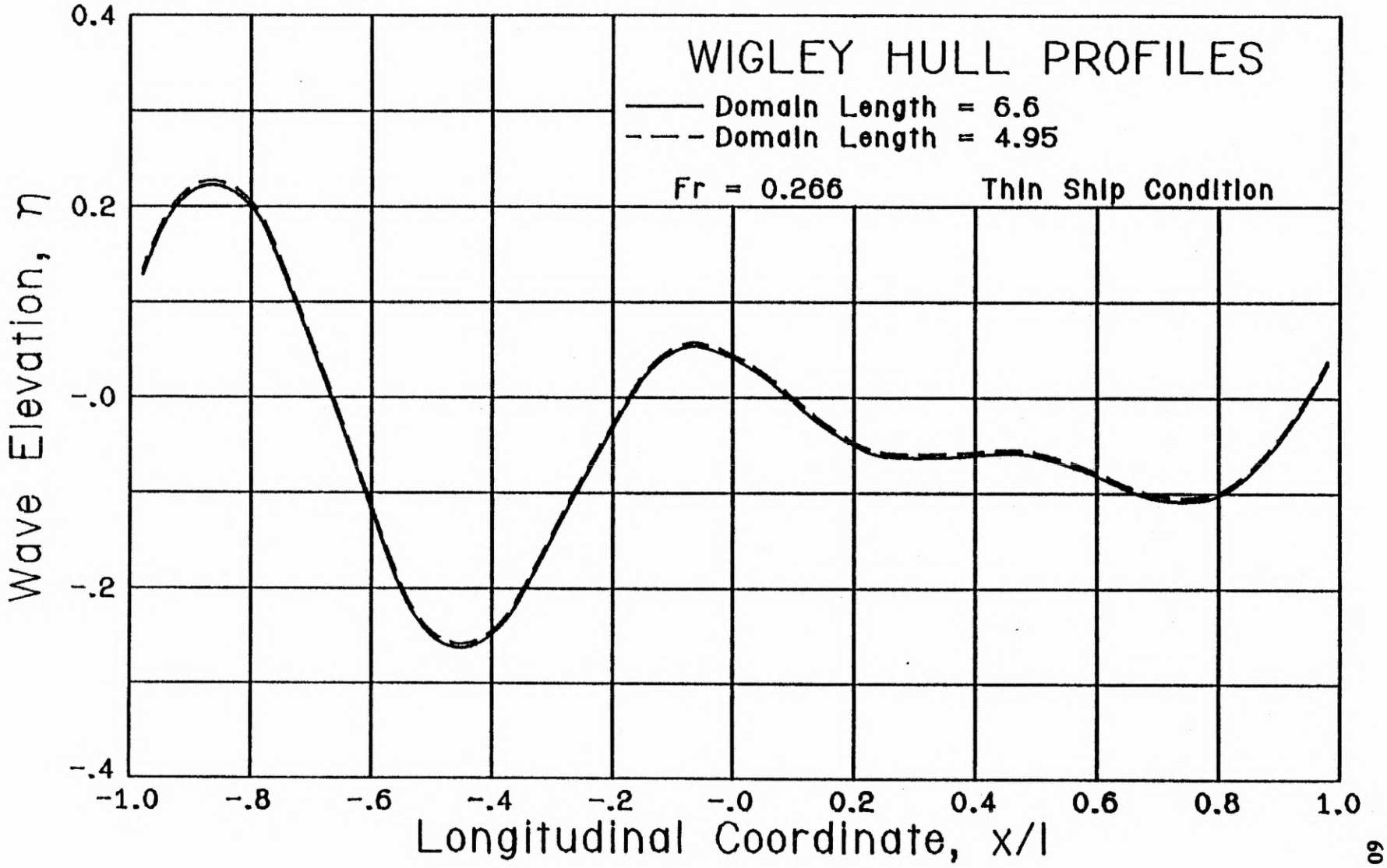

Figure 4.12 Comparison of the Wigley hull wave profiles using the thin ship condition for the domain length equal to 6.6 and 4.95 and for $Fr = 0.266$.

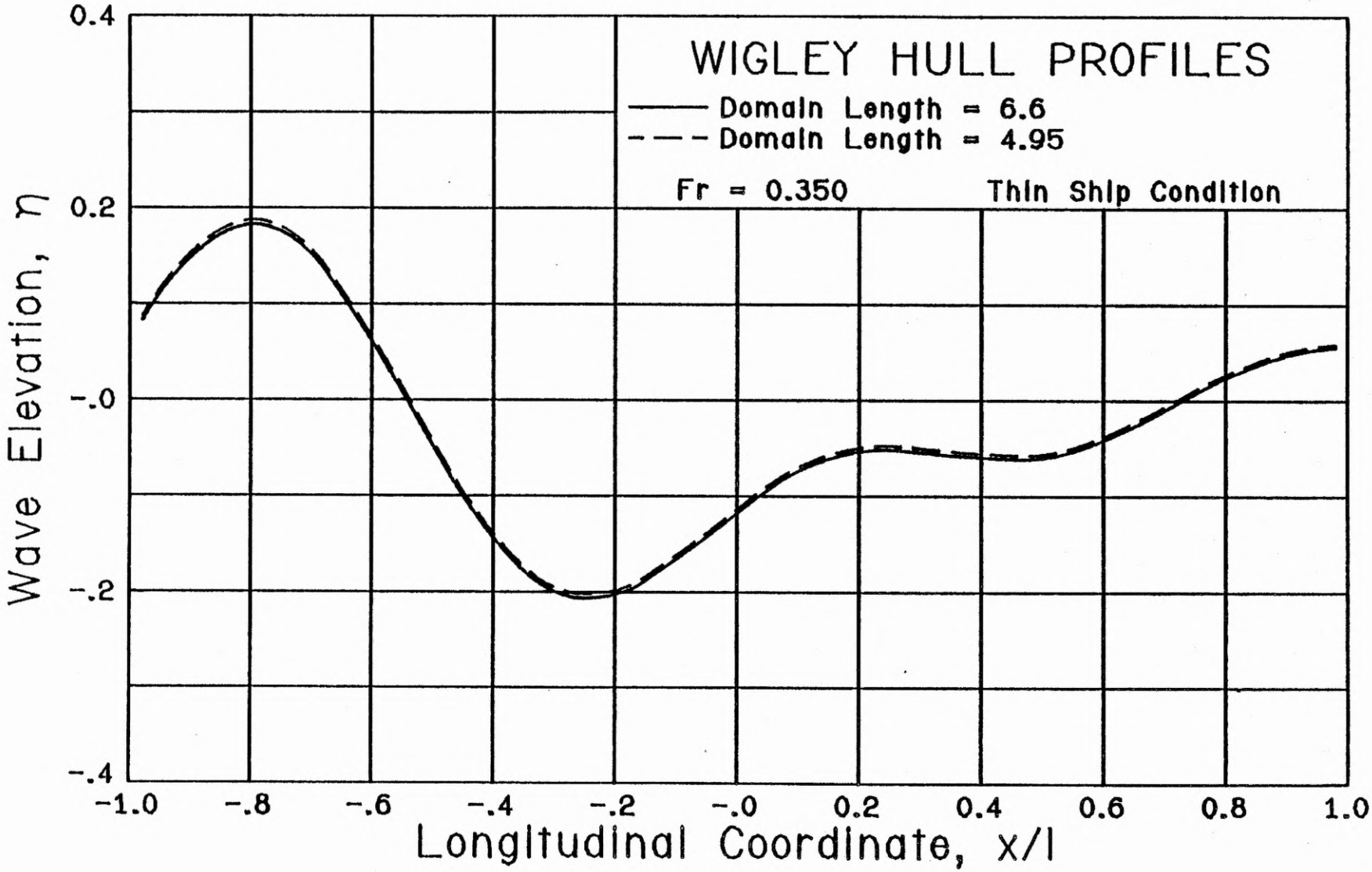

Figure 4.13 Comparison of the Wigley hull wave profiles using the thin ship condition for the domain length equal to 6.6 and 4.95 and for $Fr = 0.350$.

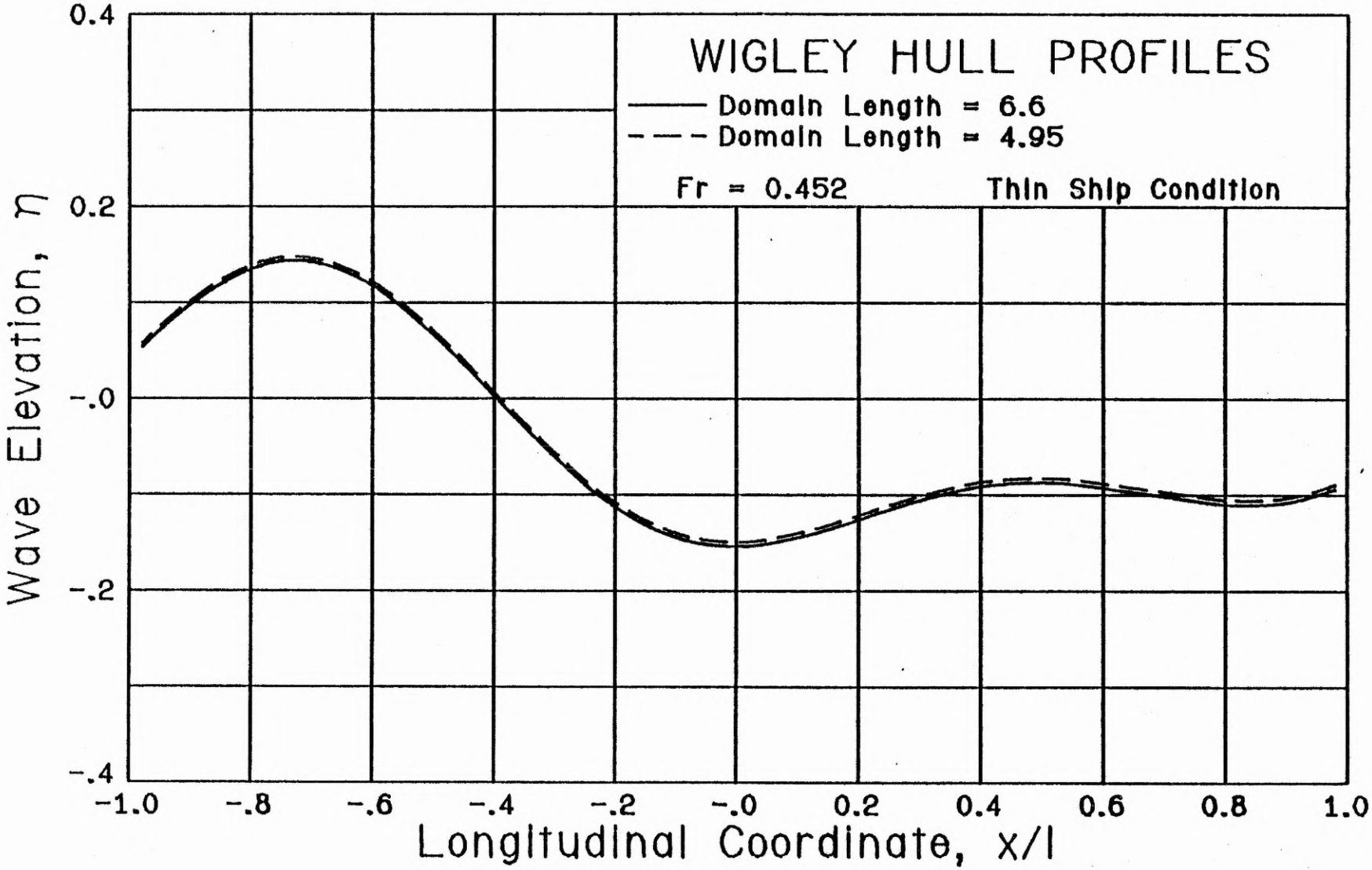

Figure 4.14 Comparison of the Wigley hull wave profiles using the thin ship condition for the domain length equal to 6.6 and 4.95 and for $Fr = 0.452$.

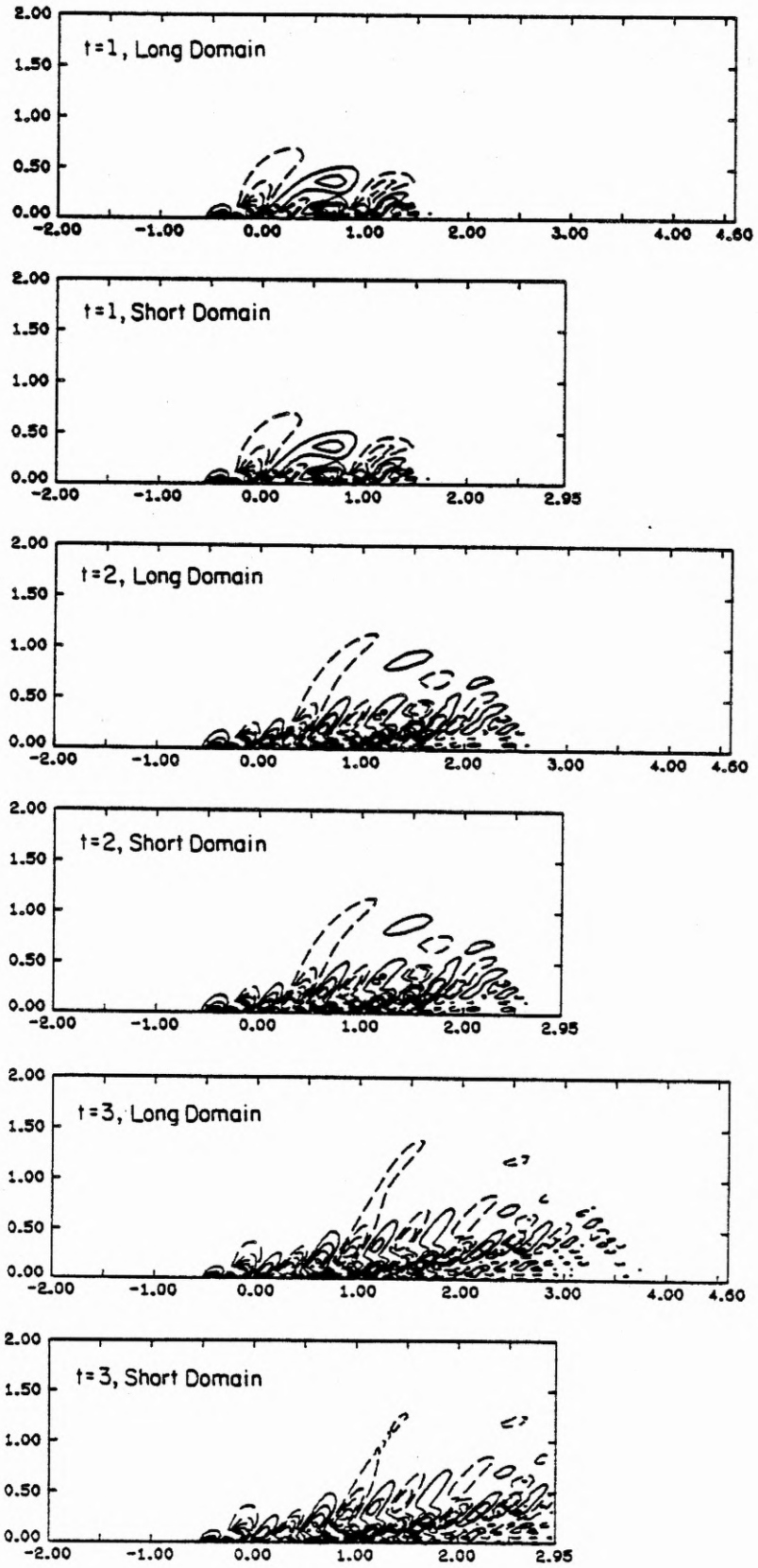

Figure 4.15 A time sequence of the thin ship wave profiles generated by the translating Wigley hull for both the Long Domain and the Short Domain. t = 1,2 and 3; Fr = 0.266.

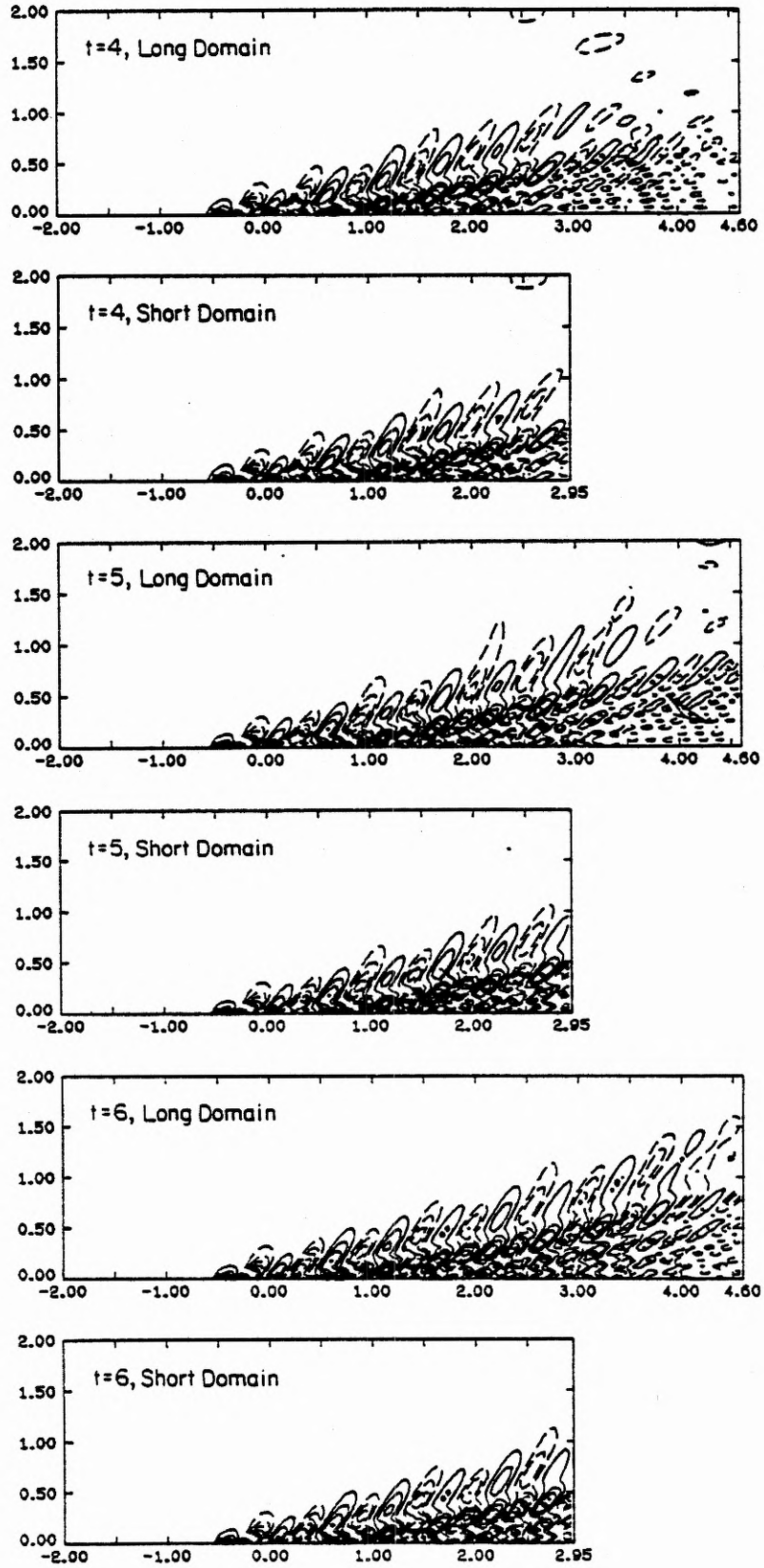

Figure 4.16 A time sequence of the thin ship wave profiles generated by the translating Wigley hull for both the Long Domain and the Short Domain. t = 4,5 and 6; Fr = 0.266.

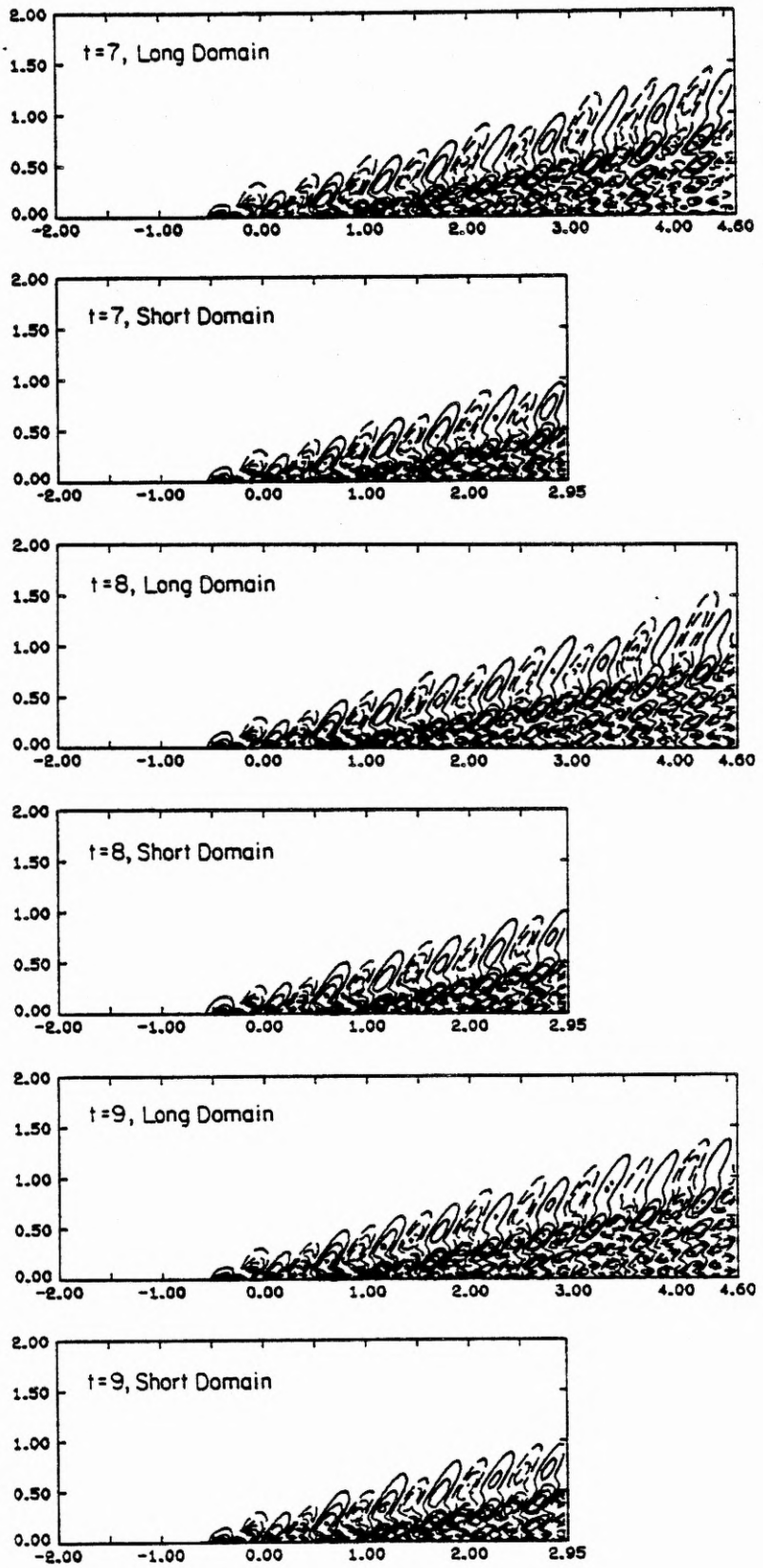

Figure 4.17 A time sequence of the thin ship wave profiles generated by the translating Wigley hull for both the Long Domain and the Short Domain. t = 7,8 and 9; Fr = 0.266.

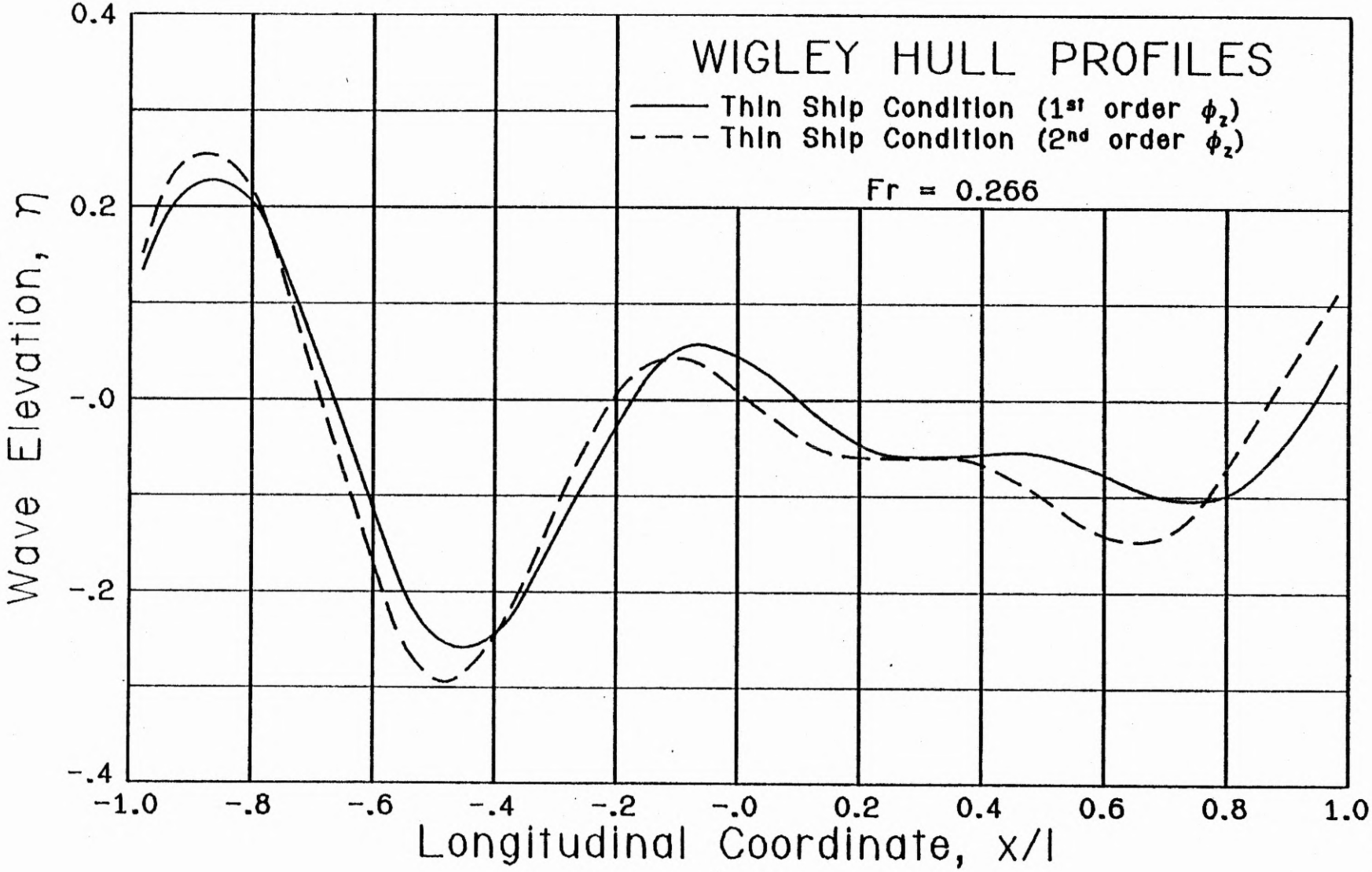

Figure 4.18 Comparison of the Wigley hull wave profiles using the thin ship condition for both first and second order one-sided differencing of the vertical velocity (ϕ_z) at the free surface. $Fr = 0.266$.

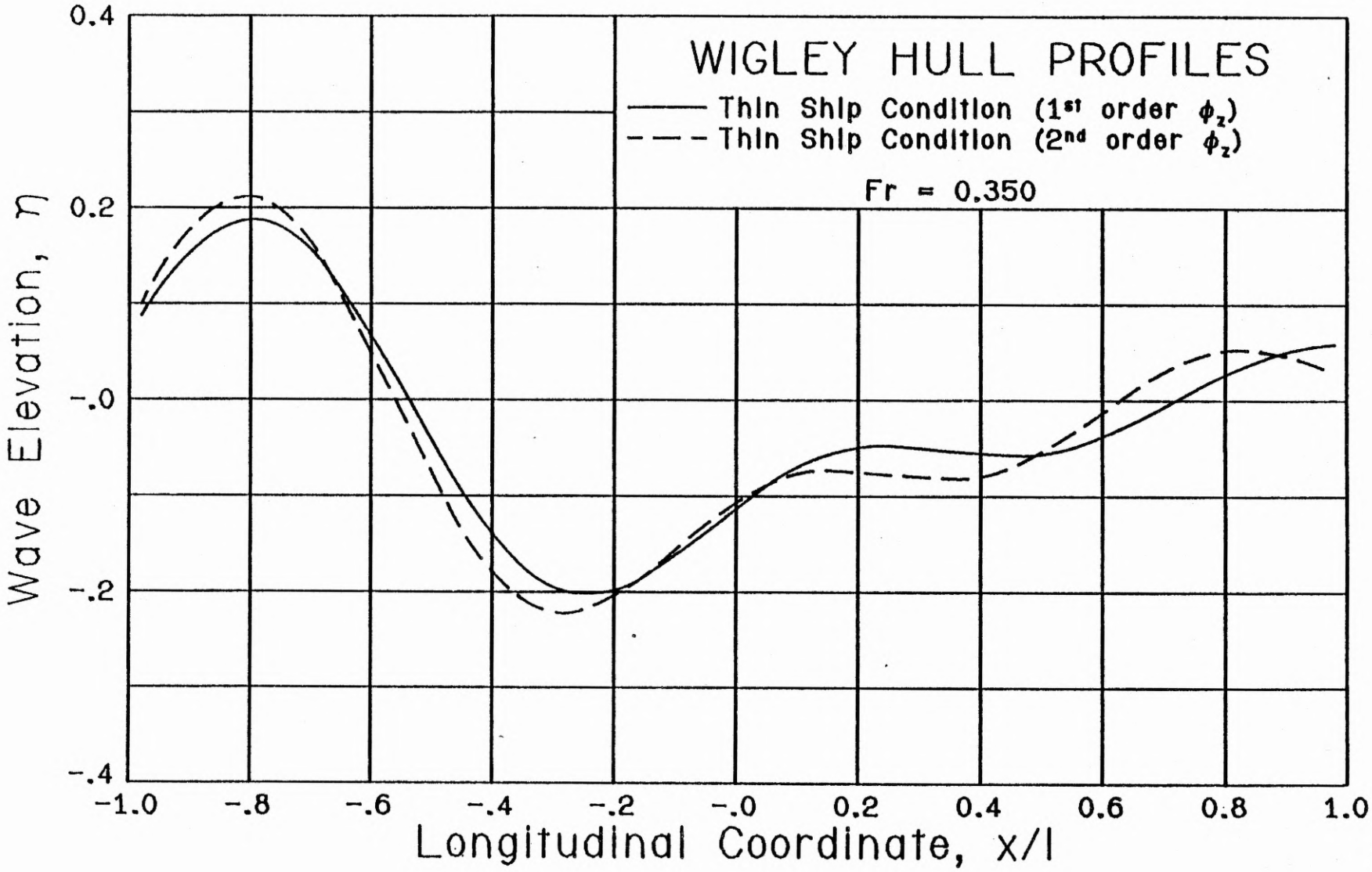

Figure 4.19 Comparison of the Wigley hull wave profiles using the thin ship condition for both first and second order one-sided differencing of the vertical velocity (ϕ_z) at the free surface. Fr = 0.350.

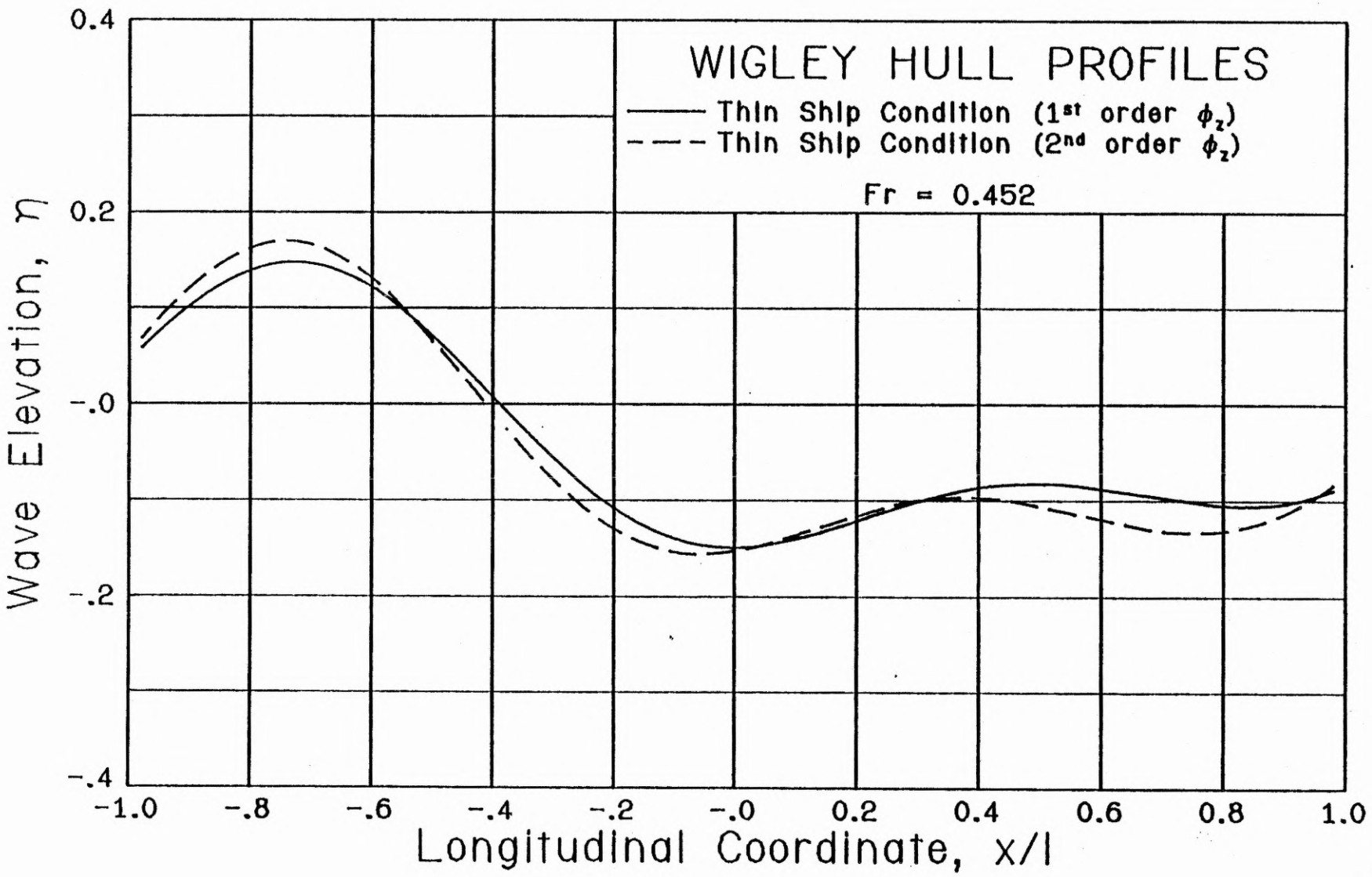

Figure 4.20 Comparison of the Wigley hull wave profiles using the thin ship condition for both first and second order one-sided differencing of the vertical velocity (ϕ_z) at the free surface. $Fr = 0.452$.

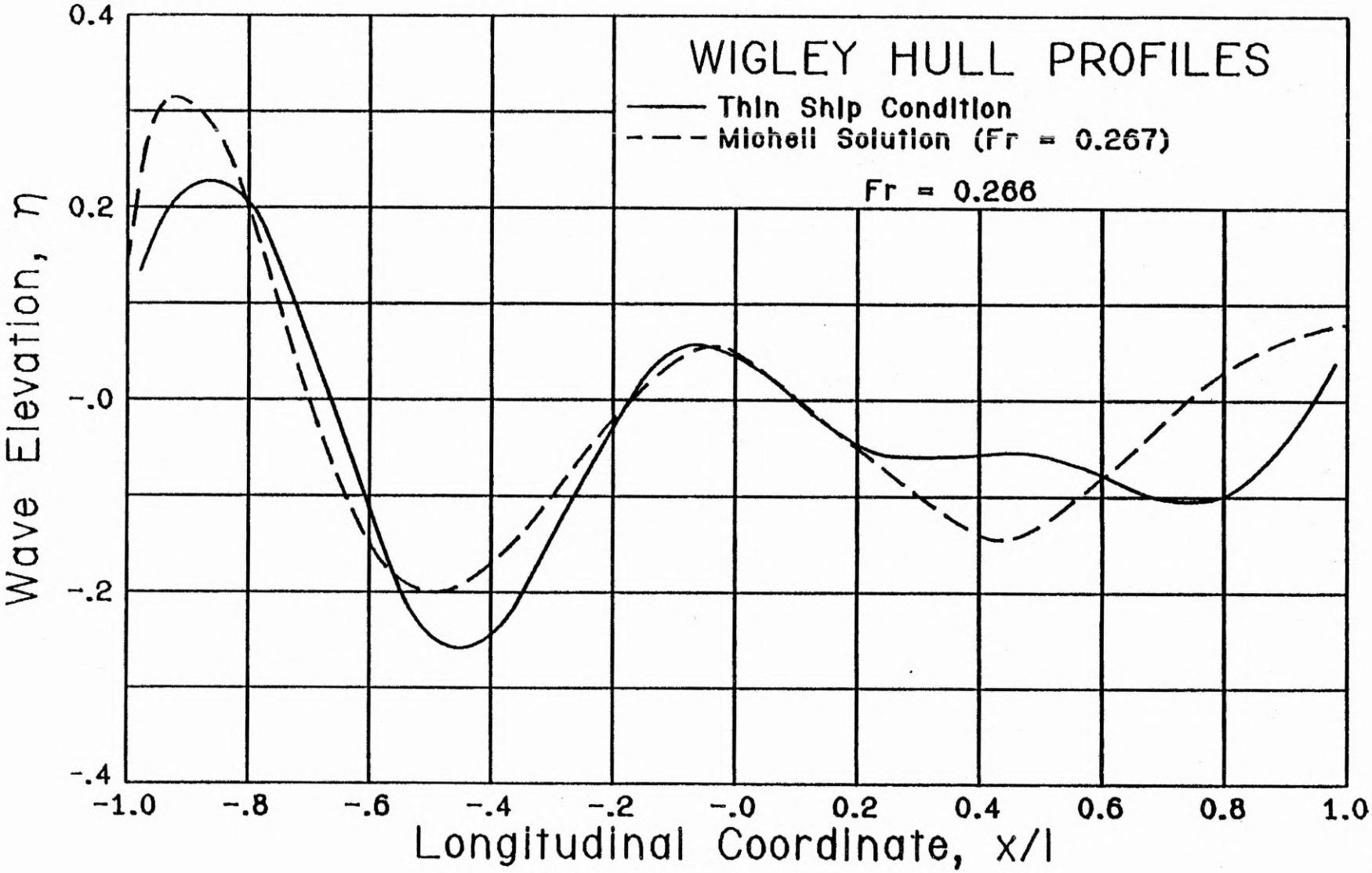

Figure 4.21 Comparison of the Wigley hull wave profile using the thin ship condition (first order ϕ_-) with the Michell solution for $Fr = 0.266$.

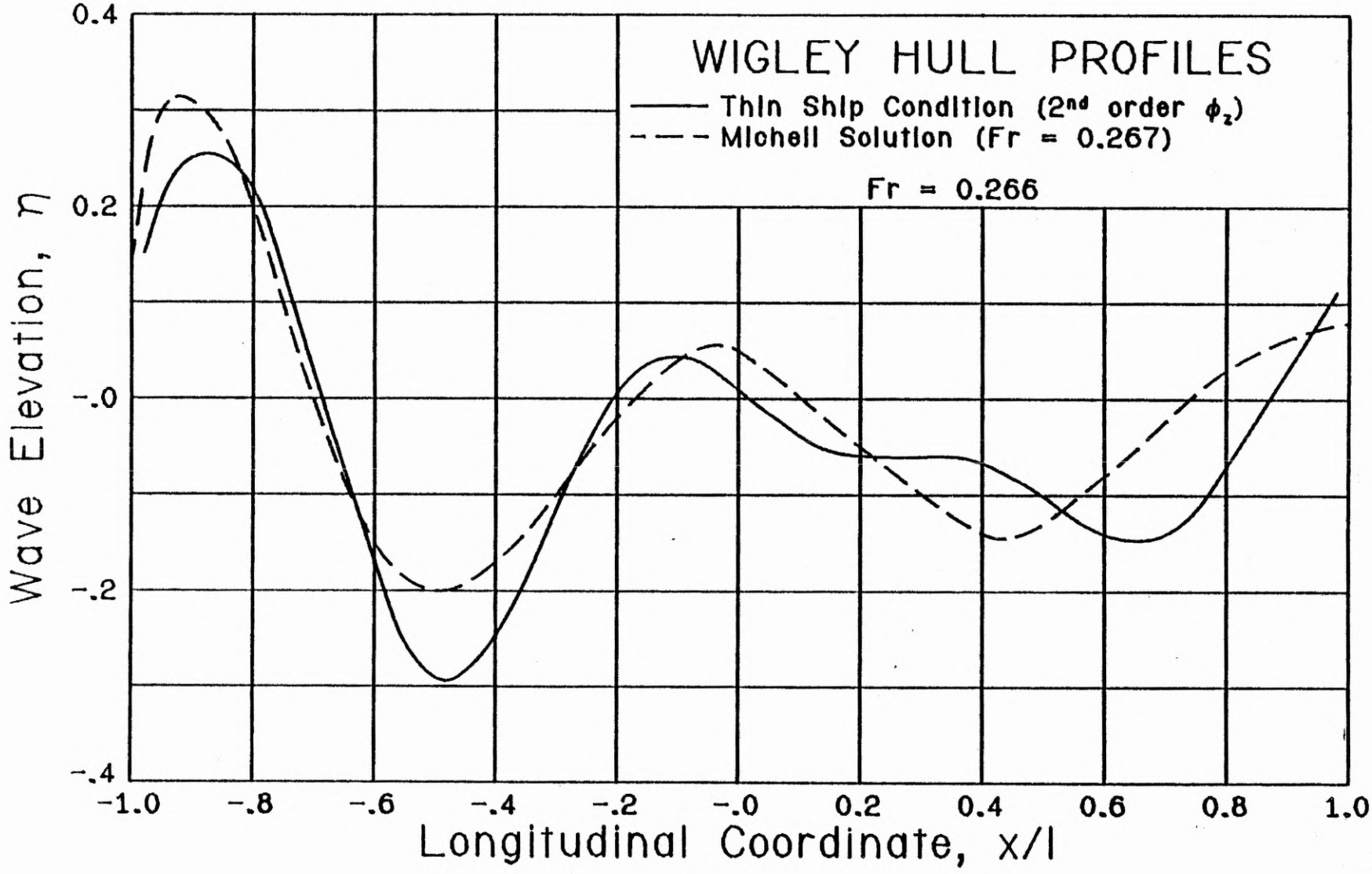

Figure 4.22 Comparison of the Wigley hull wave profile using the thin ship condition (second order ϕ_2) with the Michell solution for $Fr = 0.266$.

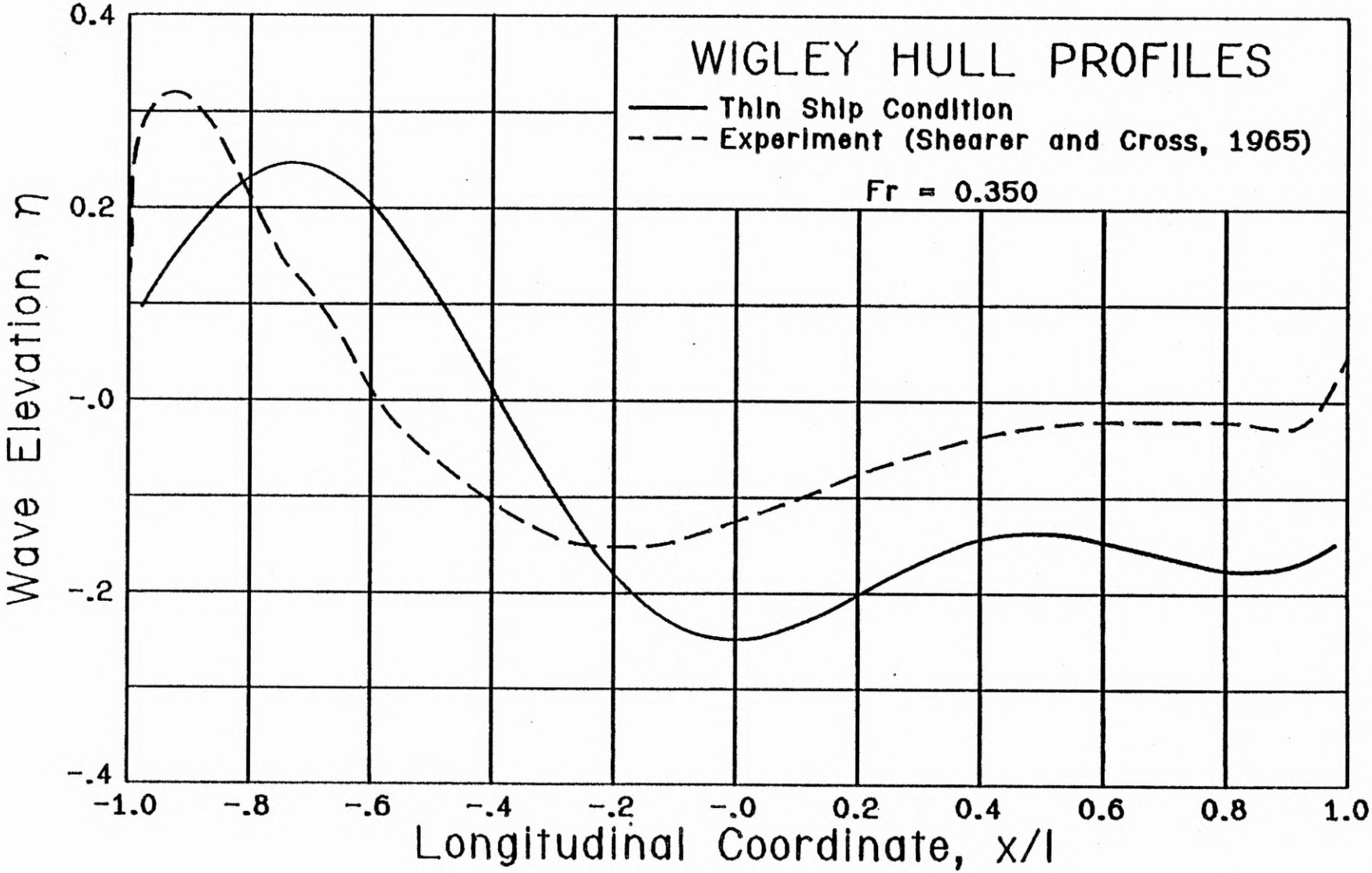

Figure 4.23 Comparison of the Wigley hull wave profile using the thin ship condition (first order ϕ_s) with an experiment for $Fr = 0.350$.

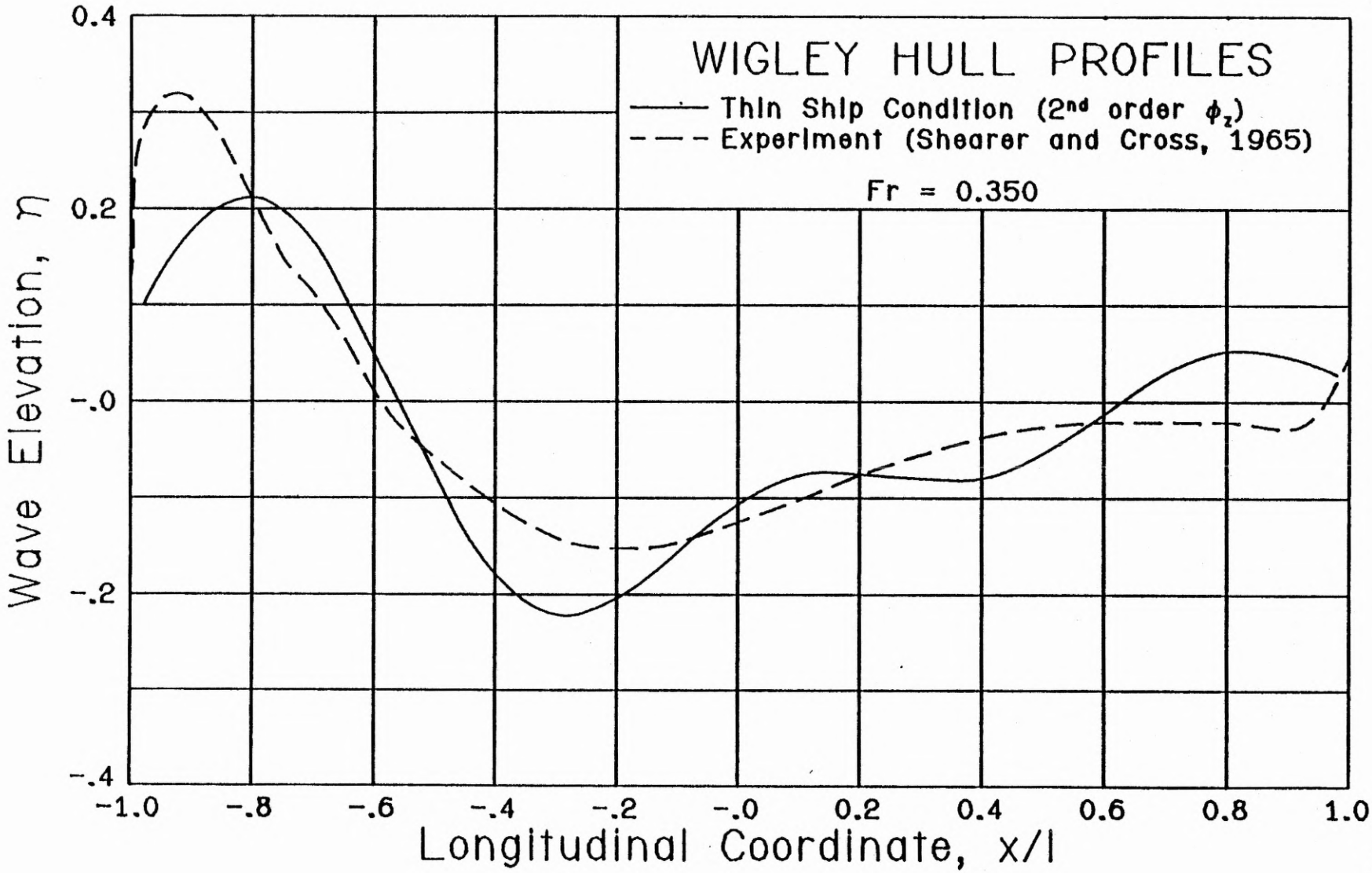

Figure 4.24 Comparison of the Wigley hull wave profile using the thin ship condition (second order ϕ_z) with an experiment for $Fr = 0.350$.

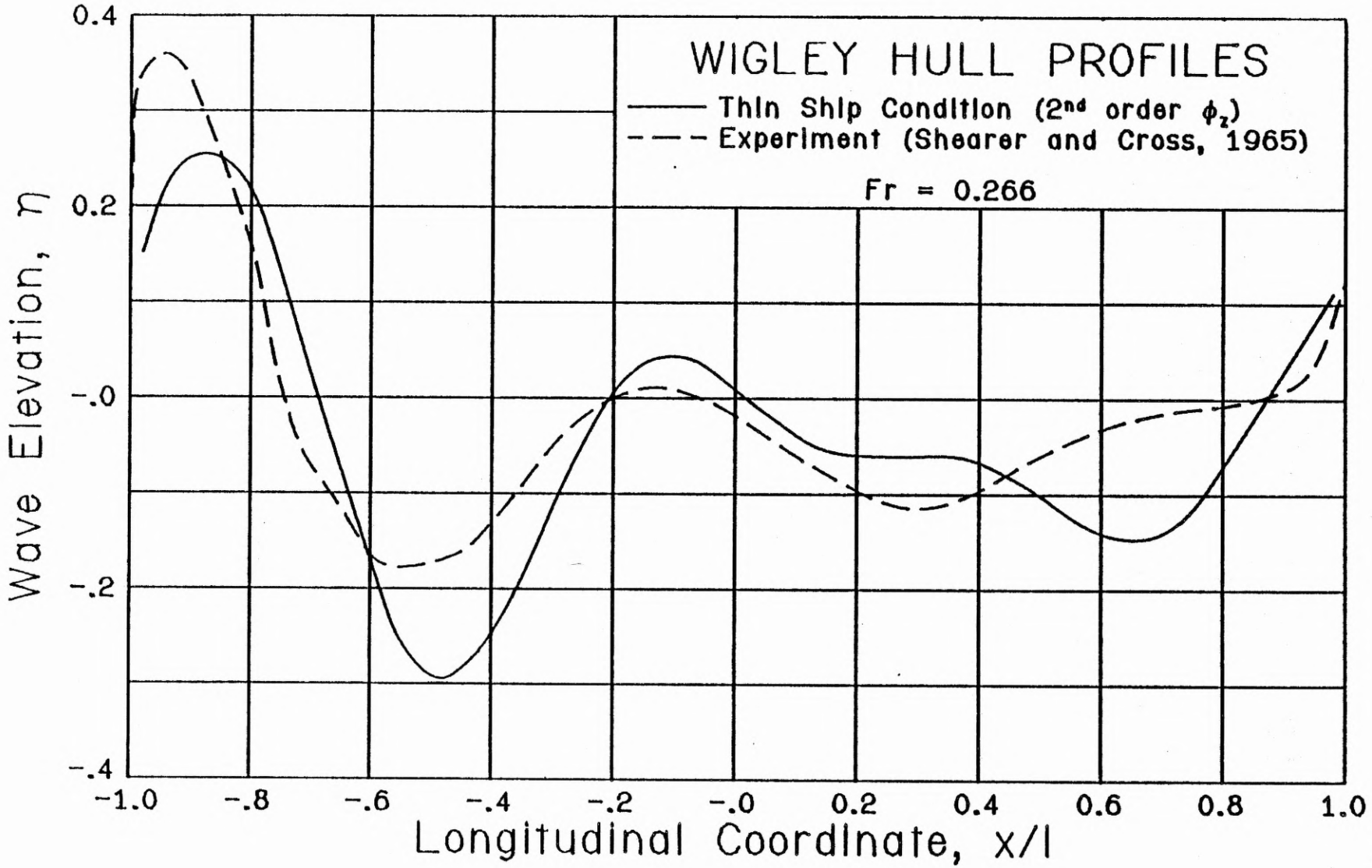

Figure 4.25 Comparison of the Wigley hull wave profile using the thin ship condition (second order ϕ_2) with an experiment for $Fr = 0.266$.

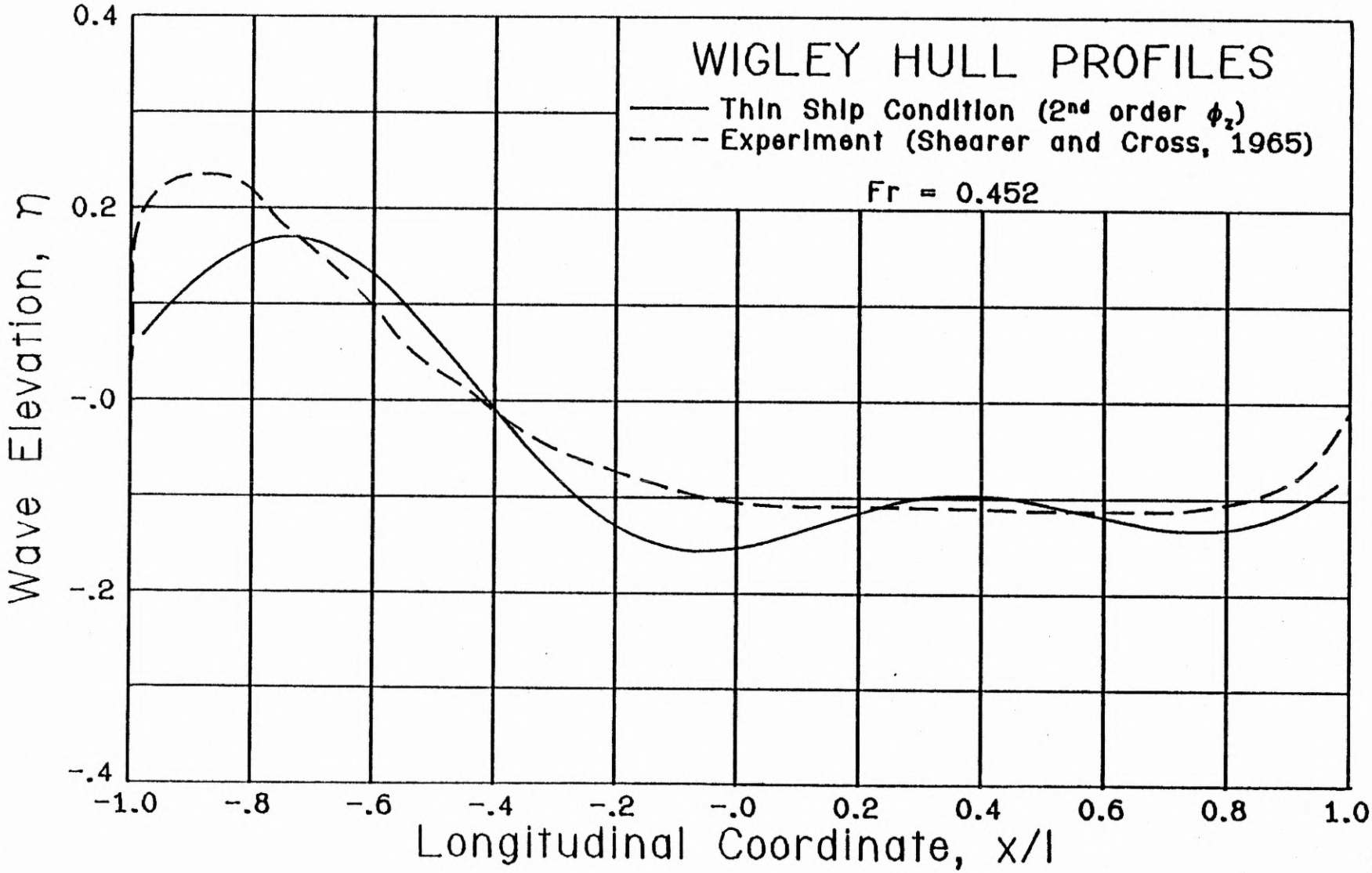

Figure 4.26 Comparison of the Wigley hull wave profile using the thin ship condition (second order ϕ_2) with an experiment for $Fr = 0.452$.

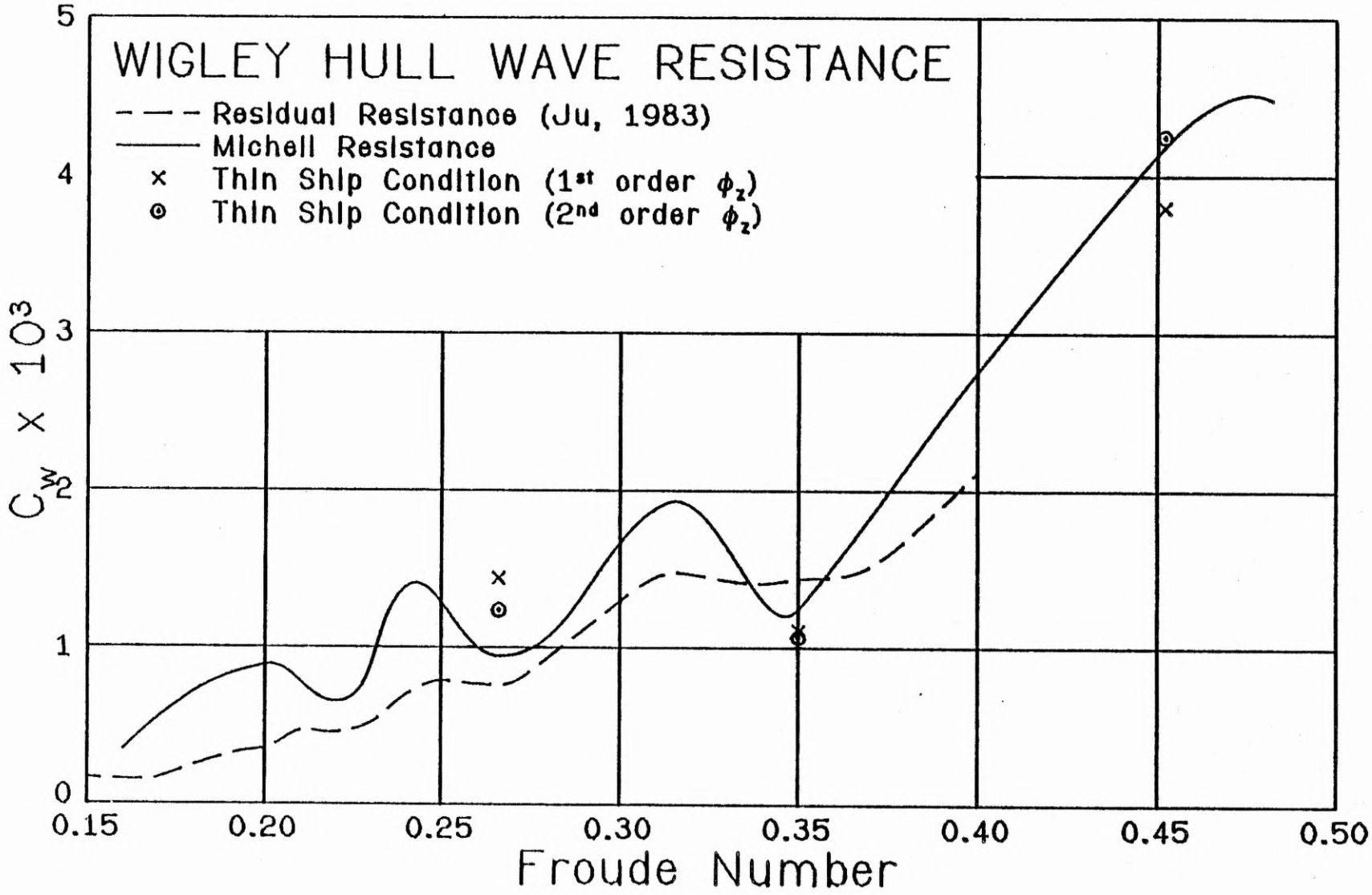

Figure 4.27 Comparison of the Wigley hull wave resistance vs. Froude number for both first and second order ϕ_z differencing.

CHAPTER 5. THE NEUMANN-KELVIN PROBLEM

In the present development of a general numerical method for the nonlinear ship wave problem, it is desired to create a new, more efficient approach to the implementation of the exact hull boundary condition (Eq. (2.11)). The development of this approach is given in the context of the Neumann-Kelvin problem in which the hull boundary condition is satisfied exactly but the free surface conditions remain linearized. This strategy allows a careful examination of the numerical features in the absence of the complexity due to the nonlinear free surface conditions. It is often argued, however, that the Neumann-Kelvin problem is mathematically inconsistent since the orders of approximation for the hull and free surface conditions are not the same. Regardless of this inconsistency, we must develop a new mesh system to accurately accommodate the Wigley hull, and we must revise the fast Poisson solver for the Laplace equation so that the exact hull boundary condition can be efficiently implemented. It is felt that this step is most effectively accomplished by considering the Neumann-Kelvin problem. Furthermore, the method developed in the present chapter will play an important role in the solution of the full nonlinear problem, which will be discussed in Chapter 6.

In this chapter, we introduce a new mesh system which allows an accurate representation of the Wigley hull in a Cartesian grid. Since the region is no longer rectangular, as in the thin ship case, is is necessary to modify the fast Poisson solver by using the capacitance matrix technique. This modification method allows the optimized elliptic solver of Chapter 3 and Appendix B to be used, even when a Neumann boundary condition must be implemented on an arbitrary curvilinear surface described in Cartesian coordinates. As a test example, the numerical solution to a simple boundary value problem, which possesses an analytical solution, demonstrates the accuracy of the present mesh system and solution technique. The method is then applied to the problem of a translating Wigley hull in the presence of a linearized free surface. The hull wave profiles and wave resistance values obtained are compared to the previous thin

ship results as well as to experiments. Based upon the numerical and experimental evidence, conclusions regarding the validity of the linearization of the free surface conditions in this case are drawn.

The Mesh System

The success of the optimized direct method for the thin ship problem motivates one to consider an immediate application of the technique to the Neumann-Kelvin problem. However, the presence of the exact Wigley hull introduces the necessity for non-Cartesian (i.e., curvilinear) mesh lines as a means of accommodating the hull geometry. Unfortunately, fast elliptic solvers, including the Fourier series method, cannot be directly applied in this situation. One alternative approach, proposed by Chan [23], is to use the mesh system shown schematically in Fig. 5.1. The physical (x,y) plane uses a body fitted coordinate system throughout the entire domain to accommodate the hull geometry. A transformation is then made to the computational (x',y') plane, which is represented in this figure by a uniform mesh with constant grid intervals. The resulting elliptic equation is extremely tedious to deal with, and its finite difference analog must be solved by SOR. The slow convergence rate coupled with the awkwardness of the field equation are considered to be the extreme disadvantages of this approach.

In the present section, we shall introduce the new concept of the locally body fitted mesh system, which is shown for the Wigley hull in Fig. 5.2. This type of mesh system is considered to be more appropriate for application to the ship wave problem. As in Chan's approach, the hull becomes a coordinate plane so that the Neumann condition can be applied at the proper location. This requires that the Laplace equation be transformed to account for the derivatives being computed on the curvilinear hull surface. Contrary to Chan's approach, however, we continue to use the Cartesian mesh system away from the hull so that the form of the Laplace equation does not change. This means that in most of the domain, the finite difference form of the Laplace equation will remain the same as that in the thin ship case. Modification of the

fast Poisson solver is required only for a few of the equations in the finite difference system (i.e., those on and near the Wigley hull) which are perturbed due to the locally body fitted coordinate transformation. This approach for implementing the exact hull boundary condition thus minimizes the awkwardness of the elliptic field equation by using the locally body fitted concept, and at the same time it maximizes the solution efficiency and accuracy by retaining the use of the fast Poisson solver.

Since the numerical experiments for the thin ship problem demonstrated that the domain size 4.95 x 2.0 x 1.0 was sufficient to approximate a much longer and deeper computational region, the grid system parameters for Mesh II (Table 4.2) will be used in the present application. In anticipation of the extension to the full nonlinear case, however, we find it necessary to redefine the vertical mesh spacing near the free surface so that finite amplitude waves can be readily accommodated without allowing any mesh lines to intersect. To meet this requirement, we choose the first interior mesh points below the free surface to be located at $z = -h/3$, i.e., at a vertical position which is equal to one third of the draft of the ship (Fig. 5.2a). The constant vertical spacing on the remaining portion of the hull is now Δz = h/5.5. Furthermore, the new vertical transition coordinates for smoothly matching the constant (but unequal) grid intervals on the hull and far below the hull are given in Table 5.2. We note that only the vertical grid spacing is modified and that all remaining aspects of the mesh system described by Eqs. (4.2) for Mesh II remain in force.

The motivation for choosing the first interior mesh points to be placed at $z = -h/3$ is that at the lower or moderate Froude numbers, the free surface height will not be large enough to allow the possibility of intersecting mesh lines. This will only be a concern when the free surface is actually allowed to move (Chapter 6). However, the new vertical spacing is introduced here for the Neumann-Kelvin problem so that a more consistent comparison with the nonlinear results can be made. Furthermore, we wish to demonstrate the accuracy afforded by the representation of the hull geometry and the flow variables in the present mesh system before

applying it to the physical problems of interest.

Vertical Mesh Spacings	
k	z
24	−0.4000
25	−0.2500
26	−0.1750
27	−0.1250
28	−0.1100
29	−0.1000
30	−0.0900
31	−0.0824
32	−0.0748
33	−0.0673
34	−0.0597

Table 5.1 The values of z vs. k in the vertical mesh transition region used for the nonlinear calculations. This region is again defined for values of k in the range $24 \leqslant k \leqslant 34$.

The Locally Body Fitted Coordinate Transformation

In this section, we shall consider the transformation of the Laplace equation to a locally body fitted coordinate system in which the Wigley hull becomes a coordinate plane. This is done solely for the purpose of facilitating the implementation of the Neumann condition on the exact hull surface. We shall see that the form of the second order derivatives of ϕ in the Laplace equation will be modified by the transformation in order to take account of the fact that the grid lines now conform to a curvilinear surface.

We first consider the following change of variables :

$$\begin{aligned} x' &= x \\ y' &= y - f(x,z) \\ z' &= z \\ t' &= t \end{aligned} \tag{5.1}$$

The (x',y',z') coordinate system is body fitted, i.e., movement in the x'- or z'-directions is along the surface of the body defined by $y = f(x,z)$. Applying the chain rule to Eqs. (5.1), we find the following relations for the derivatives of any function Q :

$$\begin{aligned} Q_x &= Q_{x'} - f_x Q_{y'} \\ Q_y &= Q_{y'} \\ Q_z &= Q_{z'} - f_z Q_{y'} \\ Q_t &= Q_{t'} . \end{aligned} \tag{5.2}$$

Using these rules of differentiation for ϕ, we transform the Laplace equation into

$$\phi_{x'x'} + \gamma_1^2 \phi_{y'y'} + \phi_{z'z'} - 2f_x \phi_{y'x'} - 2f_z \phi_{y'z'} - \gamma_2 \phi_{y'} = 0 , \tag{5.3}$$

where $\gamma_1 = (1 + f_x^2 + f_z^2)^{1/2}$ and $\gamma_2 = (f_{xx} + f_{zz})$. This equation is to be applied only on the Wigley hull surface.

The cross derivatives appearing in this equation (i.e., $\phi_{y'x'}$ and $\phi_{y'z'}$) are rather troublesome since their finite difference approximations involve several additional unknowns which lie outside of the domain. Since these additional unknowns cannot be easily eliminated from the resulting linear system, it is desirable to remove these cross derivatives from the transformed Laplace equation. This can be accomplished by using the exact hull condition, which we recall from Chapter 2 is

$$-f_x \phi_x + \phi_y - f_z \phi_z = U_s f_x \tag{2.11}$$

or, after applying the transformation of Eqs. (5.2), becomes

$$\phi_{y'} = \frac{1}{\gamma_1^2} [\gamma_1^2 \phi_n + f_x \phi_{x'} + f_z \phi_{z'}] \tag{5.4}$$

on $y = f(x,z)$ or $y' = 0$. The quantity ϕ_n is the perturbed fluid velocity normal to the hull and is equal to $\frac{U_s f_x}{\gamma_1^2}$. We now compute $\phi_{y'x'}$ and $\phi_{y'z'}$ from Eq. (5.4) and, together with Eq. (5.4), substitute these expressions into Eq. (5.3) to obtain

$$a_{11}\phi_{x'x'} + a_{22}\phi_{y'y'} + a_{33}\phi_{z'z'} + a_{13}\phi_{x'z'} + a_1\phi_{x'} + a_3\phi_{z'} = r_1 , \tag{5.5}$$

in which the coefficients are defined as

$$a_{11} = 1 - \frac{2f_x^2}{\gamma_1^2}$$

$$a_{22} = \gamma_1^2$$

$$a_{33} = 1 - \frac{2f_z^2}{\gamma_1^2}$$

$$a_{13} = -\frac{4f_x f_z}{\gamma_1^2} \tag{5.6}$$

$$a_1 = -\left[\frac{\gamma_2 f_x}{\gamma_1^2} + 2f_x\left(\frac{f_x}{\gamma_1^2}\right)_x + 2f_z\left(\frac{f_x}{\gamma_1^2}\right)_z\right]$$

$$a_3 = -\left[\frac{\gamma_2 f_z}{\gamma_1^2} + 2f_x\left(\frac{f_z}{\gamma_1^2}\right)_x + 2f_z\left(\frac{f_z}{\gamma_1^2}\right)_z\right]$$

$$r_1 = \gamma_2\phi_n + 2f_x\phi_{nx} + 2f_z\phi_{nz} .$$

Equation (5.5) represents the transformed Laplace equation which is to be applied at the exact location of the Wigley hull. We note that the cross derivatives $\phi_{y'x'}$ and $\phi_{y'z'}$ have been eliminated at the expense of introducing the term $\phi_{x'z'}$. This situation is acceptable since this derivative can be approximated without introducing any unknowns outside of the computational region. We also note that this equation reduces identically to the original (untransformed) Laplace equation in the absence of the locally body fitted coordinate transformation. We expect the finite difference form of Eq. (5.5) to be similar to that of the original Laplace equation and therefore to be a slightly perturbed form of the thin ship linear system. As we shall see in the next section, the exact hull linear system has some important differences.

Implementation of the Boundary Conditions

The Dirichlet conditions on the free surface as well as the Neumann conditions on all of the boundaries except the hull are implemented in exactly the same way as for the thin ship

case. Therefore, in this section, we shall explicitly consider only the implementation of the exact hull boundary condition as well as of the linearized free surface conditions at the points of intersection with the exact hull. The procedure is, in principle, precisely the same as that for the thin ship case. We first discretize the transformed Laplace equation (Eq. (5.5)) and then eliminate the single unknown outside of the domain using the discretized form of the hull boundary condition (Eq. (5.4)). By contrast, this procedure is illustrated schematically in Fig. 5.3a for the thin ship case. The unknown value $\phi_{i,0,k}$, which is located a distance Δy outside of the domain, is eliminated from the finite difference system by using the thin ship boundary condition. In the exact hull case, however, the presence of the Wigley hull (Fig. 5.3b) alters the y-spacing so that the grid intervals are no longer constant in this direction. It is therefore necessary to use finite difference formulas modified for nonuniform spacing when computing $\phi_{y'y'}$ and $\phi_{y'}$ on the exact hull. Using the standard Taylor series approximations for nonuniform grid intervals, we find the following finite difference representations :

$$\phi_{y'y'} \approx \alpha_{i,k}\phi_{i,0,k} - (\alpha_{i,k} + \beta_{i,k})\phi_{i,1,k} + \beta_{i,k}\phi_{i,2,k} \tag{5.7}$$

and

$$\phi_{y'} \approx \gamma_{i,k}\phi_{i,0,k} - (\gamma_{i,k} + \delta_{i,k})\phi_{i,1,k} + \delta_{i,k}\phi_{i,2,k} , \tag{5.8}$$

in which the coefficients $\alpha_{i,k}$, $\beta_{i,k}$, $\gamma_{i,k}$ and $\delta_{i,k}$ are defined as

$$\begin{aligned}
\alpha_{i,k} &= \frac{1}{\Delta y(\Delta y + f_{i,k})} \\
\beta_{i,k} &= \frac{1}{\Delta y(\Delta y - f_{i,k})} \\
\gamma_{i,k} &= -\frac{(\Delta y - f_{i,k})}{2\Delta y(\Delta y + f_{i,k})} \\
\delta_{i,k} &= \frac{(\Delta y + f_{i,k})}{2\Delta y(\Delta y - f_{i,k})} .
\end{aligned} \tag{5.9}$$

Note that we use the shorthand notation $f_{i,k}$ to represent $f(x_i, z_k)$, etc. Now, since $\phi_{i,0,k}$ lies outside of the domain, we eliminate it from Eqs. (5.7) and (5.8) to obtain

$$\phi_{y'y'} \approx -\epsilon_{i,k}\,\phi_{i,1,k} + \epsilon_{i,k}\,\phi_{i,2,k} + \frac{\alpha_{i,k}\,\phi_{y'}}{\gamma_{i,k}}, \tag{5.10}$$

where $\epsilon_{i,k} = \beta_{i,k} - \dfrac{\alpha_{i,k}\,\delta_{i,k}}{\gamma_{i,k}}$. The derivatives $\phi_{x'x'}$ and $\phi_{x'}$ in Eq. (5.5) are computed using the standard second order finite difference expressions, whereas $\phi_{z'z'}$, $\phi_{x'z'}$ and $\phi_{z'}$ require nonuniform formulas due to the unequal spacing near the free surface. Using Eqs. (5.4) and (5.10) to eliminate $\phi_{y'y'}$ and $\phi_{y'}$, we obtain the final discretized form of Eq. (5.5) as

$$\begin{aligned} &a_{11}^{-}\phi_{i-1,1,k} + a_{11}^{+}\phi_{i+1,1,k} + a_{33}^{-}\phi_{i,1,k-1} + a_{33}^{+}\phi_{i,1,k+1} + a_{22}\epsilon_{i,k}\,\phi_{i,2,k} + \\ &a_{13}^{-}(\phi_{i+1,1,k-1} - \phi_{i-1,1,k-1}) - (a_{13}^{+}a_{13}^{+})(\phi_{i+1,1,k} - \phi_{i-1,1,k}) + \\ &a_{13}^{+}(\phi_{i+1,1,k+1} - \phi_{i-1,1,k+1}) - a_0\phi_{i,1,k} = r'_1 \end{aligned} \tag{5.11}$$

in which we define

$$a_{11}^{\pm} = \frac{a_{11}}{\Delta x^2} \pm \frac{1}{2\Delta x}\left[a_1 + \frac{\alpha_{i,k}}{\gamma_{i,k}} f_x\right],$$

$$a_{33}^{+} = \frac{2a_{33} + a_3 h_{k-1}}{\Delta z^{+}}$$

$$a_{33}^{-} = \frac{2a_{33} - a_3 h_k}{\Delta z^{-}}$$

$$a_{13}^{+} = \frac{a_{13} h_{k-1}}{2\Delta x\,\Delta z^{+}}$$

$$a_{13}^{-} = -\frac{a_{13} h_k}{2\Delta x\,\Delta z^{-}}$$

$$\Delta z^{+} = h_k\,(h_k + h_{k-1})$$

$$\Delta z^{-} = h_{k-1}(h_k + h_{k-1})$$

$$h_k = z_{k+1} - z_k$$

$$\phi_n = \frac{U_s f_x}{\gamma_1^2}.$$

Equation (5.11) represents the modified (transformed) Laplace equation which is to be applied on the curvilinear surface of the Wigley hull (i.e., only for $31 \leqslant i \leqslant 50$, $j = 1$ and $34 \leqslant k \leqslant 39$). Since the hull contains 20 x 6 unknowns in the x- and z-directions, respec-

tively, we see that there are actually 120 perturbed finite difference equations of the form (5.11). In addition, the equations immediately adjacent to the hull (i.e., at $j = 2$ in Fig. 5.3b) must be modified since the y distance to the hull is not the constant Δy. These 120 additional finite difference equations are obtained simply by using a nonuniform grid spacing formula for ϕ_{yy} in the Laplace equation. No other changes or transformations are necessary. It is thus found that the total number of perturbed finite difference equations is 240. Therefore, the capacitance matrix system, described in Appendix C, will be of order 240.

We remarked at the end of the last section that the two linear systems which include the thin ship and exact hull boundary conditions are quite different. In fact, there are several crucial differences between these two linear systems. The exact hull system is not symmetric nor is it diagonally dominant, whereas the thin ship system is both symmetric as well as diagonally dominant. Furthermore, the diagonal elements in the exact hull matrix change sign on the surface of the ship as the keel is approached from above. All of these conditions are extremely detrimental to the use of iterative methods for the exact hull case since there is no guarantee that the solution will converge. In fact, an iterative procedure, based on the optimized fast Poisson solver, was originally set up as a means of handling the exact hull boundary condition. This approach was unsuccessful since the iterations diverged quite rapidly. Fortunately, these properties of the exact hull linear system do not affect the use of the capacitance matrix technique since this approach does not depend on the question of convergence. It is therefore important to keep in mind that the exact hull linear system is not amenable to the use of iterative methods and that the present direct approach appears to be the only viable alternative.

We now consider the modification of the linearized free surface boundary conditions under the transformation in Eqs. (5.2). These equations will be used only when applying the boundary conditions at the intersection of the free surface with the exact hull. Employing the appropriate relations for the derivatives of ϕ and η from Eqs. (5.2), we obtain the transformed

linearized free surface conditions (Eqs. (2.12) and (2.13)) as

$$\eta_{t'} + U_s \eta_{x'} = \phi_{z'} - f_z \phi_{y'} \tag{5.13}$$

and

$$\phi_{t'} + U_s \phi_{x'} - f_x \phi_{y'} = -\eta / Fr^2 . \tag{5.14}$$

It then follows from Eqs. (5.13) and (5.14) that the following definitions hold for u^*, v^* and Δ^* in the time marching scheme of Eq. (3.3) :

Dynamic condition for ϕ :

$$u^* = U_s$$

$$v^* = -f_x$$

$$\Delta^* = -\eta / Fr^2$$

Kinematic condition for η :

$$u^* = U_s$$

$$v^* = 0$$

$$\Delta^* = \phi_{z'} - f_z \phi_{y'}$$

These special definitions for u^*, v^* and Δ^* are necessary because of the locally body fitted coordinate system. At any free surface location away from the hull, the previous definitions from Chapter 4 (i.e., those for $f_x = f_z = 0$) remain in effect. Since the new definitions are to be used only at the intersection of the Wigley hull with the free surface, we must remember to compute $\phi_{y'}$ according to the hull boundary condition (Eq. (5.4)).

A Numerical Test Problem

In order to conclusively establish the solution accuracy provided by the present locally body fitted mesh system, we compute the numerical solution to a simple, nonphysical boundary value problem and compare the results with the analytical solution. This test problem is for-

mulated as follows. Consider a region R which is defined by

$$0 \leqslant x \leqslant \pi$$

$$0 \leqslant y \leqslant \frac{\pi}{2} \tag{5.15}$$

$$-1 \leqslant z \leqslant 0 .$$

We seek a function $\psi(x,y,z)$ which satisfies

$$\psi_{xx} + \psi_{yy} + \psi_{zz} = 0 \tag{5.16}$$

in R, subject to the conditions

$$\psi_x = 0 \quad \text{on } x = 0,\pi ,$$

$$\psi_y = 0 \quad \text{on } y = 0,\frac{\pi}{2} ,$$

$$\psi_z = 0 \quad \text{on } z = -1 , \tag{5.17}$$

$$\psi = \cosh(4\sqrt{2})\cos 4x \cos 4y \quad \text{on } z = 0 ,$$

$$\gamma_1^2 \psi_n = f_x \cosh[4\sqrt{2}(1+z)]\sin 4x \cos 4y - \cosh[4\sqrt{2}(1+z)]\cos 4x \sin 4y -$$

$$f_z \sqrt{2}\sinh[4\sqrt{2}(1+z)]\cos 4x \cos 4y \quad \text{on } y = f(x,z) .$$

The function $f(x,z)$ again describes the Wigley hull, which may be redefined for the region R as

$$f(x,z) = \frac{b}{2}[1 - 4(x - x_c)^2][1 - (z/h)^2] \tag{5.18}$$

for $x_c - \frac{1}{2} \leqslant x \leqslant x_c + \frac{1}{2}$ and $-h \leqslant z \leqslant 0$. The quantities b, h and x_c are the beam, draft and the x position of midship and have the values b = 0.10, h = 0.0625 and $x_c = \frac{65\pi}{128} + \frac{1}{2}$. The analytical solution to this boundary value problem is simply

$$\psi(x,y,z) = \cosh[4\sqrt{2}(1+z)]\cos 4x \cos 4y . \tag{5.19}$$

Using the locally body fitted mesh system and the modified direct solution technique described in Appendix C, we compute the numerical solution to this boundary value problem. The grid for this test example is chosen to be 65 x 26 x 20, with $\Delta x = \pi/64$ and $\Delta y = \pi/50$.

The z-distribution of mesh points previously discussed for application to the Neumann-Kelvin is also used in this example. We are particularly interested in the numerical solution for ψ on the actual hull surface. We thus compare this solution against the analytical solution (Eq. (5.19)) for two values of z (i.e., $z = -0.0208$ and -0.0597) in Figs. 5.4 and 5.5. These figures show the solution for ψ on the Wigley hull as a function of the longitudinal coordinate, $(x - x_c)/l$. Excellent agreement between the solutions is obtained, and we therefore conclude that the present mesh system is able to accurately resolve the correct solution on a curvilinear surface such as the Wigley hull. Furthermore, the method of treating the exact hull boundary condition by transforming the Laplace equation is also seen to be appropriate. We also conclude that the capacitance matrix technique, used to modify the fast Poisson solver of Appendix B, is an effective way to accurately handle the linear system arising from the discretization of the Laplace equation on the Wigley hull. We shall now proceed with the application of the present method and mesh system to the problem of a translating Wigley hull with a linearized free surface.

Numerical Results for the Neumann-Kelvin Problem

In this section, we shall discuss the wave profile and wave resistance results obtained for the translating Wigley hull under the approximations associated with the Neumann-Kelvin problem. The numerical experiments described in Chapter 4 for the thin ship case provide the guidelines for the operating conditions under which the present results are obtained. Specifically, we use the 4.95 x 2.0 x 1.0 domain size with second order ϕ_z differencing on the free surface and compute the solutions to $t = 9.0$. We also use the simple open boundary condition which was found to be so effective for the thin ship case. The boundary condition implementation for the Laplace equation has already been discussed, and we initialize the flow field and gradually start the Wigley hull in exactly the same manner as for the thin ship problem. The calculation of the wave resistance in the present case is the same as for the thin ship case, with the exception that the linearized expression for the pressure on the hull (Eq. (4.9)) is

subject to the coordinate transformation of Eqs. (5.2).

The first result to be discussed is the comparison of the exact hull wave profiles with the previously obtained thin ship profiles. This comparison is made so as to emphasize the differences between the exact hull and thin ship boundary conditions and is in no way meant to imply that one solution is better than the other. These wave profiles along the Wigley hull are shown in Figs. 5.6-5.8 for the Froude numbers 0.266, 0.350 and 0.452, respectively. For all three Froude numbers, the agreement is seen to be reasonably good in the bow region where the thin ship assumption for the Wigley hull is locally valid. Further downstream, however, the exact hull boundary condition shows a tendency to excite higher frequency components in the solution, with the frequency of the waves increasing as the Froude number decreases. This observation suggests that the exact hull boundary condition exerts more influence on the solution only downstream of those points on the Wigley hull at which the thickness begins to increase. This is what we might intuitively expect for any hull form which is not strictly a thin ship.

In Figs. 5.9-5.11, we compare the Neumann-Kelvin profiles for the three Froude numbers to an experiment by Shearer and Cross [45]. The bow waves are seen to be in qualitative agreement with the experimental profiles. The wave oscillations present in the numerical calculation are not observed in the experiment, but there are several good reasons for this. It is unclear to what extent the fluid viscosity affects the wave profiles, and it is thus possible that the higher frequency components are not damped out sufficiently in a model which ignores the viscous effect. It is more likely, however, that the flaws are in the Neumann-Kelvin problem itself since this full hull form is not allowed to make any physical waves whatsoever. That is, the linearization of the free surface conditions and the application of these conditions on the plane $z = 0$ may be considered to be inappropriate when the exact hull condition is applied. These conclusions, of course, depend to a significant degree upon the reliability of the physical experiments. For the ship wave problem, such experiments are extremely difficult to perform

and could be inaccurate, so one should not place absolute faith in them. They should rather be used as a guideline, along with the numerical calculations.

The final result for this problem is the wave resistance vs. Froude number curve. The wave resistance is computed for eight Froude numbers, as shown in Fig. 5.12. The results for C_w shown in this figure exhibit two definite peaks around Fr = 0.233 and 0.350. This trend is not observed in the experiment by Ju [44], which is believed to at least have defined the qualitative features of the Wigley hull wave resistance. In order to explain the behavior of the numerical solution relative to the experiment, we must again question the validity of the Neumann-Kelvin problem. We expect that for very low Froude numbers, the wave resistance could be reasonably close to the experiment since in this range the linearization of the free surface conditions is perhaps acceptable. Unfortunately, at the lower Froude numbers, the boundary layer is thicker and the wake is wider than in the higher Froude number range. These phenomena clearly affect the wave resistance, and it is therefore difficult to judge this inviscid numerical model by comparing the results to experiments.

On the other hand, for higher Froude numbers, when fairly large waves are formed, the linearization of the free surface conditions breaks down, but the viscous effects on the wave resistance become relatively less important. We therefore do not expect the Neumann-Kelvin problem to be applicable in the higher Froude number range, so it is again difficult to assess the numerical results for the wave resistance. There do seem to be stretches along this curve, however, on which C_w agrees, perhaps coincidentally, with the experiment. It may be that the Neumann-Kelvin problem is applicable for certain Froude number ranges, but it is impossible to predict these ranges in advance unless a general trend is known for all ship models. It does seem possible that the observed peaks in C_w may be due ultimately to the free surface linearization, but this point will require more careful consideration in the next chapter when we extend the method to solve the full nonlinear ship wave problem.

Summary

In this chapter, the new concept of the locally body fitted mesh system was introduced for application to the Neumann-Kelvin problem. The body fitted transformation for both the hull and free surface boundary conditions was described in detail. As a result of this local transformation, a few of the finite difference equations representing the Laplace equation had to be altered. Since iterative methods for the resulting exact hull linear system cannot be expected to converge, a modification of the optimized direct Laplace solver was implemented, and the capacitance matrix technique was used for this purpose. The solution algorithm was then tested on a simple boundary value problem in a region which contained the Wigley hull. The results of this test demonstrated the accuracy of the locally body fitted mesh system as well as of the optimized direct method. The application of the modified method to a translating Wigley hull was then carried out, and the results for the wave profiles and the wave resistance were discussed. It was generally found that the Neumann-Kelvin problem may be applicable for specified ranges of Froude numbers but that one cannot easily predict these values *a priori*. In addition, there are open questions as to the influence of viscosity on the wave profiles and the wave resistance, and this area should be investigated further.

Although the Neumann-Kelvin problem is not the final solution for ship wave resistance calculations, its significance in relation to the development of a general method for the nonlinear ship wave problem cannot be overemphasized. The finite difference approach can be successful only if it is able to accommodate the geometry accurately and to solve the field equation efficiently. The development and careful study of a numerical method which possesses these requirements is thus considered to be a priority in the present work. The final priority, however, is the implementation of the full nonlinear free surface boundary conditions. Therefore, in the next chapter, the solution method developed for the Neumann-Kelvin problem will be used in an iterative procedure which is set up to satisfy the exact nonlinear free surface conditions at their proper locations.

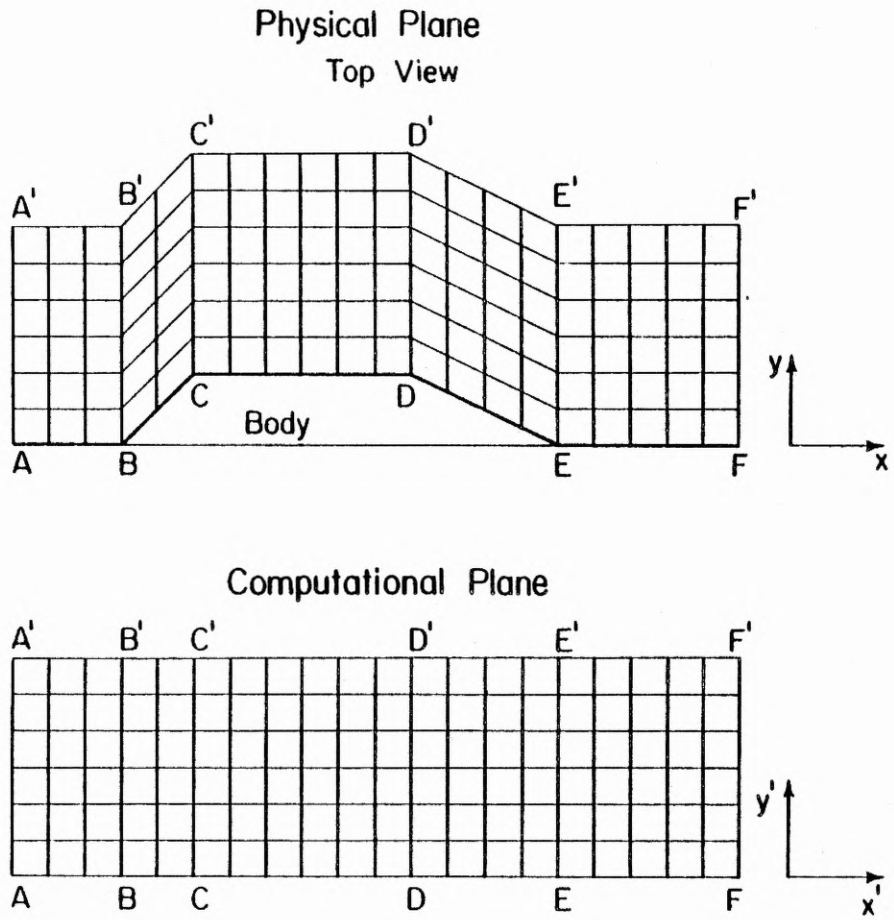

Figure 5.1 Comparison of the physical and computational planes for a body fitted coordinate system which is used throughout the entire domain. The mesh lines in the physical plane accommodate the body geometry but map into uniform intervals in the computational plane.

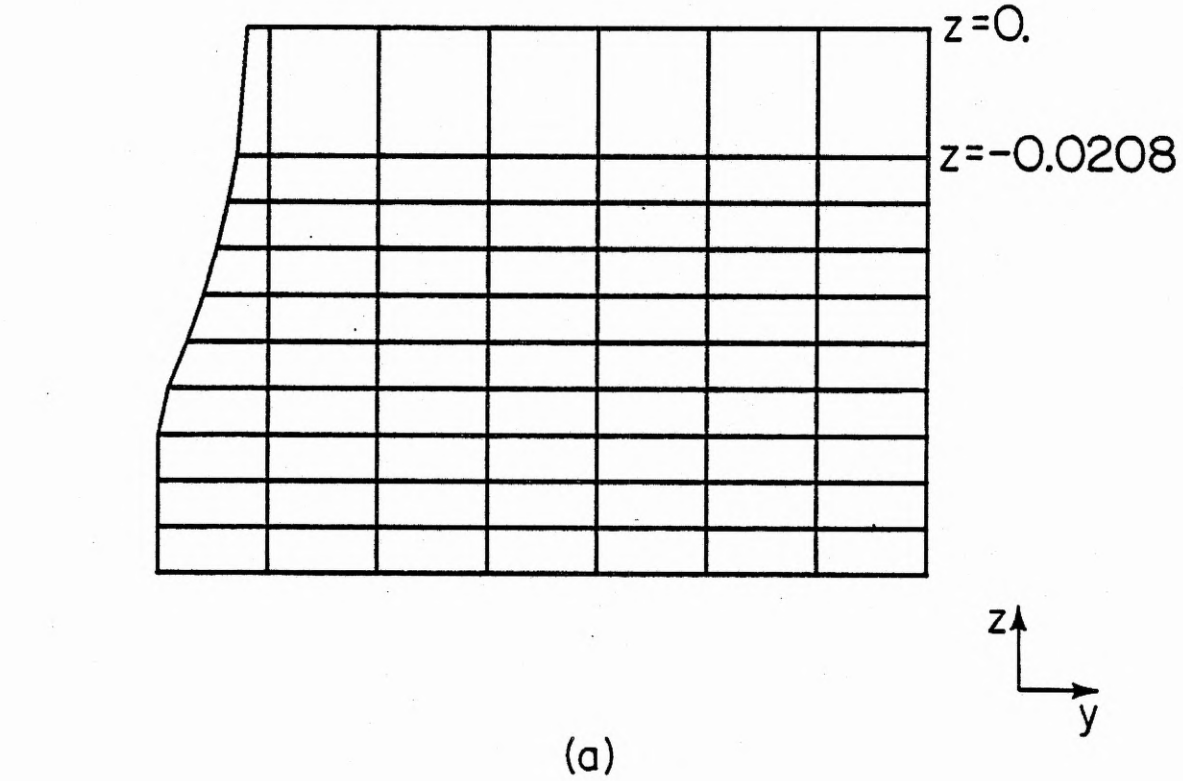

(a)

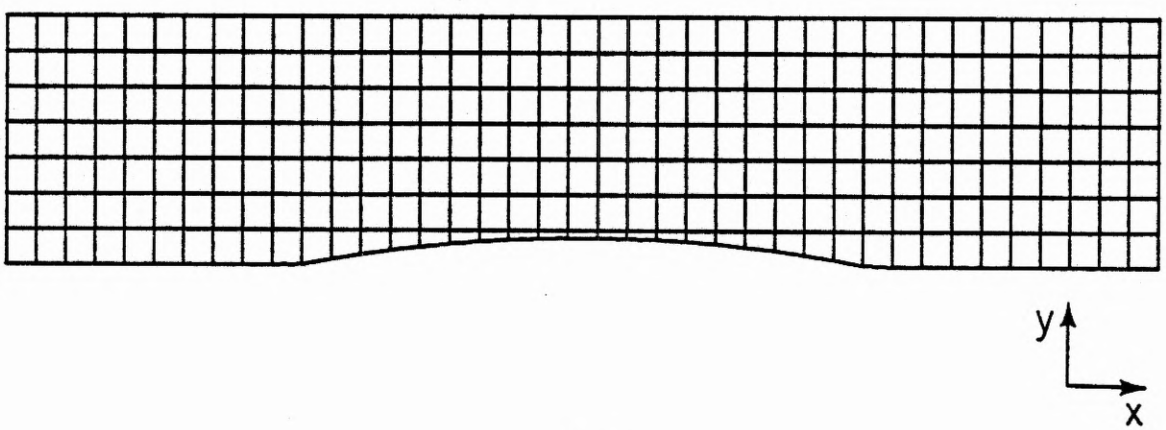

(b)

Figure 5.2 Two views of the locally body fitted mesh system for the Wigley hull. Note that only the finite difference equations on and near the hull are perturbed due to the coordinate transformation.
(a) A side view in the (y,z) plane showing the hull accommodation.
(b) A top view in the (x,y) plane.

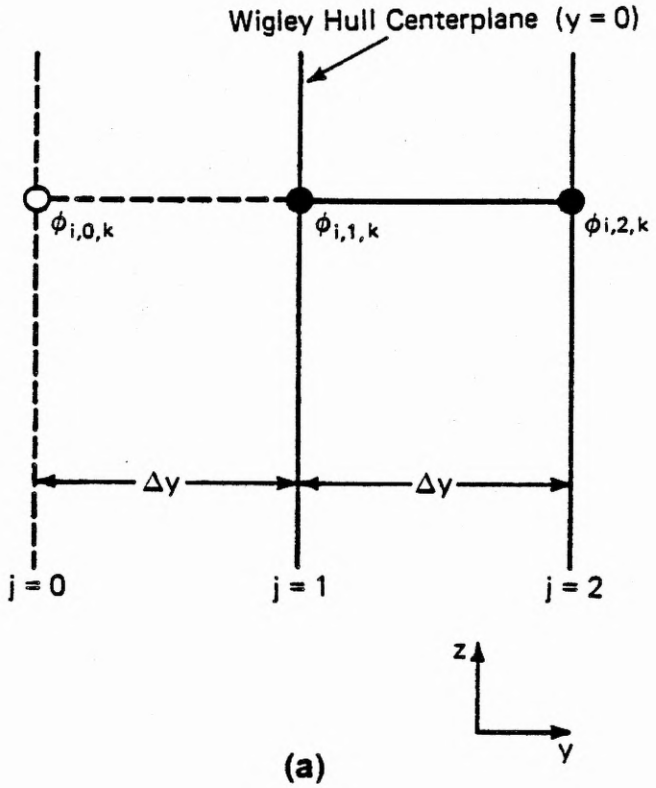

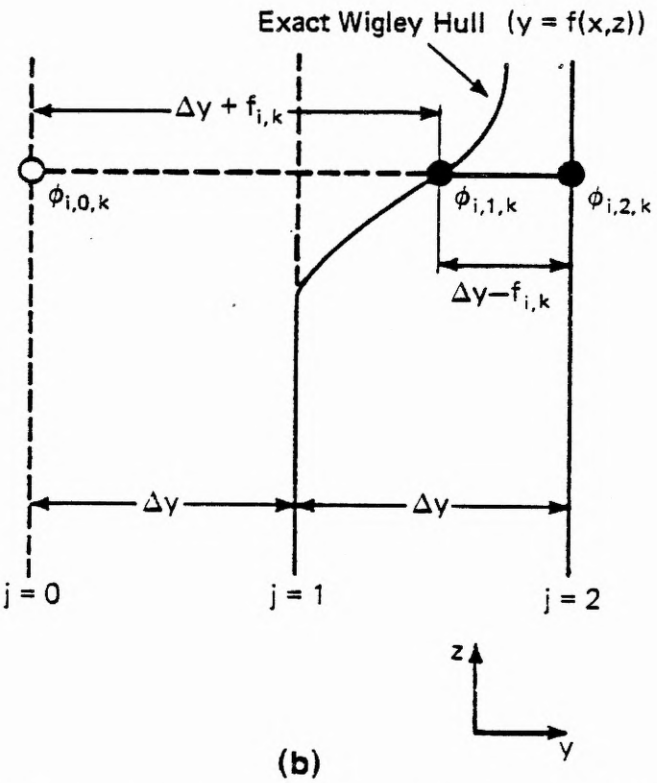

Figure 5.3 Comparison of the thin ship and exact hull mesh systems and their relationship to the implementation of the Neumann boundary condition.
(a) The unknown $\phi_{i,0,k}$ is located a distance Δy outside of the domain and is easily eliminated from the equations by using the thin ship condition.
(b) The unknown $\phi_{i,0,k}$ in the locally body fitted mesh system is no longer located a uniform distance outside of the domain. Special derivative formulas must therefore be used in order to eliminate it from the system of equations.

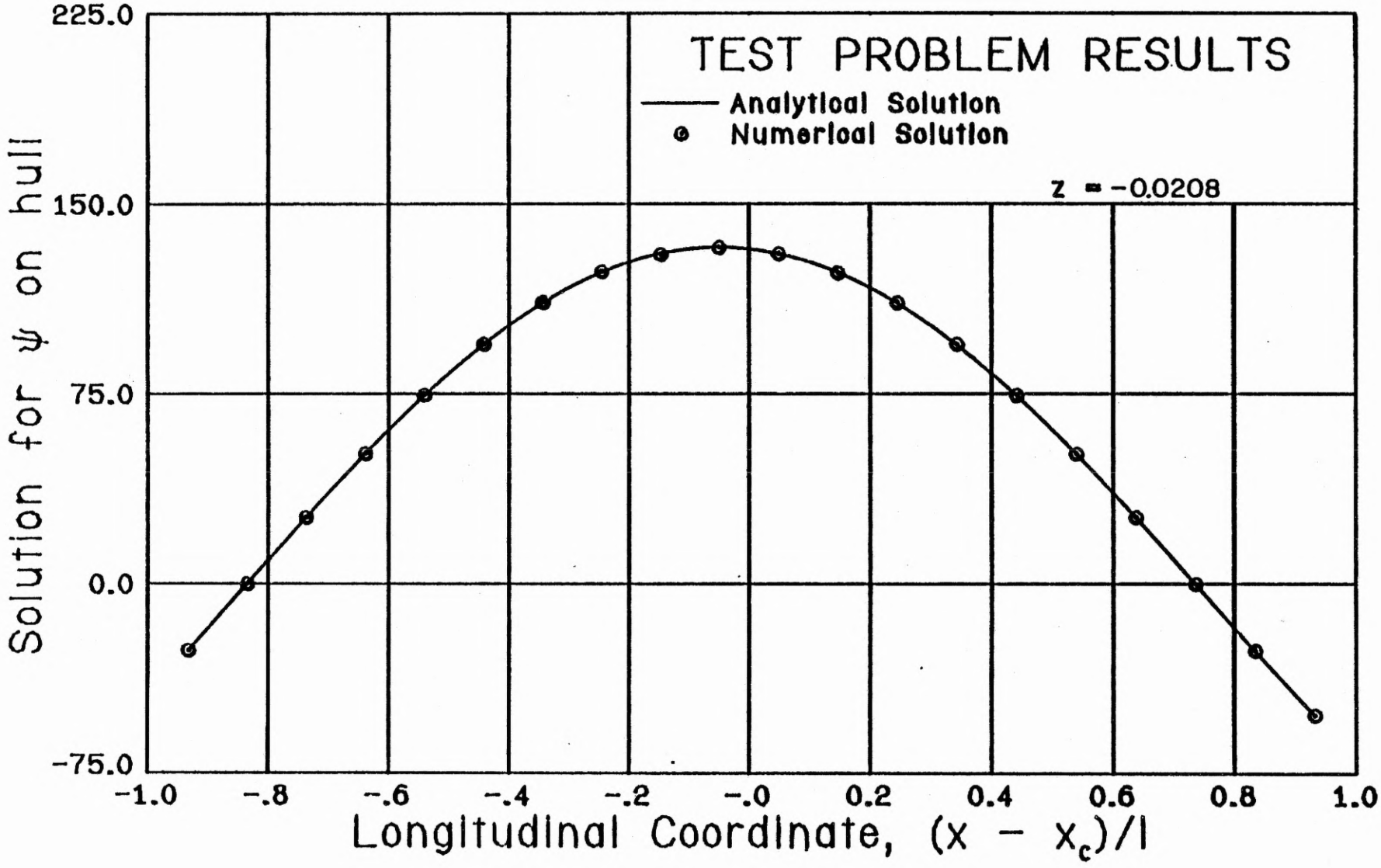

Figure 5.4 Comparison of the analytical and numerical solutions for the boundary value problem which tests the mesh system and the solution technique. The solution is plotted along the Wigley hull at $z = -0.0208$.

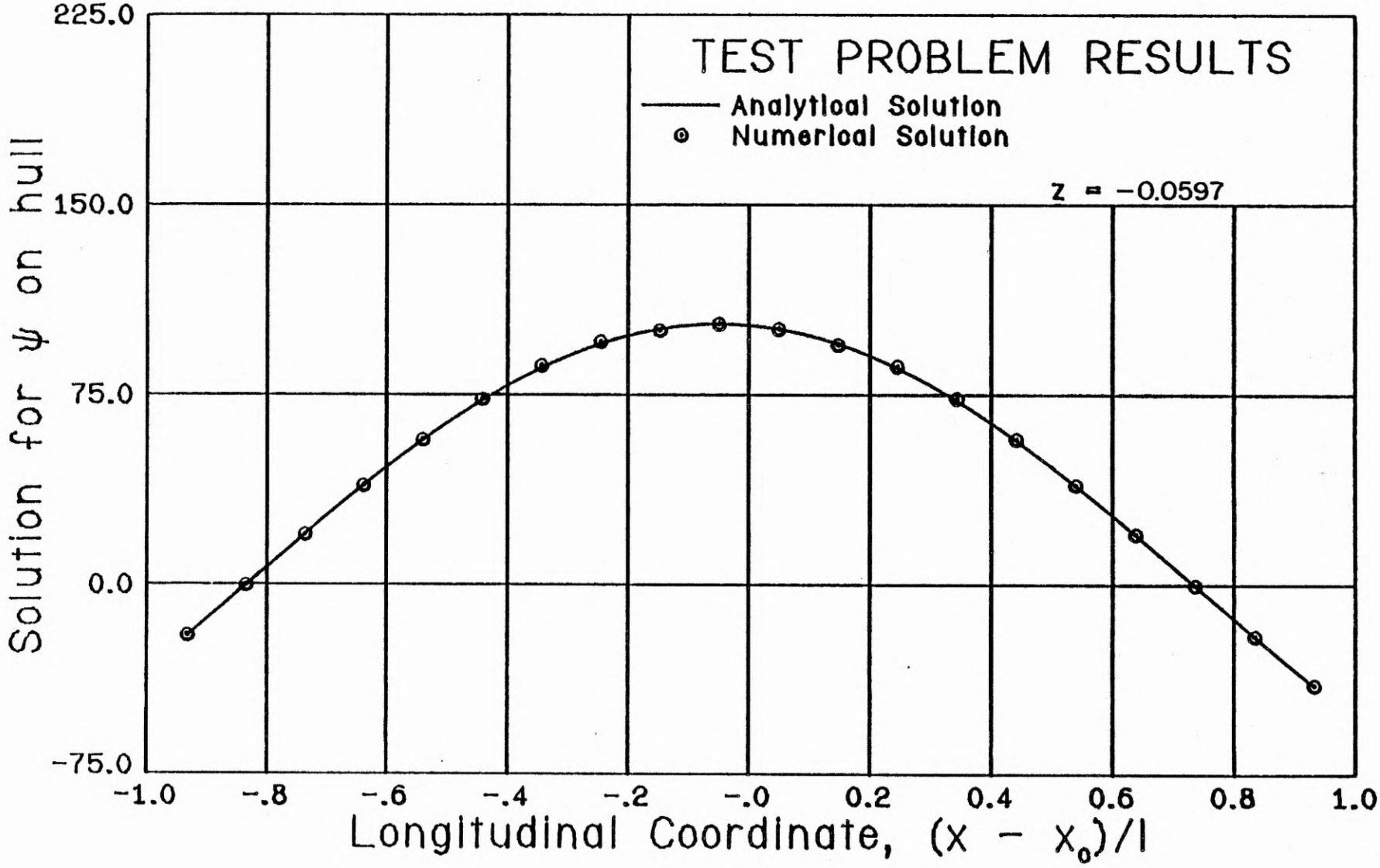

Figure 5.5 Comparison of the analytical and numerical solutions for the boundary value problem which tests the mesh system and the solution technique. The solution is plotted along the Wigley hull at $z = -0.0597$.

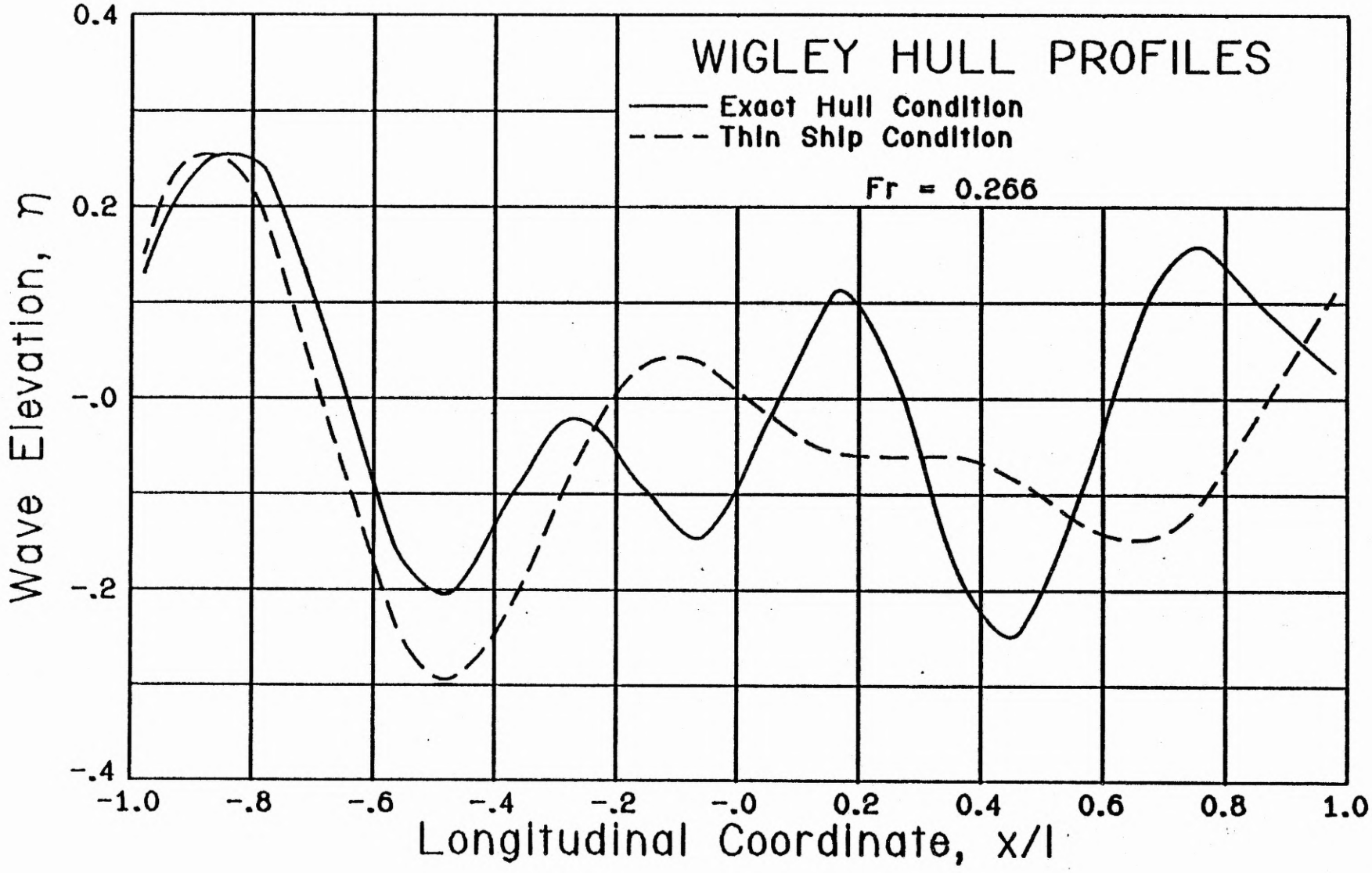

Figure 5.6 Comparison of the Wigley hull wave profiles for the thin ship and the exact hull cases (second order ϕ_z differencing) for $Fr = 0.266$.

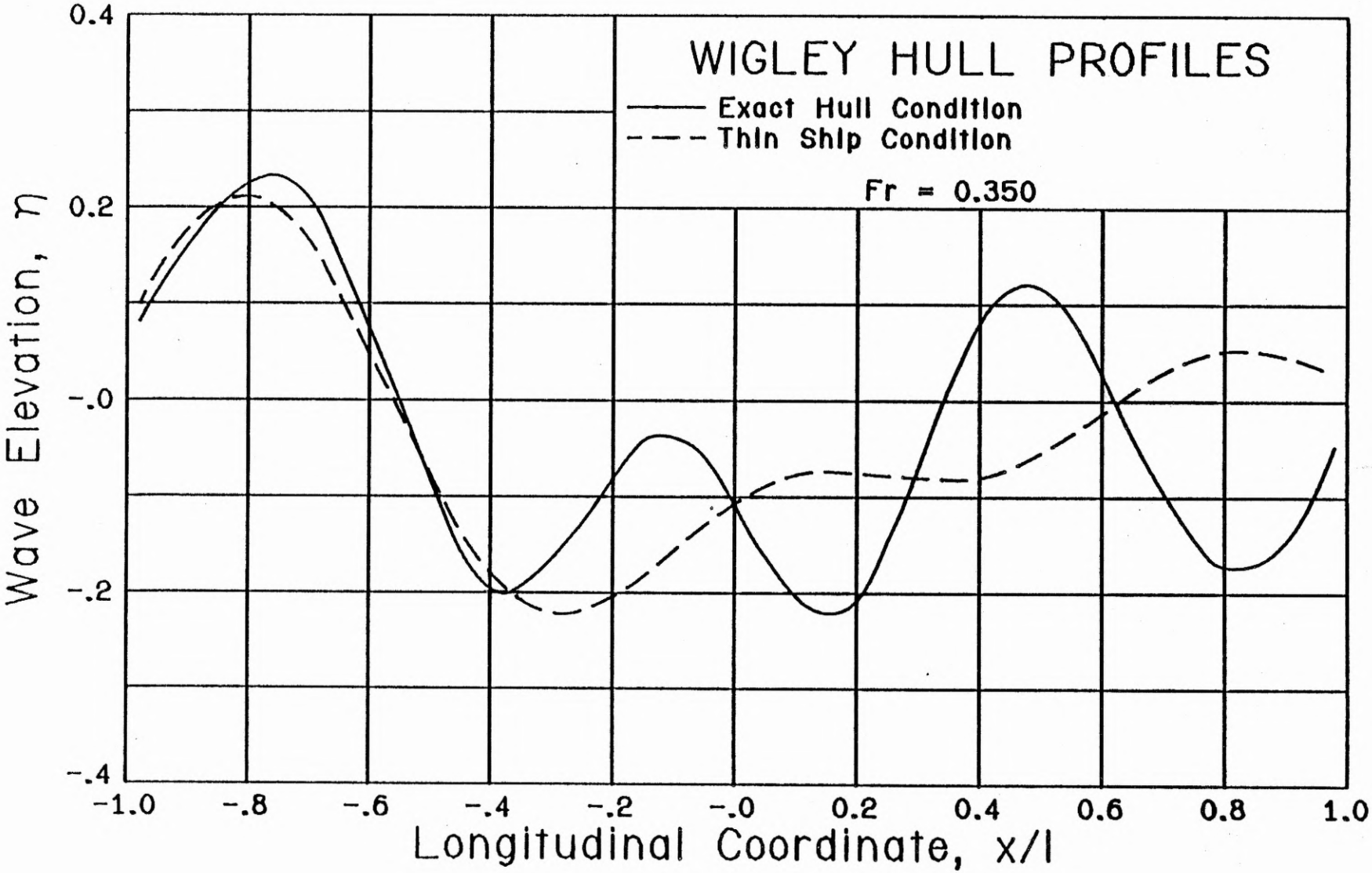

Figure 5.7 Comparison of the Wigley hull wave profiles for the thin ship and the exact hull cases (second order $\phi_{\bar{z}}$ differencing) for $Fr = 0.350$.

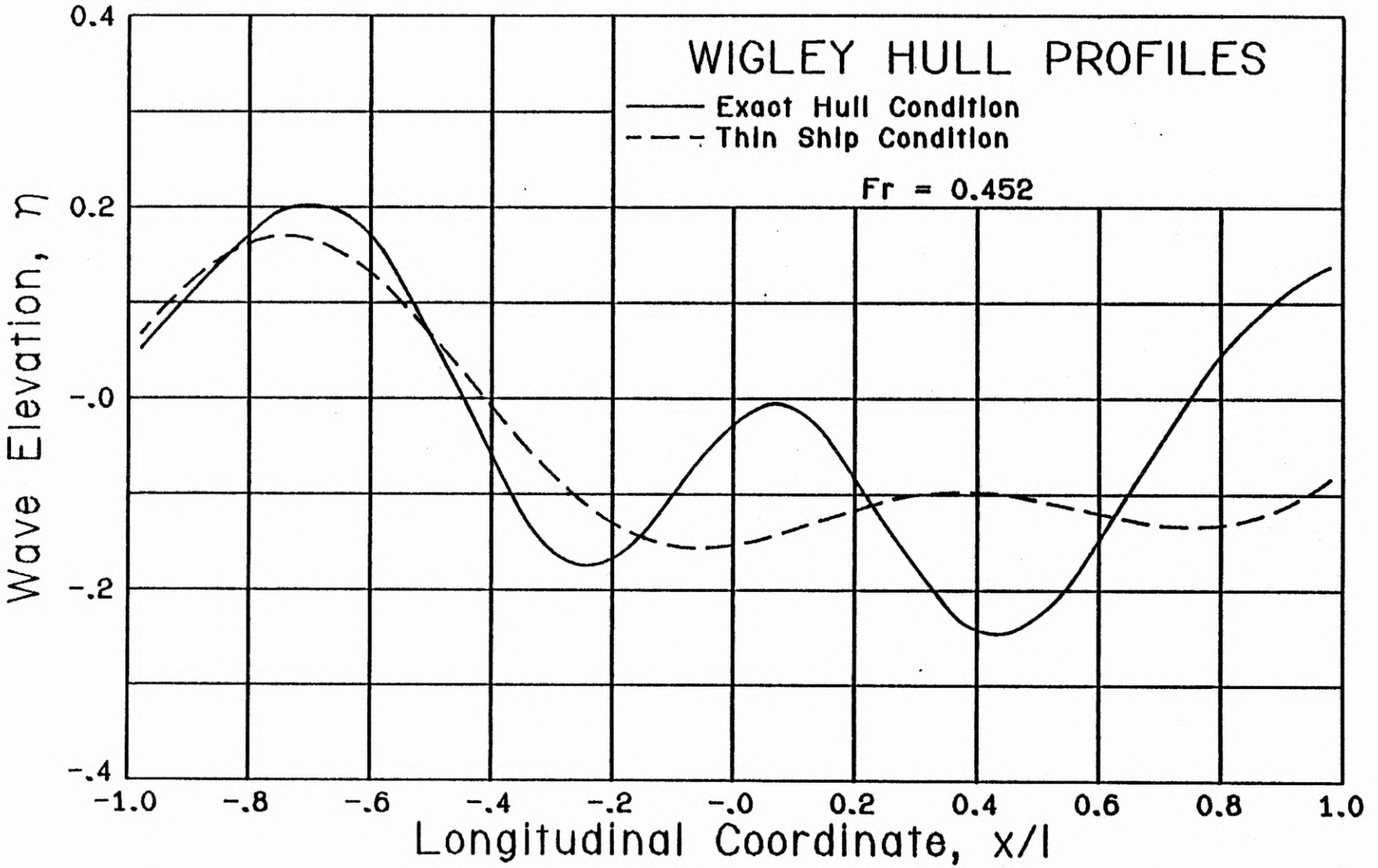

Figure 5.8 Comparison of the Wigley hull wave profiles for the thin ship and the exact hull cases (second order $\phi_{\bar{z}}$ differencing) for $Fr = 0.452$.

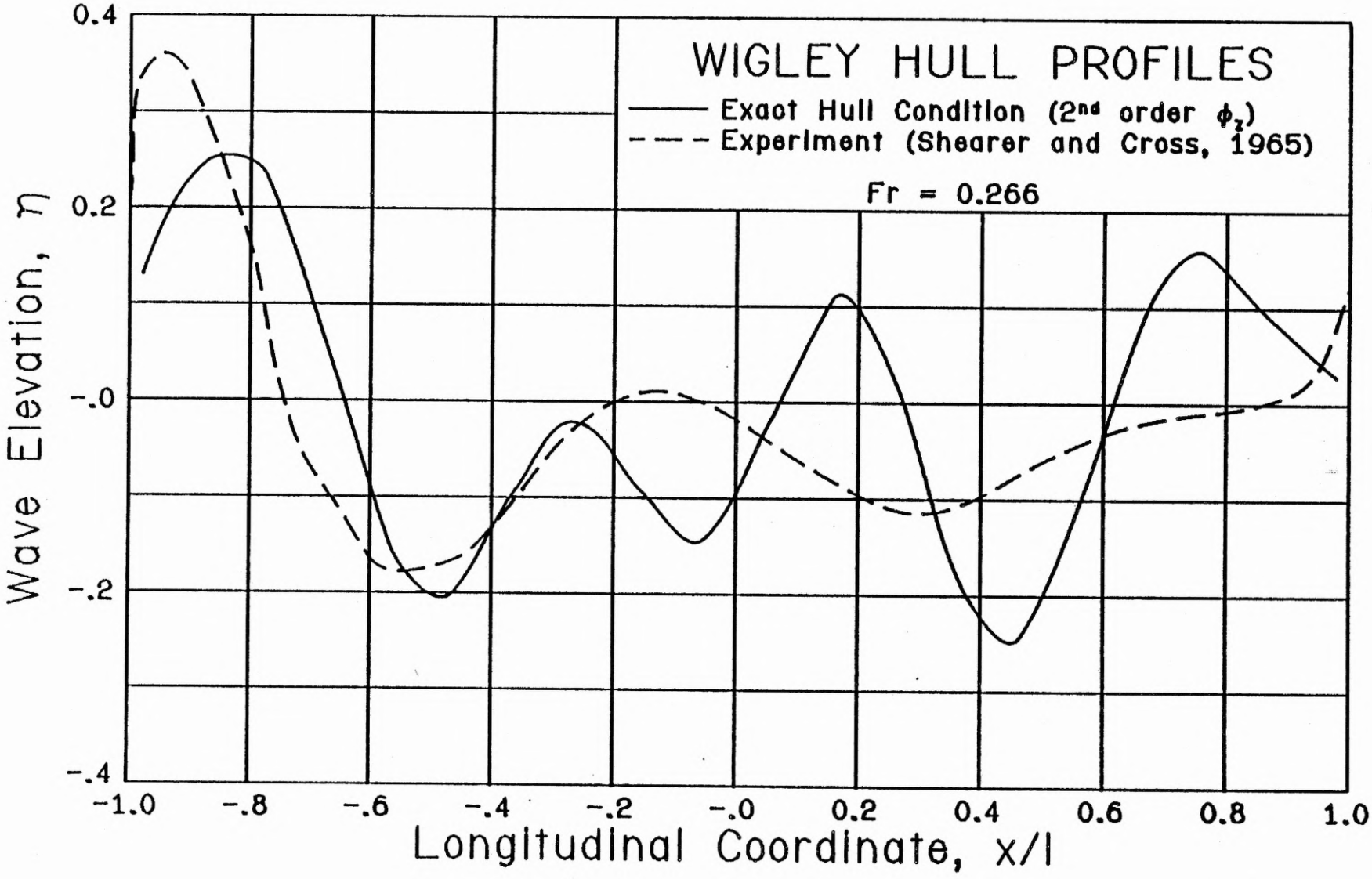

Figure 5.9 Comparison with an experiment of the Wigley hull wave profile obtained using the exact hull condition for $Fr = 0.266$.

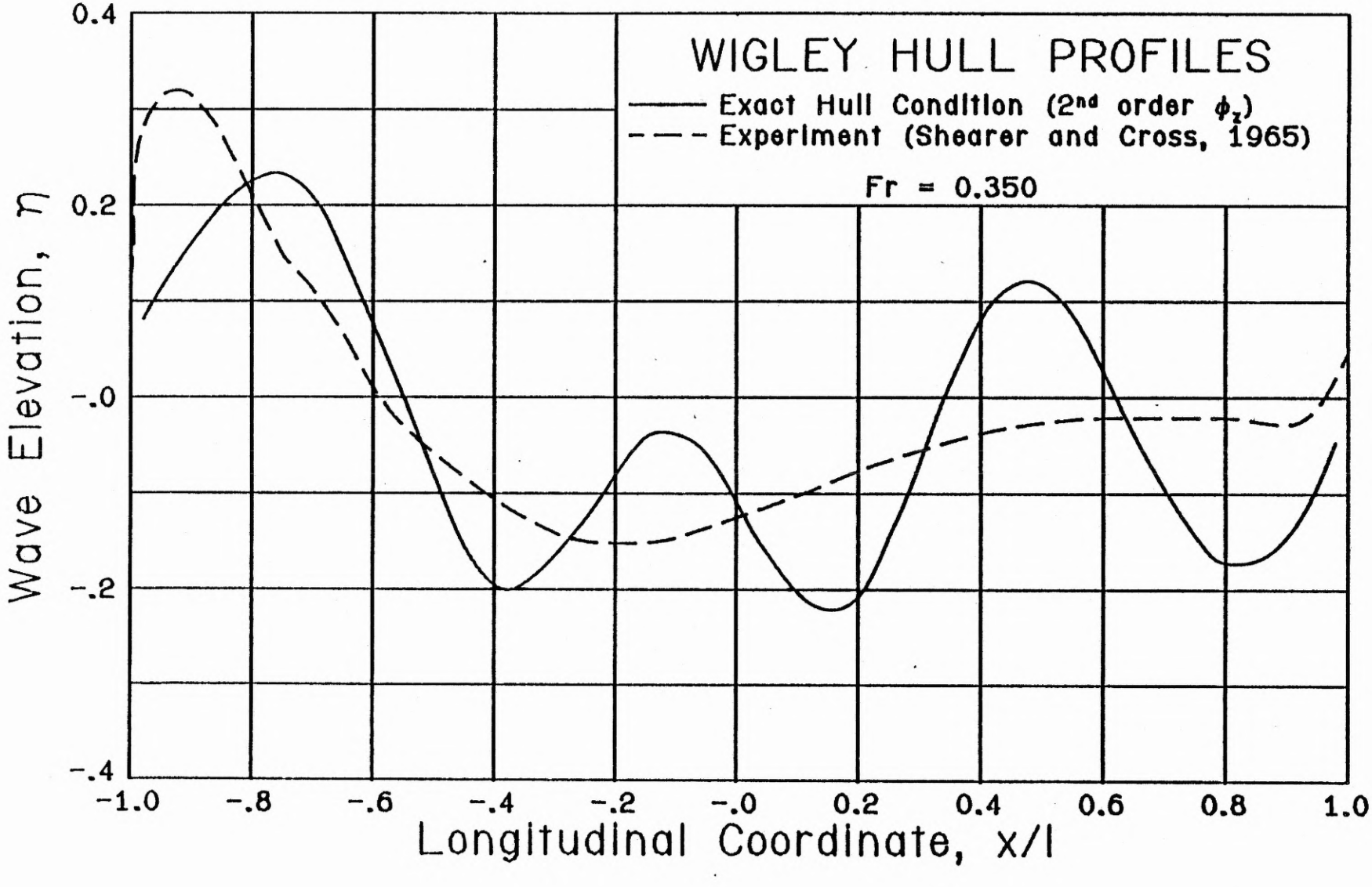

Figure 5.10 Comparison with an experiment of the Wigley hull wave profile obtained using the exact hull condition for $Fr = 0.350$.

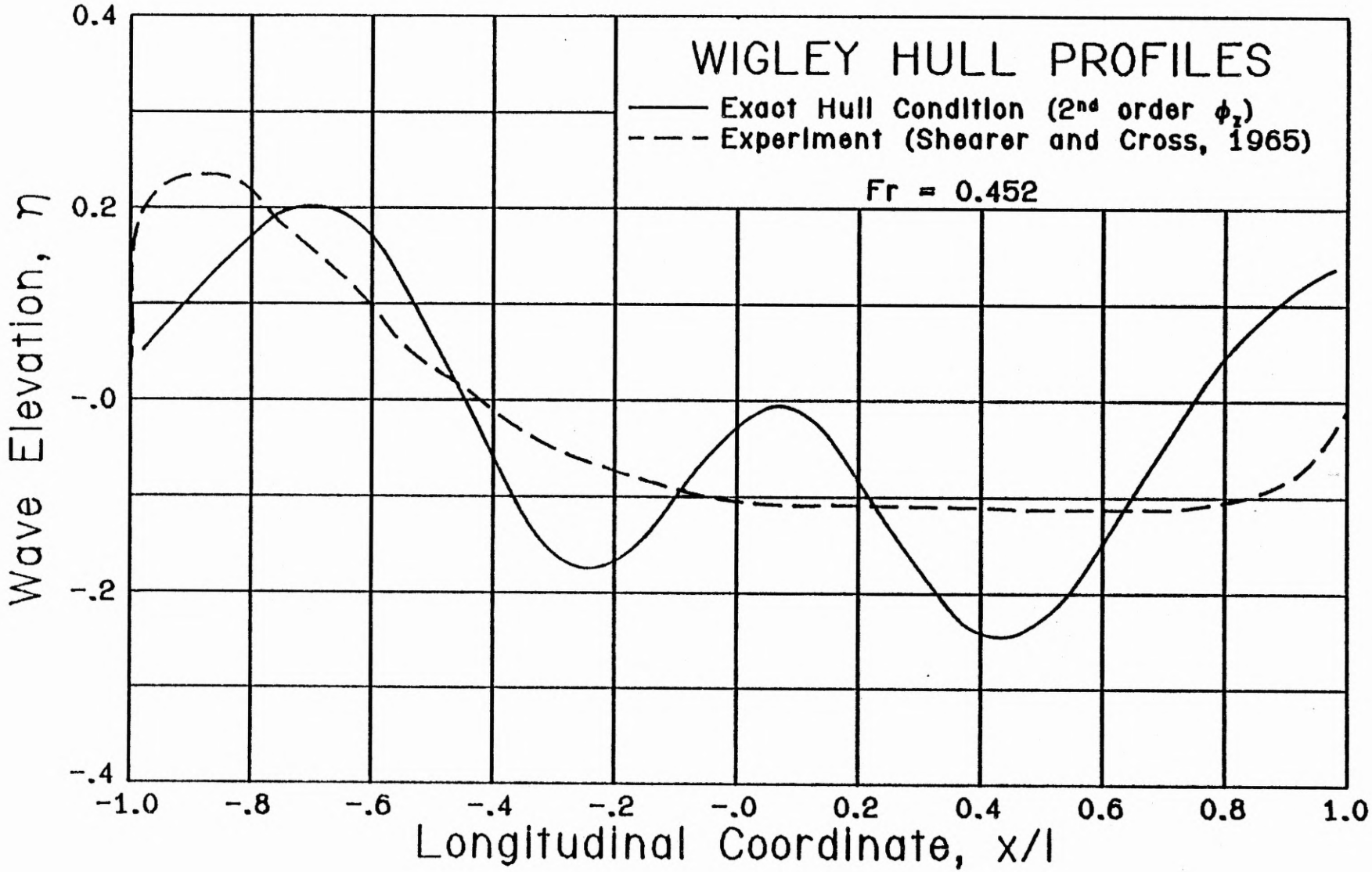

Figure 5.11 Comparison with an experiment of the Wigley hull wave profile obtained using the exact hull condition for $Fr = 0.452$.

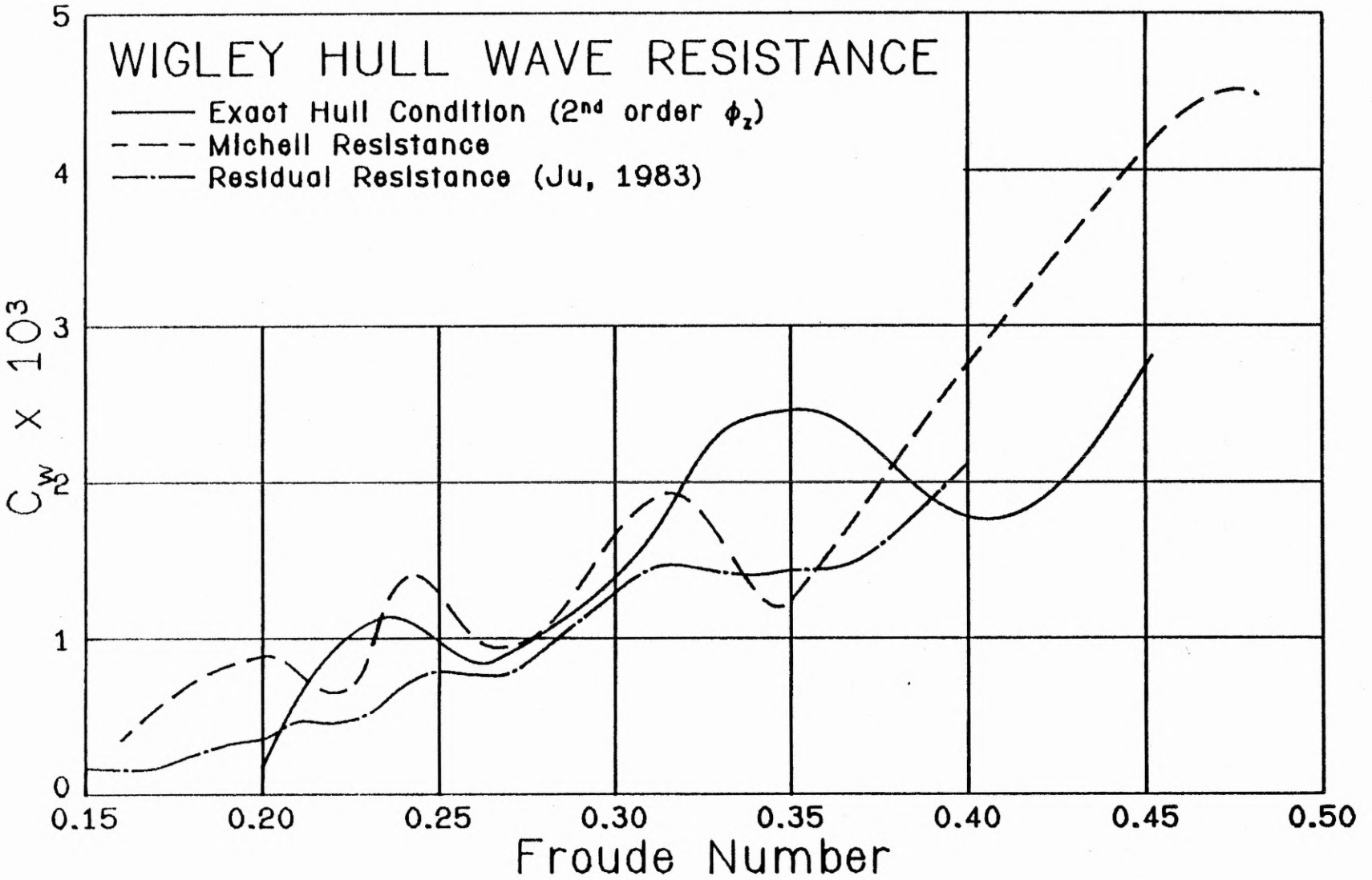

Figure 5.12 Comparison of the C_w vs. Fr curves for the the exact hull condition, the Michell solution and an experiment.

CHAPTER 6. THE NONLINEAR SHIP WAVE PROBLEM

The numerical development up to this point has proceeded with the ultimate goal of obtaining a solution to the nonlinear ship wave problem. We have seen that the computational difficulties, such as the open boundary and exact hull conditions, are successfully resolved by the present numerical approach. We have also seen that the thin ship and the Neumann-Kelvin formulations of the ship wave problem generally do not adequately predict the wave resistance of the Wigley hull over a typical Froude number range. It is therefore the purpose of this chapter to outline in detail the extension of the present time dependent finite difference method to the full nonlinear ship wave problem. We shall begin with a discussion of the new computational difficulties involved as well as with the strategy which will be used to handle them. A detailed description of the implementation of the nonlinear free surface conditions on the exact location of the moving boundary will then be presented, after which we shall describe the calculation of the wave resistance for the nonlinear case. Finally, the results for the nonlinear wave profiles will be compared to the those of the Neumann- Kelvin problem.

One new computational difficulty which is found in the nonlinear problem is the actual time advancement of the free surface boundary conditions at the exact location of the moving boundary. Since the free surface geometry is continuously changing, we must now be able to compute the free surface derivatives on a time dependent, curvilinear surface. This is accomplished by employing a time dependent mesh system which is capable of following the changing geometry. A general boundary fitted coordinate transformation is necessary in order to easily compute the required derivatives on $z = \eta(x,y;t)$. The result of this transformation is that the free surface is allowed to actually move since the top mesh plane in the Cartesian grid system conforms to the instantaneous location of the boundary.

The most difficult problem encountered in the nonlinear case, however, is the simultaneous implementation of the exact hull condition and the Dirichlet conditions for ϕ on the mov-

ing free surface. The situation is complicated by the fact that the capacitance matrix itself, used in implementing the exact hull condition, must be computed for each given geometry, including that of the free surface. As we have seen in Appendix C, the preprocessing involved in computing this matrix represents a fair amount of overhead since the fast Poisson solver must be used a number of times equal to the order of the capacitance matrix (240 in this case). This preprocessing obviously cannot be performed each time the geometry changes (i.e., at each time step), and so we must resort to a different strategy for the Laplace equation in the nonlinear case.

We have already remarked in Chapter 5 that the properties of the matrix for the exact hull linear system are not conducive to the use of iterative methods for the Laplace equation. On the other hand, it is possible to iteratively apply the Dirichlet boundary conditions on the exact location of the free surface since no coordinate transformations of the Laplace equation are necessary for this implementation. The present strategy is thus to successively refine the Laplace solution by repeatedly solving the Neumann-Kelvin problem with the correct free surface boundary conditions applied on the plane $z = 0$. The Dirichlet conditions on $z = \eta(x,y;t)$ are increasingly better approximated at each iteration by using results from the previous iteration to improve the interior solution. This strategy has been devised so that the use of the capacitance matrix technique, which relies on fixed geometry, is applicable even in the nonlinear case. These ideas concerning the new solution strategy for the Laplace equation as well as the implementation of the nonlinear free surface conditions will be developed in detail in the next section.

Implementation of the Nonlinear Free Surface Boundary Conditions

In this section, we shall first discuss the free surface fitted coordinate transformation and then formally present the new strategy for the numerical solution of the Laplace equation. We find that the time advancement of η and ϕ on the moving boundary may be accomplished

in the same manner as before, however we must now redefine the quantities u^*, v^* and Δ^* in the time marching scheme (Eq. (3.3)) so that we properly take into account the shape of the free surface on which the derivatives in Eqs. (2.8)-(2.9) are computed. This is done by performing the necessary coordinate transformations so that the free surface becomes a coordinate plane on which these derivatives may be easily evaluated. The most general situation of this sort occurs at the intersection of the hull with the free surface, and so this case is considered first.

We recall from Chapter 2 that the kinematic and dynamic conditions are

$$\eta_t + (U_s + \phi_x)\eta_x + \phi_y \eta_y = \phi_z \tag{2.8}$$

and

$$\phi_t + U_s \phi_x + \frac{1}{2}(\phi_x^2 + \phi_y^2 + \phi_z^2) + \eta/Fr^2 = 0\,. \tag{2.9}$$

In order to handle the deformation of the Cartesian mesh system due to the hull geometry, we reintroduce the transformation of Eqs. (5.1), which was already used for the Neumann-Kelvin problem, and recall that the rules of differentiation are

$$\begin{aligned} Q_x &= Q_{x'} - f_x Q_{y'} \\ Q_y &= Q_{y'} \\ Q_z &= Q_{z'} - f_z Q_{y'} \\ Q_t &= Q_{t'} \end{aligned} \tag{5.2}$$

for any function Q (i.e., either η or ϕ). The free surface geometry is handled by a similar transformation to a moving mesh system which, by definition, always conforms to the instantaneous location of the free boundary. The change of variables in this case is :

$$\begin{aligned} x'' &= x' \\ y'' &= y' \\ z'' &= z' - \eta(x', y'; t') \end{aligned} \tag{6.1}$$

$$t'' = t' ,$$

from which it follows that

$$\begin{aligned} Q_{x'} &= Q_{x''} - \eta_{x'} Q_{z'} \\ Q_{y'} &= Q_{y''} - \eta_{y'} Q_{z'} \\ Q_{z'} &= Q_{z''} \\ Q_{t'} &= Q_{t''} - \eta_{t'} Q_{z'} \end{aligned} \tag{6.2}$$

for any function Q. Using the first transformation on the free surface conditions, we obtain

$$\eta_{t'} + (U_s + \phi_x)\eta_{x'} + (\phi_y - f_x(U_s + \phi_x) - f_z\phi_z)\eta_{y'} = \phi_z \tag{6.3}$$

for the kinematic condition and

$$\phi_{t'} + U_s\phi_{x'} - U_s f_x \phi_{y'} + \frac{1}{2}(\phi_x^2 + \gamma_1^2\phi_y^2 + \phi_z^2) - f_x\phi_{x'}\phi_{y'} - f_z\phi_{y'}\phi_{z'} + \eta/Fr^2 = 0 \tag{6.4}$$

for the dynamic condition. We recall that γ_1 is defined as $\gamma_1 = (1 + f_x^2 + f_z^2)^{1/2}$.

Since Eqs. (6.3) and (6.4) are applied at the intersection of the hull with the free surface, we must compute ϕ_y (as well as $\phi_{y'}$) according to the exact hull boundary condition (Eq. (2.11)). In view of this condition, the coefficient of $\eta_{y'}$ in Eq. (6.3) is identically zero. Furthermore, after applying the second transformation to Eq. (6.3), we obtain

$$\eta_{t''} + (U_s + \phi_x)\eta_{x''} = \phi_{z'} - f_z\phi_{y'} \tag{6.5}$$

in which ϕ_x is computed using Eqs. (5.2) and (6.2), while $\phi_{y'}$ is computed using Eq. (5.4).

Under the transformation of Eqs. (6.2), Eq. (6.4) becomes

$$\phi_{t''} + U_s\phi_{x''} - f_x(U_s + \phi_{x''})\phi_{y''} + \Delta + \eta/Fr^2 = 0 , \tag{6.6}$$

in which $\Delta = \frac{1}{2}[\phi_x^2 + \gamma_1^2\phi_y^2 - (1 + \eta_x^2 + \gamma_1^2\eta_y^2 + 2\eta_{y''}(f_z - f_x\eta_{x''}))\phi_z^2]$. These two conditions are applied on $z'' = 0$ (i.e., on $z' = \eta(x', y', t')$).

From Eqs. (6.5) and (6.6), we derive the following expressions for u^*, v^* and Δ^* which are to be used in the time marching scheme of Eq. (3.3) :

Dynamic condition for ϕ :

$$u^* = U_s$$

$$v^* = -f_x(U_s + \phi_{x^*})$$

$$\Delta^* = -\Delta - \eta/Fr^2$$

Kinematic condition for η :

$$u^* = (U_s + \phi_x)$$

$$v^* = 0$$

$$\Delta^* = \phi_{z^*} - f_z \phi_{y^*}$$

The above definitions are used in the time marching scheme only when the free surface conditions are applied at the intersection of the free surface with the hull. Since the original mesh system is Cartesian away from the hull, these definitions may be simplified when the boundary conditions are applied at free surface points not in contact with the ship. We are then able to consider these expressions with all references to the hull geometry set equal to zero. Therefore, away from the hull, we use the following quantities in the time marching scheme (Eq. (3.3)) :

Dynamic condition for ϕ :

$$u^* = U_s$$

$$v^* = 0$$

$$\Delta^* = \frac{1}{2}[\phi_x^2 + \phi_y^2 - (1 + \eta_x^2 + \eta_y^2)\phi_z^2] - \eta/Fr^2$$

Kinematic condition for η :

$$u^* = (U_s + \phi_{x^*} - \eta_{x^*}\phi_{z^*})$$

$$v^* = \phi_{y^*} - \eta_{y^*}\phi_{z^*}$$

$$\Delta^* = \phi_{z^*}$$

The free surface conditions may now be advanced in time using the same explicit scheme

described in Chapter 3. This time marching scheme is thus seen to be very flexible in the ship wave problem since we are able to use it for all of the free surface boundary conditions considered in this work.

We now turn to a discussion of the method by which the Dirichlet conditions for ϕ may be implemented on the moving boundary during the numerical solution of the Laplace equation. As we mentioned earlier, this presents a special problem since the capacitance matrix technique requires that the geometry of the region remain fixed, which is not the case when we allow the free surface to move. We therefore incorporate the fast direct solution of the Neumann-Kelvin problem into an iterative procedure which successively approximates the solution to the full nonlinear problem. This is done by applying the correct conditions for ϕ on $z' = 0$ and by modifying the right hand side of the Laplace equation in such a way as to take account of the exact free surface location. We now proceed to consider this method more formally in the following discussion.

Let us define the matrix A in such a way that the linear system $A\phi = b$ describes the discretization of the Laplace equation in the region whose boundaries include the exact hull and the moving free surface. In a similar fashion, we define the matrix B to be that for the Neumann-Kelvin problem. We already know that systems involving B can be easily solved by the method of Appendix C, so we naturally consider the splitting

$$A = B - N , \tag{6.7}$$

where the matrix N describes the time dependent part of A. Thus N will account for the fact that the free surface position is $z' = \eta(x', y'; t')$ rather than $z' = 0$, as is assumed in the matrix B. Given the matrix splitting of Eq. (6.7), the following iterative process solves $A\phi = b$:

$$B\phi_{s+1} = b + N\phi_s . \tag{6.8}$$

We use here the subscript s to denote the iteration count. It is seen from Eq. (6.8) that the right hand side of the finite difference elliptic system is updated using information from the

previous step. Since N involves only the equations adjacent to the moving boundary, this accounts for the fact that the Dirichlet conditions on the free surface are successively better approximated after each iteration.

The entire numerical method to solve the full nonlinear ship wave problem is now summarized in the following steps :

(1) Initialize the flow field by setting $\phi = \eta = 0$ throughout the domain.

(2) Advance the free surface boundary conditions in time using the scheme in Eq. (3.3) with the nonlinear definitions for u^*, v^* and Δ^*.

(3) Solve the Laplace equation using the iterative process defined in Eq. (6.8). The exact hull condition is satisfied at each iteration while the Dirichlet conditions at the precise location of the free surface are successively approximated by this process.

(4) Repeat steps (2) and (3) until the steady state is reached.

We remark at this point that we have not entirely relaxed our restrictions on the use of iterative methods for the ship wave problem. Comments made previously in this work suggested that the exclusive use of iterative methods for the solution of the Laplace equation in the ship wave problem would be inefficient and possibly inaccurate. It should be pointed out that the present method for the nonlinear problem still uses an efficient direct method for the bulk of the flow field and only incorporates this method into an iterative procedure to facilitate the implementation of the Dirichlet conditions at the free surface. It is still felt that the use of fast direct methods should dominate the solution process of the ship wave problem.

Calculation of the Wave Resistance

We now briefly describe the formula which is used to calculate the wave resistance in the nonlinear problem. The pressure integral is different in two respects from the previous linear-

ized cases. First, the full Bernoulli equation is used to compute the pressure, and second, the limits of integration are modified by the presence of the exact free surface, $z = \eta(x,y;t)$. The Bernoulli equation (Eq. (2.9)) applied on the hull can be written as

$$P = -[\phi_t + U_s \phi_x + \frac{1}{2}(\phi_x^2 + \phi_y^2 + \phi_z^2) + z/Fr^2 . \tag{6.9}$$

The derivatives in this expression must be computed according to Eqs. (5.2), and the exact hull condition (Eq. (2.11)) must be used to compute ϕ_y. Using the wave resistance formula given by Eqs. (4.8) and (4.10), we compute C_w in the nonlinear case from

$$C_w = \frac{4}{S} \int_{-h}^{\eta(x,y;t)} \int_{-1/2}^{1/2} P f_x \, dx \, dz . \tag{6.10}$$

We recall that S is the wetted hull area at rest and is given by Eq. (4.12).

Numerical Results for the Nonlinear Problem

The iterative procedure for numerically solving the Laplace equation subject to the exact hull condition as well as the exact nonlinear free surface conditions is now applied to the case of a translating Wigley hull. The iteration is initialized by assuming that the matrix N in Eq. (6.8) has all zero elements for the first step. This corresponds to applying the exact Dirichlet conditions on the plane $z = 0$ and is intended to represent a good first approximation to the interior flow. For each successive iteration, the matrix N contains the elements which correspond to the finite difference approximations to ϕ_{zz} at all the mesh points which are adjacent to the moving free surface (i.e., at $z = -0.0208$ in Fig. (5.2a)). We use two iterations to obtain the present solution, and this strategy corresponds to a predictor-corrector type method.

The nonlinear wave profile result is obtained for $Fr = 0.266$ and is compared to the corresponding result for the Neumann-Kelvin problem at $t = 3.0$ in Fig. 6.1. We note that the profiles in the bow region are very similar but they begin to exhibit their own characteristics at downstream locations. The nonlinear wave amplitudes are slightly reduced, especially near the

stern. This is an interesting result since it indicates that the nonlinear terms have a strong influence on the solution in the stern region. This region is also affected by the wake, and it is likely that further nonlinear-viscous interaction would take place in a model which included viscosity.

Summary

In this chapter, we have described the logical extension of the present numerical method to the full nonlinear ship wave problem. Two additional computational difficulties, not present in the linearized cases, were identified. The first concerned the calculation of the free surface derivatives on a time dependent, curvilinear boundary. A general boundary fitted coordinate transformation was performed so that the required derivatives could be easily evaluated. The second difficulty, considered to be more severe than the first, involved the simultaneous satisfaction of all of the boundary conditions at their proper locations. In order to resolve this problem, the solution of the Neumann-Kelvin problem was used in an iterative procedure such that at each iteration, the hull condition was satisfied exactly, and the Dirichlet conditions on the free surface were successively refined in accuracy. The next discussion concerned the modification of the wave resistance calculation due to the introduction of the nonlinear terms as well as to the replacement of the upper limit of the pressure integration in the z-direction by the bound $z = \eta(x,y;t)$. Finally, the nonlinear wave profile result for $Fr = 0.266$ was compared to that of the Neumann-Kelvin problem, and it was found that the nonlinear terms most affect the solution in the stern region.

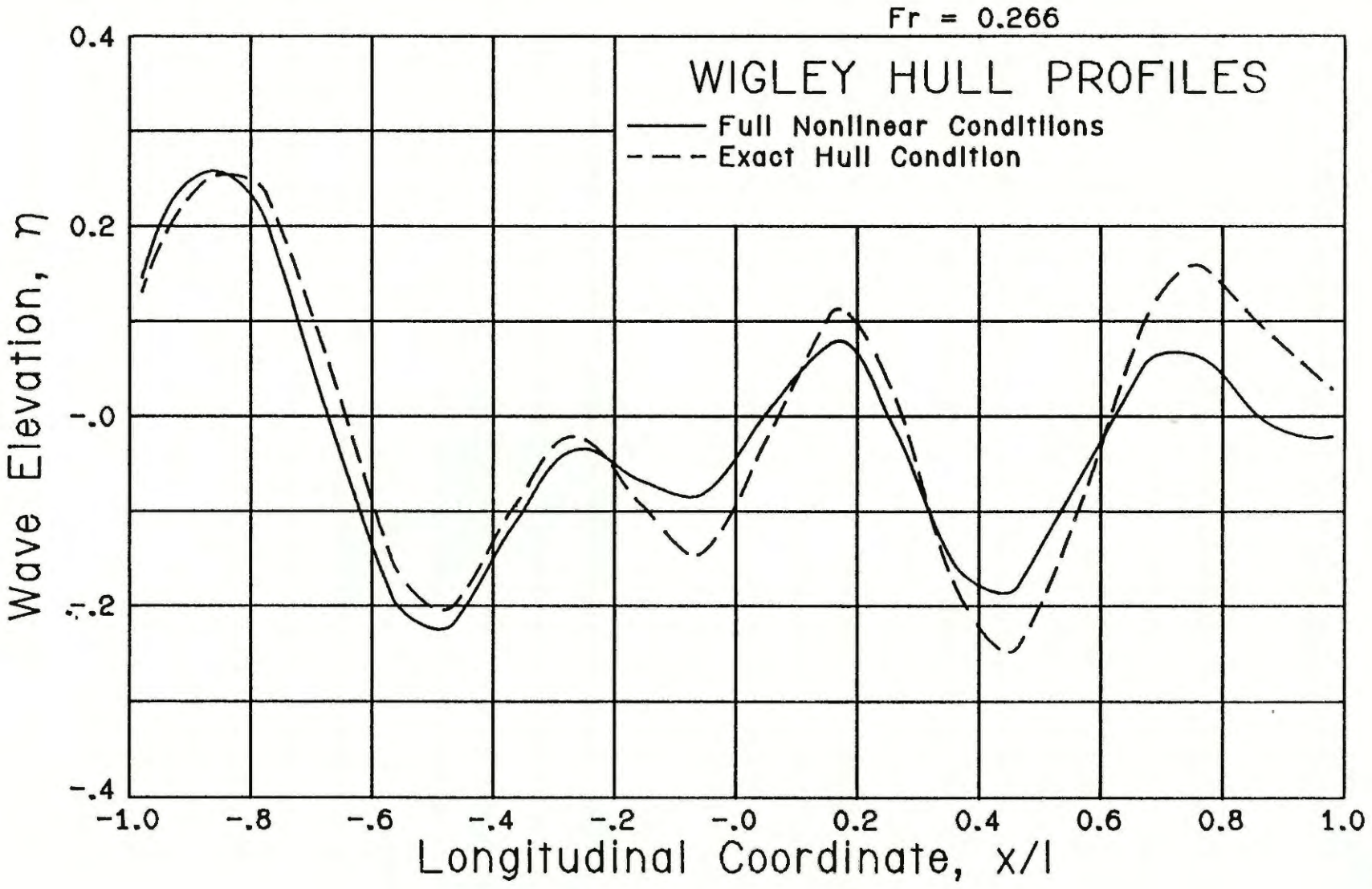

Figure 6.1 Comparison of the hull wave profiles for the full nonlinear and Neumann-Kelvin problems at $t = 3.0$ for $Fr = 0.266$.

CHAPTER 7. SUMMARY AND CONCLUSIONS

This thesis represents a unified and systematic development of a general numerical method to solve the full nonlinear ship wave problem. The approach has been to divide the task into three distinct phases which progress successively in levels of both difficulty and reality. This strategy allows the computational difficulties in each phase to be identified, studied and resolved. Furthermore, the importance of numerical experiments during the initial development cannot be overemphasized since they provide valuable insight into both the characteristics of the numerical method as well as into the effects of changes in the computational parameters on the solutions. In this chapter, we shall review the overall numerical approach and highlight the major results and conclusions of this research. We shall then conclude with some indications for further numerical ship hydrodynamics research which is identified as a result of the present study.

One of the main contributions of this work is the development of an optimized direct method for the numerical solution of the Laplace equation both in rectangular and nonrectangular regions. The solution technique is considered to be optimized in the sense that it is neither necessary to compute or store the solution in the entire domain. The reason for this is that the Fourier series method for solving the finite difference form of the Laplace equation is able to take advantage of the fact that the right hand side vector consists entirely of zero elements in the region below the keel of the ship. Using this method, it is possible to efficiently compute the solution in regions which are very much larger than could be handled by any other solution procedure. The present Laplace solution method is thus considered to be essential to the success of the time dependent finite difference approach to the ship wave problem.

The numerical strategy for the time dependent solution of the thin ship, Neumann-Kelvin and nonlinear ship wave problems is essentially the same. We first initialize the flow field, then update the free surface conditions in time and finally solve the Laplace equation subject to

the appropriate boundary conditions. This updating and Laplace solution process is repeated until the steady state solution is attained. The major difference between each of these problems lies exclusively in the solution of the Laplace equation. The elliptic solution strategy for the thin ship and the Neumann-Kelvin problems differs significantly due to the locally body fitted coordinate transformation. The strategy for the nonlinear problem differs due to the iterative refinement of the Dirichlet conditions which must be imposed on a time dependent boundary of arbitrary shape. The optimized direct solution technique used in the thin ship problem (Appendix B) is modified by the capacitance matrix method (Appendix C) so as to allow the direct solution of the Laplace equation in an irregular (i.e., non-Cartesian) region which arises from the presence of the exact hull geometry. This modified direct Laplace solver is then used in an iterative procedure as a means of solving the nonlinear ship wave problem.

The solution accuracy, speed and storage requirements of the present optimized direct method are considered to be superior to those of any iterative method for the numerical solution of the Laplace equation. The use of the fast direct method based on the FFT is further enhanced by the locally body fitted mesh system. This mesh allows the majority of the domain to be represented by an orthogonal Cartesian grid, while at the same time it accurately accommodates arbitrary hull geometry in a localized portion of the region. The concept of the locally body fitted mesh is thus essential to the applicability of the optimized direct method to the solution of the Neumann-Kelvin and the nonlinear problems.

It is interesting to note that the use of the locally body fitted mesh system is currently recognized by the aircraft design industry as an essential tool in the rapid solution of transonic flow problems. For example, Johnson, et. al. [46] have described a panel method in which rectangular grids are used to represent the bulk of the flow field which surrounds complex aircraft configurations. This new direction in the grid generation for elliptic problems, taken in the present numerical approach to the nonlinear ship wave problem, has been found to be necessary given the fact that the Laplace equation must be solved efficiently many times during

the course of the calculation. The field of numerical ship hydrodynamics is thus beginning to share at least one of the concepts which is considered to be important in the more established field of numerical aerodynamics.

Another issue in numerical ship hydrodynamics which has been dealt with successfully is the implementation of the open boundary condition. We recall that in the steady state approach, which disregards the transient solution, the appropriate conditions at the downstream boundary are unknown *a priori*. One way to circumvent this difficulty is to use the time dependent approach so that an open boundary must exist downstream of the ship. Although the open boundary condition is known, its correct implementation is the subject of an ongoing debate. The usual one dimensional advection models presently in use are often difficult to implement in practice, and two dimensional models have never been considered. Furthermore, these approaches can be inaccurate due to numerical errors in the calculation of the proper wave speed. It was found in the present work, however, that a much simpler approach to this issue is possible. The downstream boundary is placed a large distance from the ship, and the correct condition for no disturbance (i.e., uniform flow) is specified. This condition has been found to be a good approximation even when transient waves are present since the depth of the domain is large compared to the wave height. This in turn means that the mass flux across the downstream boundary is still approximately correct (i.e., equal to that at the inflow boundary). Furthermore, no wave reflection or distortion at the open boundary are observed, and there is no adverse influence on the solution near the Wigley hull due to this treatment, even long after the waves have reached the downstream boundary. It is interesting to note that Chan [23] placed the open boundary very close to the ship with the hope that the SOR iteration would converge more rapidly. However, without using his complicated open boundary treatment, the present approach, using a relatively long domain and the optimized fast Laplace solver, can actually outperform the SOR procedure used in a much shorter region. Therefore, if the time dependent approach is to be used, it is much simpler and faster to use the present method. We are thus able to conclude that the open boundary issue is not as severe as is now generally

believed by the numerical ship hydrodynamics community.

One final comment which concerns the open boundary condition is that colleagues in fields other than naval hydrodynamics have obtained results which concur with the present implementation. Rudy [47] considers a propagating vortex as a test example for several different open boundary implementations, all of which are based on the Sommerfeld radiation model. He tests a simple outflow condition similar to the present one as well as both one and two dimensional advection models in which the exact phase speed is known. He reports that there is no reflection at the outflow boundary for any of the boundary treatments, although the vortex is allowed to pass more cleanly out of the region as the level of sophistication of the open boundary condition increases. The important point here is that Rudy's results for an entirely different problem are in agreement with the present findings as far as the lack of wave reflection is concerned, even when the open boundary treatment is as simple as possible.

We now briefly review the numerical experiments which were described in Chapter 4 for the thin ship problem. These experiments demonstrated that the domain size 4.95 x 2.0 x 1.0 was sufficient to approximate a much longer and deeper domain. This is significant because we can maximize the computational efficiency in a relatively small region while obtaining the same results that would be expected in a much larger region. The numerical experiments also showed that second order one sided differencing for the vertical free surface velocity (ϕ_z) gave more accurate results relative to the semi-analytical classical solution of Michell. The guide-lines for the choices of the computational parameters, having thus been established, were then followed throughout the rest of the work.

The wave profile and wave resistance results obtained shall now be briefly reconsidered. The validity of the time dependent approach to the ship wave problem was first verified by comparing the thin ship wave profile and wave resistance results to those computed from the first order Michell theory. The qualitative features of these results for the Wigley hull were certainly reproduced by the present method. While the thin ship theory seemed to reproduce

some aspects of the hull wave profiles which have been observed in experiments, it seemed to have difficulty in accurately predicting the experimental wave resistance. It has been argued that this is due to the thin ship approximation, especially in the low Froude number range in which the linearization of the free surface conditions is usually assumed to be tolerable. The results for the Neumann-Kelvin problem, however, have apparently refuted this argument. Relative to the thin ship and experimental profiles, these results exhibited higher frequency components which were not previously observed. Furthermore, the wave resistance results predicted two peaks in the C_w vs. Fr curve which were also not observed. Since one of these peaks occurred at $Fr = 0.233$, it may not be justified to assume that the Neumann-Kelvin problem will accurately predict the wave resistance, even at low Froude numbers.

We now conclude with some indications, based on the results of this study, for further research in the area of numerical ship hydrodynamics. The Wigley hull has been considered in this work because of its simple mathematical representation and because of its wide acceptance as a research standard. However, since the method developed here for the ship wave problem is generally applicable to any hull form, it would be of interest to consider other shapes as well. Using the present method, this is quite simple to do, even if the hull has no algebraic definition. This is in fact one of the great advantages of numerical methods in ship research since new models do not have to be built and tested in a towing tank. However, without a large database created from many runs in a numerical towing tank for a variety of different hull forms, it is too early to tell how effective purely numerical methods will be in augmenting modern ship design. It is felt that research on the numerical aspects of ship hydrodynamics should continue and should follow the guidelines set forth in the present work.

APPENDIX A

The linear von Neumann stability analysis for Chan's advection scheme is now presented. We consider the two dimensional model equation

$$\phi_t + u\phi_x + v\phi_y = 0 \tag{A.1}$$

in which u and v are constant (≥ 0). We replace the derivatives in Eq. (A.1) with the finite difference approximations from Eqs. (3.2) to obtain

$$\frac{1}{2\Delta t}\left[\phi_{i,j}^{n+1} + \phi_{i-1,j}^{n} - \phi_{i,j}^{n} - \phi_{i-1,j}^{n-1}\right] + \frac{u}{\Delta x}\left[\phi_{i,j}^{n} - \phi_{i-1,j}^{n}\right] +$$

$$\frac{v}{4\Delta y}\left[\phi_{i,j+1}^{n} - \phi_{i,j-1}^{n} + \phi_{i-1,j+1}^{n} - \phi_{i-1,j-1}^{n}\right] = 0 . \tag{A.2}$$

In order to analyze this scheme, we assume that the solution $\phi_{i,j}^{n}$ can be written in the form

$$\phi_{i,j}^{n} = \lambda^n \, e^{i(kx_i + ly_j)} , \tag{A.3}$$

where λ^n is the amplitude (damping) factor at time $t = n\Delta t$, which must be ≤ 1 for stability, and $e^{i(kx_i + ly_j)}$ represents the spatial variation of the solution. Furthermore, $k = \frac{2\pi}{\lambda_x}$, $l = \frac{2\pi}{\lambda_y}$ and $i = \sqrt{-1}$, in which λ_x and λ_y are the wavelengths in the x- and y-directions, respectively. Substituting Eq. (A.3) into Eq. (A.2), we obtain the following relation for the damping factor

$$\lambda^2 + b\lambda - z = 0 , \tag{A.4}$$

in which we have introduced the following definitions

$$b = (2c_x - 1)(1 - z) + i c_y \sin l\Delta y (1 + z) ,$$

$$z = e^{-ik\Delta x} = \cos k\Delta x - i \sin k\Delta y ,$$

$$c_x = \frac{u\Delta t}{\Delta x}$$

and

$$c_y = \frac{v\Delta t}{\Delta y} .$$

The solution to Eq. (A.4) has two roots, which can be written as

$$\lambda_\pm = -\frac{b}{2} + \frac{1}{2}[b^2 + 4z]^{1/2} . \tag{A.5}$$

Using the identities

$$(1-z)^2 = -4z \sin^2 \frac{k\Delta x}{2} ,$$

$$(1+z)(1-z) = 2(1 - z\cos k\Delta x) ,$$

$$(1+z)^2 = 2z(1 + \cos k\Delta x) ,$$

$$\frac{1}{z} - \cos k\Delta x = i \sin k\Delta x ,$$

we obtain for Eq. (A.5)

$$\lambda_\pm = -a \sin \frac{k\Delta x}{2} \pm \cos \frac{k\Delta x}{2} (1-a^2)^{1/2}$$

$$- i[a \cos \frac{k\Delta x}{2} \pm \sin \frac{k\Delta x}{2} (1-a^2)^{1/2}] , \tag{A.6}$$

in which $a = c_y \sin l\Delta y \cos \frac{k\Delta x}{2} + (2c_x - 1)\sin \frac{k\Delta x}{2}$.

We see that Eq. (A.6) has the form $\lambda_\pm = x + iy$, so that $|\lambda_\pm|^2 = x^2 + y^2$. Using this fact, we find that

$$|\lambda_\pm|^2 = 1 . \tag{A.7}$$

Thus, Chan's scheme is neutrally stable, meaning that pure advections (i.e., u,v = constant) will theoretically propagate with no changes in amplitude. This is a very desirable numerical property for the ship wave problem since no physical viscosity is assumed to be present.

Equation (A.7) guarantees that the scheme in Eq. (A.2) will be stable, but it does not indicate for which combination of Δx, Δy or Δt. Therefore, we must also find the conditions under which Eq. (A.7) holds. This is accomplished by requiring that the imaginary part of Eq. (A.6) remain entirely imaginary. That is, we must have $1-a^2 \geq 0$, or

$$|c_y \sin l\Delta y \cos \frac{k\Delta x}{2} + (2c_x - 1)\sin \frac{k\Delta x}{2}| \leqslant 1 . \qquad (A.8)$$

We take the maximum absolute value of this expression to occur when $\sin l\Delta y = 1$ and $\cos \frac{k\Delta x}{2} = \sin \frac{k\Delta x}{2} = \frac{\sqrt{2}}{2}$. The stability condition thus becomes

$$|c_y + 2c_x| \leqslant 1 + \sqrt{2} . \qquad (A.9)$$

For the one dimensional case, in which v = 0, we reconsider Eq. (A.8) with $c_y = 0$. We now take the maximum absolute value to occur when $\sin \frac{k\Delta x}{2} = 1$, giving us the one dimensional stability requirement

$$|\frac{u\Delta t}{\Delta x}| \leqslant 1 . \qquad (A.10)$$

This is the usual Courant condition which states that information must not propagate faster than one mesh interval per time step.

APPENDIX B

We consider in this section the reduction of the three dimensional finite difference Poisson (Laplace) equation, via the finite Fourier transform, to a sequence of tridiagonal systems which must be solved for the Fourier coefficients. Once obtained, these coefficients are used to reconstruct the exact solution to the finite difference equations by Fourier synthesis.

The second order seven point difference operator for the Poisson equation is written as

$$C_1[\phi_{i-1,j,k} - 2\phi_{i,j,k} + \phi_{i+1,j,k}] + C_2[\phi_{i,j-1,k} - 2\phi_{i,j,k} + \phi_{i,j+1,k}]$$
$$+ a_k\phi_{i,j,k-1} - b_k\phi_{i,j,k} + c_k\phi_{i,j,k+1} = r_{i,j,k} . \qquad \text{(B.1)}$$

Standard finite difference notation is used so that $\phi_{i,j,k}$ represents the solution ϕ at the grid point $[i\Delta x, j\Delta y, k\Delta z]$. The coefficients C_1 and C_2 are constant and equal to $\frac{1}{\Delta x^2}$ and $\frac{1}{\Delta y^2}$, respectively. The coefficients in the z- (k-) direction are defined as

$$a_k = \frac{2}{h_{k-1}(h_k + h_{k-1})}$$
$$b_k = \frac{2}{h_k h_{k-1}} \qquad \text{(B.2)}$$
$$c_k = \frac{2}{h_k(h_k + h_{k-1})} ,$$

where $h_k = z_{k+1} - z_k$. These definitions are used so as to allow the use of nonuniform grid spacing in the vertical direction. The above coefficients have been derived by considering the standard Taylor series expansion about a point $\phi_{i,j,k}$ which is located a distance h_{k-1} and h_k from its neighboring points, $\phi_{i,j,k-1}$ and $\phi_{i,j,k+1}$, respectively.

We now assume that the solution and the right hand side of Eq. (B.1) can be written as

$$\phi_{i,j,k} = \sum_{l=1}^{L} E_{l,k}\ \bar{\phi}^{l}_{j,k}\ \cos(l-1)\theta_i \qquad \text{(B.3a)}$$

and

$$r_{i,jk} = \sum_{l=1}^{L} E_{l,L}\, \bar{r}^{1}_{jk} \cos(l-1)\theta_i \,, \tag{B.3b}$$

where $\theta_i = \dfrac{(i-1)\pi}{(L-1)}$ and $i = 1,2,\ldots,L$. We also define the normalizing factor, $E_{i,j}$, as

$$E_{i,j} = \begin{cases} \tfrac{1}{2} & \text{if } i = 1 \text{ or } i = j \\ 1, & \text{otherwise.} \end{cases}$$

In the x-direction, the Fourier coefficients of the solution and the right hand side are represented by $\bar{\phi}^{1}_{jk}$ and $\bar{r}^{1}_{jk}$, respectively. It can be seen from Eqs. (B.3a) and (B.3b) that the number of coefficients required to exactly represent the solution and the right hand side in the x-direction is just L, the total number of x-grid points. Furthermore, the cosine transform is used since the boundary conditions in this case are $\phi_x = 0$ at the extreme values of x, and the cosine series in Eq. (B.3a) satisfies these boundary conditions exactly.

The procedure is now to substitute the Eqs. (B.3) into Eq. (B.1) so that we obtain an equation involving only the Fourier coefficients. We thus obtain

$$\begin{aligned}
&C_1 \sum_{l=1}^{L} E_{l,L}\, \bar{\phi}^{1}_{jk} \cos(l-1)\theta_{i-1} - 2C_1 \sum_{l=1}^{L} E_{l,L}\, \bar{\phi}^{1}_{jk} \cos(l-1)\theta_i \\
&\qquad + C_1 \sum_{l=1}^{L} E_{l,L}\, \bar{\phi}^{1}_{jk} \cos(l-1)\theta_{i+1} \\
&+ C_2 \sum_{l=1}^{L} E_{l,L}\, \bar{\phi}^{1}_{j-1,k} \cos(l-1)\theta_i - 2C_2 \sum_{l=1}^{L} E_{l,L}\, \bar{\phi}^{1}_{jk} \cos(l-1)\theta_i \\
&\qquad + C_2 \sum_{l=1}^{L} E_{l,L}\, \bar{\phi}^{1}_{j+1,k} \cos(l-1)\theta_i \\
&+ a_k \sum_{l=1}^{L} E_{l,L}\, \bar{\phi}^{1}_{j,k-1} \cos(l-1)\theta_i - b_k \sum_{l=1}^{L} E_{l,L}\, \bar{\phi}^{1}_{jk} \cos(l-1)\theta_i \\
&+ c_k \sum_{l=1}^{L} E_{l,L}\, \bar{\phi}^{1}_{j,k+1} \cos(l-1)\theta_i \;=\; \sum_{l=1}^{L} E_{l,L}\, \bar{r}^{1}_{jk} \cos(l-1)\theta_i \,.
\end{aligned} \tag{B.4}$$

We now multiply Eq. (B.4) through by $E_{i,L} \cos(m-1)\theta_i$ and sum over i. Using the orthogonality relations

$$\sum_{i=1}^{L} E_{i,L}\cos(l-1)\theta_i\cos(m-1)\theta_i = \begin{cases} (L-1)/2 & \text{if } l = m \neq 1 \text{ or } L \\ L-1 & \text{if } l = m = 1 \text{ or } L \\ 0 & \text{if } l \neq m \end{cases}$$

and

$$\sum_{i=1}^{L} E_{i,L}\sin(l-1)\theta_i\cos(m-1)\theta_i = 0\,,$$

we obtain the system

$$C_2[\,\bar{\phi}^l_{j-1,k} - 2\bar{\phi}^l_{j,k} + \bar{\phi}^l_{j+1,k}\,] + a_k\bar{\phi}^l_{j,k-1} - b_k\bar{\phi}^l_{j,k} + c_k\bar{\phi}^l_{j,k+1} - \lambda_l\bar{\phi}^l_{j,k} = \bar{r}^l_{j,k}\,, \tag{B.5}$$

in which $\lambda_l = 4C_1\sin^2\dfrac{(l-1)\pi}{2(L-1)}$ for $l = 1,2,\ldots,L$.

By applying the above procedure in the x-direction, we have uncoupled the finite difference equations so that there is no longer any x (i) dependence. We now have a sequence of L two dimensional linear systems to be solved. This sequence can be further reduced to $L \times M$ tridiagonal systems by transforming in the y (j) direction, which contains M unknowns per mesh line. A completely analogous transformation then yields

$$a_k\bar{\bar{\phi}}^{l,m}_{k-1} - [b_k + \lambda_l + \lambda_m]\bar{\bar{\phi}}^{l,m}_{k} + c_k\bar{\bar{\phi}}^{l,m}_{k+1} = \bar{\bar{r}}^{l,m}_{k}\,, \tag{B.6}$$

in which $\lambda_m = 4C_2\sin^2\dfrac{(m-1)\pi}{2(M-1)}$ for $m = 1,2,\ldots,M$.

The right hand side of Eq. (B.6) is obtained in two steps, each carried out by using the cosine transform in the x- and y-directions. Thus,

$$\bar{r}^l_{j,k} = \sum_{i=1}^{L} E_{i,L}\, r_{i,j,k}\cos(l-1)\theta_i \tag{B.7}$$

holds for the x-direction ($l = 1,2,\ldots,L$ and all j,k), while we have

$$\bar{\bar{r}}^{l,m}_{k} = \sum_{j=1}^{M} E_{j,M}\,\bar{r}^l_{j,k}\cos(m-1)\theta_j \tag{B.8}$$

for the y-direction ($m = 1,2,\ldots,M$ and all l,k). The quantity θ_j is defined analogously as

$$\theta_j = \frac{(j-1)\pi}{(M-1)} .$$

Equation (B.6) represents $L \times M$ tridiagonal systems which must be solved for the Fourier coefficients, $\bar{\bar{\phi}}_k^{lm}$. The order of the system is just the number of unknowns in the z- (k-) direction. The exact solution is then obtained from the coefficients by Fourier synthesis. Performing the inverse transformation in reverse order, we have for the y-direction

$$\bar{\phi}_{j,k}^{l} = \sum_{m=1}^{M} E_{m,M}\, \bar{\bar{\phi}}_k^{lm} \cos(m-1)\theta_j \tag{B.9}$$

for $j = 1,2,...,M$ and all l,k. The final inverse transform in the x-direction yields the solution as

$$\phi_{i,j,k} = \sum_{l=1}^{L} E_{l,L}\, \bar{\phi}_{j,k}^{l} \cos(l-1)\theta_i \tag{B.10}$$

for $i = 1,2,...,L$ and all j,k.

The Fourier sums in Eqs. (B.7) - (B.10) are performed by the routine COST in the Fishpak library. If the methods of Cooley and Tukey [48] are used, then the values of $(L-1)$ and $(M-1)$ must be of the form $2^p + 1$, where p is an integer (> 0). The COST subroutine, however, removes this restriction and performs the summations for arbitrary L and M. This is found to offer greater flexibility in the choice of mesh spacing and domain size.

The solution procedure for the Poisson (Laplace) equation by the Fourier series method is now summarized in the following steps :

(1) Transform the right hand side, $r_{i,j,k}$, in the x- and y-directions to obtain $\bar{\bar{r}}_k^{lm}$ (Eqs. (B.7) and (B.8)).

(2) Solve $L \times M$ tridiagonal systems (Eq. (B.6)) to obtain the Fourier coefficients of the solution, $\bar{\bar{\phi}}_k^{lm}$.

(3) Inverse transform these coefficients in the y- and x-directions (Eqs. (B.9) and (B.10)) to obtain the exact solution, $\phi_{i,j,k}$.

APPENDIX C

In this section, we describe the capacitance matrix technique for efficiently solving elliptic finite difference systems in irregular regions. The development of this method has been carried out by Buzbee and Dorr [49], however we shall follow the treatment given by Buzbee [50].

We suppose that we are to solve the N x N elliptic finite difference system Ax = b in which A is not amenable to the Fourier series method due to the irregular hull geometry. The matrix A, however, is very close to a matrix B which describes the thin ship problem in an entirely rectangular domain and for which fast direct methods are applicable. The only difference between these two matrices occurs on and near the hull where an irregular body fitted grid must be used to accommodate the hull geometry. This motivates us to change A into B so that the Fourier series method can be used. Thus, instead of solving Ax = b, we shall solve Bx = c by the optimized direct method. We use the capacitance matrix technique to find the modified right hand side c from the original right hand side b.

We now assume that we must modify only p rows of A to make it identical to B. We then let

$$R = \{1,2,\ldots,N\},$$

$$S = p \text{ element subset of } R$$

and

$$Ax = b\,. \tag{C.1}$$

We note that row j of A is identical to row j of B for all j in R-S. Now we define

$$Bg_i = e_i \text{ for all } i \text{ in } S\,,$$

$$B\hat{x} = b$$

and

$$z = \hat{x} + \sum_S \beta_i g_i \ .$$

The vector e_i is the i^{th} column of the N x N identity matrix, and the scalars β_i (for all i in S) are to be determined. We then have

$$(Az)_j = (Bz)_j = b_j \text{ for all } j \text{ in R—S} \ .$$

The notation $(Az)_j$ means that the j^{th} row of A multiplies the vector z. Thus, z satisfies the N-p unmodified equations of (C.1). Our objective is to determine the β_i so that the remaining p equations of (C.1) are also exactly satisfied. Once this is done, we will have satisfied the hull boundary condition at the precise location of the hull. We now simply require

$$(Az)_i = b_i = (A\hat{x})_i + \sum_S \beta_k (Ag_k)_i \qquad \text{(C.2)}$$

for all i in S. The quantity $(Ag_k)_i$ is the k^{th} element of the i^{th} row in the capacitance matrix, so that Eq. (C.2) defines the p x p linear system for β as

$$C\beta = \gamma \ ,$$

where C is the capacitance matrix and $\gamma_i = b_i - (A\hat{x})_i$ for all i in S. The algorithm is divided into two phases, a preprocessing and a solution phase. The preprocessing involves computing and factoring C and can be performed independently of the right hand side b. The solution phase then uses these results to obtain the solution vector x for a given right hand side.

The complete capacitance matrix algorithm is then summarized as follows :

Preprocessing:

(1) Solve $Bg_i = e_i$ for all i in S.

(2) Calculate and factor C, defined by $(Ag_k)_i$ for all i,k in S.

Solution:

(3) Solve $B\hat{x} = b$.

(4) Solve $C\beta = \gamma$.

(5) Solve $Bx = y + \sum_S \beta_i e_i$.

We note that the solution phase consists of two fast direct solutions involving the matrix B, so that solving the exact hull problem is roughly twice as expensive as the thin ship problem. We also remark that C is factored by Crout reduction with partial pivoting into C = LU. Thus, $C\beta = \gamma$ is solved very efficiently by forward and backward substitution.

For the present locally body fitted mesh system under consideration, there are 240 perturbed finite difference equations on and near the exact Wigley hull. This means that the set S contains 240 elements. From step (1) above, we see that by far the greatest amount of preprocessing effort is spent on solving the systems involving B for all i in S (i.e., the systems involving B are solved 240 times). This must be done once for each hull geometry under consideration and is roughly analogous to constructing a new ship model before it is tested in a towing tank, although the cost for the present preprocessing is far less.

REFERENCES

1. Michell, J.H., "The Wave Resistance of a Ship," *Phil. Mag.* **45** (1898), p. 106.

2. Guilloton, R., "L'etude Theorique Du Bateau En Fluide Parfait," *Bull. De L'Assoc. Tech. Maritime Et Aeronautique* **64** (1964), p. 537.

3. Emerson, A., "The Calculation of Ship Resistance: An Application of Guilloton's Method," *Trans. RINA* **109** (1967), p.241.

4. Gadd, G.E., "Wave Resistance Calculations by Guilloton's Method," *Trans. RINA* **115** (1973), p.377.

5. Brard, R., "The Representation of a Given Ship Form by Singularity Distributions When the Boundary Condition on the Free Surface is Linearized," *J. Ship Res.* **16** (1972), p. 79.

6. Gadd, G.E., "A Method for Calculating the Flow over Ship Hulls," *Trans. RINA* **112** (1970), p. 335.

7. Gadd, G.E., "Ship Wavemaking in Theory and Practice," *Trans. RINA* **111** (1969), p. 487.

8. Baba, E. and K. Takekuma, "A Study on Free Surface Flow Around Bow of Slowly Moving Full Forms," *J. Soc. Nav. Arch. of Japan* **137** (1975), p. 1.

9. Baba, E. and M. Hara, "Numerical Evaluation of a Wave Resistance Theory for Slow Ships," Second Int. Conf. on Num. Ship Hyd., Univ. of Calif., Berkeley, Sept. 1977, p. 17.

10. Baba, E., "Wave Resistance Computations by Low Speed Theory," Proc. of the Workshop on Ship Wave Resistance Computations, DTNSRDC, Bethesda, MD, Nov. 1979, p. 306.

11. Tulin, M.P., "Wave Resistance - State of the Art 1980," Proc. of the Continued Workshop on Ship Wave Resistance Computations, Izu Shuzenji, Japan, Oct. 1980, p. 5.

12. Dawson, C.W., "A Practical Computer Method for Solving Ship Wave Problems," Second Int. Conf. on Num. Ship Hyd., Univ. of Calif., Berkeley, Sept. 1977, p. 1.

13. Israeli, M. and S.A. Orszag, "Approximation of Radiation Boundary Conditions," *J. Comp. Phys.* **41** (1981), p. 115.

14. Dawson, C.W., "Calculations with the XYZ Free Surface Wave Program for Five Ship Models," Proc. of the Workshop on Ship Wave Resistance Computations, DTNSRDC, Bethesda, MD, Nov. 1979, p. 232.

15. Gadd, G.E., "A Method of Computing the Flow and Surface Wave Patterns Around Full Forms," *Trans. RINA* **118** (1976), p. 207.

16. Gadd, G.E., "Contribution to the Workshop on Ship Wave Resistance Computations," Proc. of the Workshop on Ship Wave Resistance Computations, DTNSRDC, Bethesda, MD, Nov. 1979, p. 117.

17. Oomen, A.C.W.J., "Ship Wave Resistance Computations by Finite Element Method," Proc. of the Workshop on Ship Wave Resistance Computations, DTNSRDC, Bethesda, MD, Nov. 1979, p. 396.

18. Oomen, A.C.W.J., "Free Surface Potential Flow Computation Using a Finite Element Method," Third Int. Conf. on Num. Ship Hyd. **1**, Paris, June 1981.

19. Korving, C. and A.J. Hermans, "The Wave Resistance for Flow Problems with a Free Surface," Second Int. Conf. on Num. Ship Hyd., Univ. of Calif., Sept. 1977, p. 285.

20. Bai, K.J., "A Note on Numerical Radiation Condition," Proc. of the Continued Workshop on Ship Wave Resistance Computations, Izu Shuzenji, Japan, Oct. 1980, p. 65.

21. Wu, D.-M. and T.Y. Wu, "Three Dimensional Nonlinear Long Waves Due to Moving Surface Pressure," Fourteenth Symp. on Naval Hyd., Univ. of Mich., Ann Arbor, Aug. 1982, p. 103.

22. Orlanski, I., "A Simple Boundary Condition for Unbounded Hyperbolic Flows," *J. Comp. Phys.* **21** (1976), p. 251.

23. Chan, R.K.-C., "Finite Difference Simulation of the Planar Motion of a Ship," Second Int. Conf. on Num. Ship Hyd., Univ. of Calif., Berkeley, Sept. 1977, p. 39.

24. Yeung, R.W., "Numerical Methods in Free Surface Flows," *Ann. Rev. Fluid Mech.* **14** (1982), p. 395.

25. Yen, S.M. and D.R. Hall, "Implementation of Open Boundary Conditions for Nonlinear Free Surface Wave Problems," Third Int. Conf. on Num. Ship Hyd. **2**, Paris, June 1981.

26. Shapiro, R., "Linear Filtering," *Math. Comp.* **29** (1975), p. 1094.

27. Ohring, S., "A Fast Fourth Order Laplace Solver for Application to Numerical Three Dimensional Water Wave Problems," First Int. Conf. on Num. Ship Hyd., Gaithersburg, MD, Oct. 1975, p. 641.

28. Ohring, S. and J. Telste, "Numerical Solutions of Transient Three Dimensional Ship Wave Problems," Second Int. Conf. on Num. Ship Hyd., Univ. of Calif., Berkeley, Sept. 1977, p. 88.

29. Ohring, S. and J. Telste, "The Direct Matrix Imbedding Technique for Computing Three Dimensional Potential Flow About Arbitrarily Shaped Bodies," *Comp. Meth. in Apl. Mech.* and *Eng.* **21** (1980), p. 315.

30. Young, D., *Iterative Solution of Large Linear Systems*, Academic Press, New York, 1971.

31. Hestenes, M. and E. Stiefel, "Methods of Conjugate Gradients for Solving Linear Systems," *J. Res. NBS* **49** (1952), p. 409.

32. Reid, J.K., "On the Method of Conjugate Gradients for the Solution of Large Sparse Systems of Linear Equations," *Proc. Conf. on Large Sparse Sets of Linear Equations*, Academic Press, New York, 1971.

33. Concus, P., G.H. Golub and D.P. O'Leary, "A Generalized Conjugate Gradient Method for the Numerical Solution of Elliptic Partial Differential Equations," *Sparse Matrix Computations*, J. Bunch and D. Rose (eds.), Academic Press, New York, 1976.

34. Concus, P. and G.H. Golub, "A Generalized Conjugate Gradient Method for Nonsymmetric Systems of Linear Equations," Stan-CS-76-535.

35. Meijerink, J.A. and H.A. van der Vorst, "An Iterative Solution Method for Linear Systems of Which the Coefficient Matrix is a Symmetric M-Matrix," *Math. Comp.* **31** (1977), p. 148.

36. Kershaw, D.S., "The Incomplete Cholesky Conjugate Gradient Method for the Iterative Solution of Systems of Linear Equations," *J. Comp. Phys.* **26** (1978), p. 43.

37. Khosla, P.K. and S.G. Rubin, "A Conjugate Gradient Iterative Method," *Computers and Fluids* **9** (1981), p. 109.

38. Rubin, S.G. and P.K. Khosla, "Navier-Stokes Calculations with a Coupled Stringly Implicit Method – I," *Computer and Fluids* **9** (1981), p. 163.

39. Buzbee, B.L., G.H. Golub and C.W. Nielson, "On Direct Methods for Solving Poisson's

Equations," *SIAM J. Num. Anal.* **7** (1970), p. 627.

40. Dorr, F.W., "The Direct Solution of the Discrete Poisson Equation on a Rectangle," *SIAM Review* **12** (1970), p. 248.

41. Hockney, R.W., "A Fast Direct Solution of Poisson's Equation using Fourier Analysis," *J. Assoc. Comp. Mach.* **12** (1965), p. 95.

42. Hockney, R.W., "The Potential Calculation and Some Applications," *Methods in Comp. Phys.* **9** (1970), p. 135.

43. Wigley, W.C.S., "Calculated and Measured Wave Resistance of a Series of Forms Defined Algebraically, the Prismatic Coefficient and Angle of Entrance Being Varied Independently," *Trans. RINA* **84** (1942), p. 52.

44. Ju, S., "Study of Total and Viscous Resistance for the Wigley Parabolic Ship Form," Iowa Inst. of Hydraulic Research, Rept. No. 261, April 1983.

45. Shearer, J.R. and J.R. Cross, "The Experimental Determination of the Components of Ship Resistance for a Mathematical Model," *Trans. RINA* **107** (1965), p. 459.

46. Johnson, F.T., R.M. James, J.E. Bussoletti and A.C. Woo, "A Transonic Rectangular Grid Embedded Panel Method," AIAA paper 82-0953, June 1982.

47. Rudy, D., private communication.

48. Cooley, J.W. and J.W. Tukey, "An Algorithm for the Machine Computation of Complex Fourier Series," *Math. Comp.* **19** (1965), p. 297.

49. Buzbee, B.L. and F.W. Dorr, "The direct solution of the biharmonic equation on rectangular regions and the Poisson equation on irregular regions," *SINUM* **11** (1974), p.753.

50. Buzbee, B.L., "A Capacitance Matrix Technique," *Sparse Matrix Computations*, J. Bunch and D. Rose (eds.), Academic Press, New York, 1976.

VITA

Robert Rexford Chamberlain, Jr. was born on November 24, 1956 in Port Chester, New York. He graduated high school from the Rye Country Day School in 1974. He then attended Denison University where, in 1978, he received his B.S. degree in Physics. During the period from 1976 to 1978, Mr. Chamberlain was enrolled in the Platoon Leaders Class of the United States Marine Corps and attended the summer training camp in Quantico, Virginia.

Upon graduation from Denison University, Mr. Chamberlain became a research assistant in the Department of Aeronautical and Astronautical Engineering at the University of Illinois at Urbana-Champaign. He received his M.S. degree from that department in 1980. The title of his thesis was "An Experimental Determination of Methane Concentration Profiles in a Vertical Square Flammability Tube."

After graduation, Mr. Chamberlain was the recipient of the Richard D. DuPont Fellowship award at the Massachussetts Institute of Technology. He attended the Insitute for one year and returned in 1981 to the University of Illinois where he joined the computational fluid dynamics research group in the Coordinated Science Laboratory. From that time, he has held a research assistantship and has been involved in the ongoing research activities of the Laboratory.